Wissenschaftszentrum Weihenstephan für Ernährung, Landnutzung und Umwelt, Technische Universität München

---

The Role and Molecular Regulation of microRNAs and their Targets in Adipogenesis

---

Christina Glantschnig

Vollständiger Abdruck der von der promotionsführenden Einrichtung
Wissenschaftszentrum Weihenstephan für Ernährung, Landnutzung und Umwelt, Technische Universität München
der Technischen Universität München zur Erlangung des akademischen Grades
eines Doktors der Naturwissenschaften
genehmigten Dissertation.

Vorsitzende/-r: Prof. Dr. Michael Schemann

Prüfende/-r der Dissertation:

1. Prof. Dr. Martin Klingenspor

---

2. Prof. Dr. Stephan Herzig

Die Dissertation wurde am 04.04.2017 bei der Technischen Universität München
eingereicht und durch die promotionsführende Einrichtung
Wissenschaftszentrum Weihenstephan für Ernährung, Landnutzung und Umwelt, Technische Universität München am 26.06.2017 angenommen.

THE ROLE AND MOLECULAR REGULATION OF MICRORNAS AND THEIR TARGETS IN ADIPOGENESIS

Dissertation

presented to the

Faculty Wissenschaftszentrum Weihenstephan

for the degree of

Doctor of Natural Sciences

by

CHRISTINA GLANTSCHNIG

Abstract

Adipose tissue, rather than being just a passive storage for excess energy, is a highly dynamic organ actively balancing energy storage and release, and besides liver and muscle is a core contributor to the systemic metabolic state. With the surge in obesity and related metabolic comorbidities in recent years, adipogenesis comes into focus. Overfeeding can lead to overloading of adipocytes, the detrimental consequences of which can in turn impair one of the potential alleviators to this situation: recruitment of preadipocytes to adipocyte differentiation.
Adipocyte differentiation is controlled not only by protein-coding genes, but also by non-coding RNAs, and particularly microRNAs (miRNAs): ~22nt RNAs that regulate gene expression by targeting the microRNA-induced silencing complex (miRISC) to the miRNA recognition element (MRE) in target mRNAs and basepairing to their seed match.

miR-29a had been identified in preliminary studies to be downregulated during adipocyte differentiation of our human adipogenesis model, human Multipotent Adipose-Derived Stem (hMADS) cells. Previous studies had implicated it in insulin resistance and diabetes, however, none of these addressed its role in adipocyte differentiation. Thus, the goal of this thesis was to elucidate the role of miR-29 in human adipocyte differentiation, and identifying a direct target that mediates this effect.
We found that miR-29a was downregulated during adipogenesis, and that increasing its abundance by transfection into preadipocytes inhibited subsequent adipocyte differentiation. From a gene expression screen, we identified eight potential target genes, five of which were directly bound by the miR-29a *in vitro.* One candidate, mesoderm-specific transcript (MEST), unexpectedly had the opposite of the expected effect on adipocyte differentiation and was pursued as a stand-alone project, since silencing MEST, contrary to published data in murine cell lines, enhanced adipogenesis in hMADS cells. Out of the remaining four candidates, only silencing of NR3C1, the glucocorticoid receptor (GR) gene, phenocopied the miR-29 effect on differentiation.

In search of an upstream regulatory mechanism of miR-29 expression, we found that miR-29a is induced by glucocorticoids *in vitro* and *in vivo*, and that GR binds upstream of the miR-29a gene locus, thus creating a negative feedback loop between the target and the targeting miRNA. The identification of this novel and unexpected feedback loop opens up interesting research perspectives on the phenomenon of GR downregulation upon long-term treatment with glucocorticoids.

In summary, this dissertation examines the role of the miR-29 and its targets in human adipocyte differentiation *in vitro*, associated correlations in murine and human tissue and identifies a novel feedback mechanism between miR-29 and GR that could serve as a starting point for exciting further research.

Zusammenfassung

Fettgewebe ist nicht nur ein passiver Speicherort für überschüssige Energie, sondern ein hochdynamisches Organ, das Energiespeicherung und Energiefreigabe aktiv ausbalanciert. Neben Leber und Muskeln ist Fettgewebe damit eines der Organe, die am meisten zum systemischen Stoffwechselstatus beitragen. Mit dem steilen Anstieg von Adipositas und den zugehörigen Begleiterkrankungen in den letzten Jahren liegt der Fokus verstärkt auf Adipogenese, da Überernährung zu einem Überladen der Fettzellen führen kann, dessen negative Konsequenzen wiederum eine der möglichen Lösungen für diese Situation inhibieren können: nämlich die Differenzierung von weiteren Präadipozyten zu reifen Fettzellen.

Fettzelldifferenzierung wird nicht nur von protein-kodierenden Genen, sondern auch nicht-kodierenden RNAs gesteuert; im Speziellen von microRNAs (miRNAs): Diese ~22nt langen RNAs regulieren die Genexpression indem sie den für die Inhibierung zuständigen microRNA-induced silencing complex (miRISC) zum respektiven „miRNA Erkennungselement", miRNA recognition element (MRE) leiten und dort Basenpaarung mit dem „seed match" des Targets eingehen.

miR-29 wurde in präliminären Versuchen als eine der miRNAs identifiziert, deren Expression während der Adipogenese unseres menschlichen Zellmodells, den humanen multipotenten Fettgewebe-stämmigen Stammzellen (Multipotent Adipose-Derived Stem (hMADS)cells), zunehmend verringert wird. Publizierte Studien hatten miR-29 mit Diabetes und Insulinresistenz assoziiert, jedoch wurde die Rolle der miRNA in der Fettzellentwicklung nie untersucht. Daher war das Ziel dieser Dissertation, die Rolle der miR-29 in der humanen Fettzellentwicklung zu untersuchen und das Target zu identifizieren, durch welches ein potenzieller Effekt vermittelt wird.

Unsere Ergebnisse zeigen, dass miR-29a während der Fettzellentwicklung verringert exprimiert wird, und das künstliches Erhöhen der miR-29 Levels durch Transfektion in Präadipozyten die Fettzelldifferenzierung verringert. Durch einen Genexpressions-Screen identifizierten wir acht Kandidatengene, von denen fünf *in vitro* direkt durch die miRNA gebunden wurden. Einer der Kandidaten, mesoderm-specific transcript (MEST), hatte unerwarteterweise den gegenteiligen Effekt auf Fettzellentwicklung humaner Zellen als von der Literatur über Versuche in Mauszellen zu erwarten war, weshalb daraus ein eigenständiges und mittlerweile publiziertes Projekt verfolgt wurde. Von den übrigen vier Kandidaten reproduzierte nur das Silencen eines Genes den Effekt der miR-29 auf die Fettzelldifferenzierung: NR3C1, das Glukokortikoidrezeptor (GR)-Gen.

Auf der Suche nach einem Regulator der miR-29 Expression entdeckten wir, dass miR-29a *in vitro* und *in vivo* von Glukokortikoiden induziert wird, und dass GR vor dem miR-29a Genlokus bindet, was eine negative Rückkopplung zwischen dem miRNA-Target und der miRNA erzeugt. Die Identifikation dieser neuen und unerwarteten Feedbackschleife eröffnet spannende Perspektiven bzgl. des Phänomens, dass GR Proteinlevel bei längerfristiger Behandlung mit Glukokortikoiden geringer werden.

Zusammengefasst untersucht diese Dissertation die Rolle der miR-29 und ihrer Targets in der humanen Fettzelldifferenzierung *in vitro*, assoziierte Korrelationen in Maus- und Menschengewebe und identifiziert einen neuen Feedbackmechanismus zwischen miR-29 und dem Glukokortikoidrezeptor, der als Startpunkt für spannende weiterführende Forschung dienen kann.

Acknowledgements

Science is no one-man show – therefore I would like to thank everyone who has supported me throughout the course of my doctoral work. First of all, I would like to thank PI Dr. Marcel Scheideler for taking me up as his PhD student in Graz, Austria, and for finding a way out of a crumbling institute into a better future. Consequently, my deepest gratitude belongs to Prof. Dr. Stephan Herzig for granting me the opportunity to complete my PhD thesis in the exciting, challenging and supportive environment of the Institute for Diabetes and Cancer (IDC) at the Helmholtz Zentrum München. I would also like to thank the DIABAT EU project, which funded the first 1.5 years of my thesis, and the Austrian Academy of Sciences (ÖAW), by virtue of whose DOC scholarship I was privileged to continue and finish my PhD work in Germany. It was an exceptional honor and inspiration to receive this endorsement through a peer-reviewed process by the Austrian government at this stage in my scientific development.

This thesis would not have been possible without the mentoring and support by Dr. Michael Karbiener, who helped get my project off the ground and taught me all the basic techniques needed to accomplish this. I appreciate the insights on scientific publishing I gained from working with Michael. Additionally, even across the alps he remained an inspirational, humorous and supportive influence on my PhD career.

I am deeply thankful to all of Division B for pleasant personal interaction and scientific support, especially Dr. Anastasia Georgiadi and Dr. Frits Mattijssen, whose input on scientific discussions where tremendously helpful in shaping the direction of my project. Also, thanks to Sabine Hartig for TA support in the lab. Outside of Division B, I owe special gratitude to Dr. Götz Hartleben for continued scientific discussion and inspiring me with his vibrant ideas, Dr. Manuel Gil Lozano for sharing his mouse samples and expertise with me as well as Dr. Anne Loft and Dr. Søren Fisker-Schmidt, who aided me on the ChIP-qPCR experiments with their marvelous expertise in epigenetics, even before they had arrived at the IDC. Additional gratitude goes to Lara Shahidian for sharing her know-how on the ChIP process.

I would also like to express my gratitude to our collaboration partners: In Nice, PI Dr. Amri Ez-Zoubir and Dr. Didier Pisani, who graciously gave us the hMADS cells and contributed not only mouse experiments but also their invaluable expertise, and hosted me for two research stays with incredible hospitability and warmth. In Leipzig, Prof. Dr. Matthias Blüher for performing RT-qPCR experiments in his treasured cohort of well-characterized human fat samples.

On a more personal note, I would like to thank my good colleagues and friends inside the lab –Lea, Eveline and most of all Susi, my "one mind" soulmate – as well as outside the lab – Lisa, Markus, Thomas, Niki and Gerhild for their continued emotional support (or depreciation in Markus' case) which made tough times more tolerable and the fun times way more awesome. You're the spice in my life! Lastly, I would like to apologize to my

dog, Kaya, for having to listen to yet another scientific monologue she was unable to voice her opinion on due to evolutionary constraints.

Last but not least, my gratitude is owed to my parents, without whose support neither my undergraduate nor my PhD studies would have been possible. My heartfelt appreciation goes especially to my Dad for strategic mentoring drawing from his rich experiences.

So long, and thanks for all the fish.

Contents

"The first principle is that you must not fool yourself — and you are the easiest person to fool."

Richard Feynman

Introduction

Adipose tissue

The adipose organ

Over the last decades of research, it has become clear that rather than being just a passive "store room" for excess energy, adipose tissue is a highly dynamic organ that performs functions of energy storage, energy release as well as modulation of systemic metabolic parameters, for example by releasing free fatty acids, as well as hormones, termed adipokines (Cinti, 2001). This makes adipose tissue an endocrine organ affecting aspects of metabolism as diverse as insulin sensitivity, satiety and lipid metabolism (Galic et al., 2010). Additionally, secreted adipokines have also been found to be involved in cardiovascular disease (Rega-Kaun et al., 2013).

Shades of adipose tissue

Adipose tissue is mainly composed of mature adipocytes embedded in a matrix of fibroblasts, preadipocytes, endothelial cells, nerves, immune cells and a varying degree of blood vessels(Cinti, 2005). Different adipose tissue types characterized by distinct location, molecular markers and metabolic phenotype have been described in mammals: white adipose tissue (WAT), brown adipose tissue, and the so called brown-in-white (brite) or beige adipose tissue. While white adipose tissue is characterized at the cellular level by large, unilocular lipid droplets and few mitochondria, its main function being energy storage, brown fat in contrast can increase energy expenditure by uncoupling oxidation of metabolites from production of the cell's energetic currency, ATP (Cinti, 2005; Gesta et al., 2007).

Brown fat cells have higher metabolic rate than white adipocytes, giving them a brownish appearance under the microscope, as well as higher metabolic rate and many, so called multilocular, lipid droplets. They can be distinguished molecularly from WAT by expression of the brown marker genes DIO2, PRDM16, PGC-1α and Cidea (Gesta et al., 2007). Until 2007, it was assumed that functional BAT in adult humans was virtually non-existent, despite radiology publications repeatedly having reported small, non-tumor regions of adipose tissue that showed up in PET/CT scans due to their high uptake of 18F-fluorodeoxyglucose, i.e. were highly metabolically active, unless patients were kept warm prior to the scan (Cohade et al., 2003; Hany et al., 2002). The watershed moment for BAT research came when in 2007, when Cannon & Nedergaard compiled a comprehensive review of evidence, mostly from radiological journals, for the existence of BAT in adult humans (Nedergaard et al., 2007). Shortly after, in 2009, five independent groups reported the presence of active BAT in adult humans, also using 18F-FDG PET/CT (Cypess et al., 2009; van Marken Lichtenbelt et al., 2009; Saito et al., 2009; Virtanen et al., 2009; Zingaretti et al., 2009). In young men exposed to 16°C cold, active BAT was detected in 23 out of 24 individuals, suggesting it might be substantially prevalent among the general population (van Marken Lichtenbelt et al., 2009).

Brite adipocytes share characteristics of both brown and white adipocytes. They resemble brown adipocytes in their metabolic activity and uncoupling of electron transport from energy production, but are found in classically "white" fat depots, usually surrounded by white fat cells. Whether there are distinct brite preadipocytes, they share a common

progenitor with white or brite adipocytes or they originate from transdifferentiation of mature white adipocytes is still up for scientific debate (Berry et al., 2014; Lee and Cowan, 2013). It has been argued that in contrast to murine BAT, human BAT demonstrates a gene expression signature more similar to beige/brite cells than to classical brown adipocytes (Sharp et al., 2012).

Origins and locations of different types of fat

In addition to distinction by the types of adipocytes they mainly comprise, there is variation in adipose tissue characteristics depending the depot it is located in (Girard and Lafontan, 2008), resulting in e.g. distinct depot-specific gene expression patterns (Gesta et al., 2007). Another finding contributing to this view is that the stromavascular fraction isolated from the subcutaneous vs. the intraabdominal depot of obese women shows increased differentiation potential (Hauner and Entenmann, 1991).

White adipose tissue depots are mainly divided into subcutaneous (abdominal, gluteal, cranial, facial) and intra-abdominal (omental, retroperitoneal and visceral), with additional retro-orbital, periarticular, intramuscular, pericardial and bone marrow located depots being less relevant to systemic metabolism. Brown adipose tissue in humans can be found at the interscapular depot in babies, while it is more prevalent at the cervical, paravertebral and mostly, supraclavicular location in adult humans (Gesta et al., 2007).

Adipose tissue is generally thought to originate from the mesoderm. Since the mesoderm arises from a layer of cells that spreads along the "belly to back" and reverse axes, i.e. the anteroposterior and dorsoventral axes during embryo development, and each region supposedly gives rise to its own distinct adipose depot, the functional and sometimes morphological diversity of adipose depots fits with its diverse origins. Despite the lack of precise lineage studies, the fact that mesenchymal stem cells can be differentiated into adipocytes in culture reinforces this interpretation of adipose tissue origins (Berry et al., 2014; Gesta et al., 2007). Brown adipose tissue can be traced to Myf5 positive precursor cells, which distinguishes them from WAT precursors (Seale et al., 2008). However, Myf5 precursors are not the only source of brown adipocytes and were also found to contribute to the white and brite adipocyte populations (Sanchez-Gurmaches and Guertin, 2014; Sanchez-Gurmaches et al., 2012).

Adipocyte differentiation

Adipocyte differentiation is the process of adipocyte precursor cells developing into fully mature, lipid-laden and metabolically functional adipocytes. This process is commonly divided into two parts: The commitment stage, in which multipotent stem cells are transformed into committed adipocyte precursor cells by virtue of epigenomic changes as well as changes in gene expression, despite being morphologically almost indistinguishable from its precursor cell (Cristancho and Lazar, 2011; Rosen and Spiegelman, 2006). The second part is the terminal differentiation phase, in which the preadipocyte develops into a mature adipocyte by acquiring essential metabolic machinery for lipid accumulation, transport, insulin sensitivity and secretion of

adipokines. During this stage, the cells visibly transform morphologically from a fibroblast type precursor to a lipid-laden, round cell (Rosen and Spiegelman, 2006).

In vivo, brown adipose tissue already develops in utero (Frontini and Cinti, 2010), while white fat depots emerge during late gestation (Gesta et al., 2007). In humans, adipocyte number increases throughout childhood and adolescence, then stabilizes and remains mostly constant in adults. The difference in adipocyte number found between lean and obese adults therefore seems to arise from the initial number set during the growth and development phase (Knittle et al., 1979; Spalding et al., 2008a). A study by Peter Arner and colleagues found that in contrast to previous assumptions, adipogenesis does play a role in adult humans, since there is a turnover of about 10% of adipocytes per year, according to analysis of integration of the 14C isotope derived from nuclear bomb detonations in genomic DNA of adipocytes (Spalding et al., 2008a). However, a limitation of this study is the exclusive analysis of early onset obesity patients, and therefore does not apply to patients who start out at a normal weight but gradually gain weight over the subsequent years. This critical view is supported by studies of short-term overfeeding in adult humans, which showed an increase in the number of adipocytes (Linhart et al., 2001).

Adipogenesis is studied *in vitro* using several mouse cell lines, such as the immortalized Swiss mouse 3T3-L1 and 3T3-F442 fibroblast cell lines, which spontaneously accumulate lipids after confluence (Green and Kehinde, 1975; Green and Meuth, 1974), and can be differentiated efficiently into mature adipocytes by applying a cocktail including insulin (Green and Kehinde, 1975), IBMX (Russell and Ho, 1976a), and glucocorticoids (Miller et al., 1978; Rubin et al., 1978).
Differentiation of human multipotent stem cells (e.g. hMADS cells) and primary cells usually requires the additional application of PPARγ agonists, e.g. Rosiglitazone, or indomethacin, a compound affecting prostaglandin synthesis. Both drive lipid accumulation even in uncommitted mesenchymal stem cells (Styner et al., 2010).

Commitment of precursor multipotent stem cells to the preadipocyte lineage

Several transcriptional regulators are known to be involved in the commitment of multipotent precursors to adipocyte differentiation. Wnt signaling, a signaling pathway involving secreted glycoproteins crucially involved in development (and therefore classified as "morphogens") negatively affects adipogenesis. Activation of canonical Wnt signaling (Ross et al., 2000) by addition of Wnt10b inhibits adipogenesis of committed preadipocytes, and mice expressing Wnt10b have lower adipose tissue mass in both white and brown depots (Longo et al., 2004). Activation of the non-canonical Wnt pathway, mostly acting via ligand Wnt5a, can additionally inhibit adipogenesis by inhibiting PPARγ activity and promoting osteogenesis in mesenchymal stem cells. On the other hand, Wnt10b plays a role for the survival of adipocyte precursors and Wnt1 targets IGF1 and IGF2 to protect preadipocytes from apoptosis during serum starvation. The non-canonical Wnt5b seems to increase adipocyte differentiation as well (Cristancho and Lazar, 2011). cAMP agonists like IBMX, required for adipogenesis of most *in vitro* models (Russell and Ho, 1976b), can besides their activation of PKA (Essayan, 2001) and

inhibition of TNFα also feed into Wnt signaling by repressing Wnt10b expression (Deree et al., 2008; Marques et al., 1999). All in all, canonical as well as non-canonical Wnt signaling controls adipogenesis in a variety of ways and integrates a diverse range of upstream signals.

Another morphogen affecting commitment to the preadipocyte lineage are Transforming Growth factor-β (TGFβ) ligands. Though the role of TGFβ in adipogenesis is unclear, as it correlates with obesity in humans but inhibits *in vitro* adipogenesis of committed mouse preadipocytes, other members of the family, bone morphogenetic proteins (BMPs), promote adipogenesis by activating SMAD proteins and signalling through the p38 kinase pathway (Cristancho and Lazar, 2011). Prominent members impacting adipogenesis are BMP2 and BMP4 which increase differentiation capacity (Böttcher et al., 2009; Huang et al., 2009), while BMP7 induces brown adipocyte differentiation (Tseng et al., 2008).

One more factor influencing adipogenesis is the stiffness, composition and tension of the extracellular matrix (ECM). ECM proteins like fibronectin, integrins and collagens contribute to the determining properties affecting adipocyte differentiation. Cells can influence their ECM by regulating the activity of matrix metalloproteinase peptidases (MMPs), which explains why several MMPs have been implicated with varying effects on preadipocyte differentiation (Cristancho and Lazar, 2011).
Confluency as well as cell shape influence commitment of MSCs as well. Confluency boosts adipogenic differentiation over e.g. osteoblast differentiation, which seems to be a consequence of cell shape and internal structure rather than inability to undergo cell division, since 3T3-L1 cells have a last mitotic clonal expansion round upon stimulation with the adipogenic cocktail. Changes in cell shape can be influenced RHO GTPase-RHO-associated kinase (ROCK) signaling, which controls internal cell structure, while GAPs and GEFs that regulate ROCK signaling can in turn also affect adipogenesis, adding yet another layer to an already complex regulatory system (Cristancho and Lazar, 2011).

Terminal differentiation of preadipocytes to mature fat cells

Terminal differentiation of committed precursor cells is orchestrated by a harmony of several transcription factors, the most prominent of which are PPARɣ, the master regulator of adipogenesis, and the C/EBPα, C/EBPβ and C/EBPɣ proteins (Cristancho and Lazar, 2011), which act as its co-activators. Among the earliest events in adipogenic differentiation of committed preadipocytes is the fast induction of C/EBPβ by cAMP agonists, mediated by phosphorylation of cAMP-responsive element-binding (CREB) (Reusch 2000, Zhang CREB 2004 JBC). The transcription factor KLF4 (Birsoy 2008) and the JAK2-STAT3 signaling pathway (Wang 2010, Zhang 2011) also promote C/EBPβ expression and activity, with its phosphorylation by MAP kinases and GSK3β being a prerequisite for its DNA binding ability crucial to the activation (Tang 2005).
Upon adipogenic stimulation via cocktails commonly including cAMP agonists like IBMX and glucocorticoids like dexamethasone, adipogenic transcription factors like C/EBP, STAT5a, RXR and the glucocorticoid receptor (GR) are recruited to hitherto

quiescent hotspot regions in the genome, most of which already harbour C/EBPβ. C/EBPβ and -δ, induced within 4h of the stimulus, seem to cooperate in early terminal differentiation, while C/EBPα expression rises much later and is directly modulated by C/EBPβ (Cristancho and Lazar, 2011). All of the C/EBP family members have a DNA-binding domain and a C-terminal leucine zipper motif that allows formation of heterodimers, which is essential for DNA binding (Birkenmeier et al., 1989).

Glucocorticoids (GCs) affect differentiation by binding to the glucocorticoid receptor (GR), which has long been known to regulate C/EBPβ activity via acetylation, or by non-transcriptional interaction with HDAC1, which depletes a co-repressor complex of C/EBPβ (Park and Ge, 2017; Wiper-Bergeron et al., 2003, 2007). Epigenomic regulation has been revealed to play an important role in modulating GR activity, which is further discussed in "GC-GR molecular action".

Three known isoforms of PPARɣ exist, with PPARɣ2 being the primary adipocyte specific variant. PPARɣ forms a heterodimer with the retinoid X receptor (RXR) (Tontonoz and Spiegelman, 2008) after induction by C/EBPβ, then together with C/EBPα induces adipocyte gene expression. Upon stable activation, PPARɣ and C/EBPα cross-activate each other through their C/EBP regulatory elements, contributing to maintenance of the mature adipocyte phenotype (Lefterova et al., 2008; Tang and Lane, 2012). Additionally, during adipogenesis, triglyceride accumulation is accompanied by an increase in the rate of lipogenesis and expression of related enzymes in the fatty acid and triglyceride biosynthesis pathways (MacDougald and Lane, 1995; Tang and Lane, 2012).

Glucocorticoids in obesity and adipocyte differentiation

Glucocorticoids (GCs) in the context of metabolism are often seen as antagonists of the anabolic action of insulin (Saltiel and Kahn, 2001). Upon fasting- or exercise-induced low blood glucose levels, GCs released from the adrenal cortex cooperate with glucagon produced by α-cells of the pancreas to change systemic energy utilization (Vegiopoulos and Herzig, 2007a).

Relevance of GC in pathology

A role for GC in excess fat accumulation is hinted at by the symptoms of Addison's disease and Cushing's syndrome. In the former, adrenal cortex dysfunction and lack of GC action leads, among other symptoms such as decreased stress resistance, to weight loss, while the latter is characterized by chronic GC excess due to pituitary adenomas or ACTH-secreting tumors, a common symptom of which is visceral obesity (Shibli-Rahhal et al., 2006). Despite this compelling evidence for a role of GCs in metabolism, the devil is in the details, which are slightly contradictory. High GC levels have been associated with metabolic syndrome (Reynolds et al., 2001), but not necessarily with obesity, where it was hypothesized that local GC action contributes more than systemic GC levels (Phillips et al., 1998). On the other hand, treating obese Zucker rats with RU486, a GR antagonist, for 15 days restored their body composition to lean levels (Langley and York, 1990)

Previous studies suggested that in non-diabetic obese patients, circulating GC levels were lower, which would seem paradoxical and had been explained by local increases in tissue GC levels produced by GC-metabolizing enzymes like 11βHSD1 (Seckl and Walker, 2001; Vegiopoulos and Herzig, 2007a). However, in our own data acquired from cooperation with M. Blüher, cortisol levels are significantly positively correlated with BMI in all NGT patients.

Regulation of GC release

GC secretion by the adrenal cortex is controlled by feedback through the hypothalamo-pituitary-adrenal (HPA) axis. Secreted corticotropin releasing hormone (CRH) activates POMC gene transcription and subsequent secretion of its adrenocorticotropic hormone (ACTH). ACTH stimulates GC synthesis, whereas GCs in turn inhibit CRH gene expression, completing the negative feedback loop (Vegiopoulos and Herzig, 2007a).
It has been purported that chronic stress can lead to glucocorticoid receptor resistance (GCR), which is characterized by a lack of correlation of plasma cortisol levels with the ratio of neutrophils to lymphocytes, and has been demonstrated in patients that had experienced a significant stressful life event during the year previous to the study. GCR is assayed by a dexamethasone suppression test that measures the ability of dexamethasone to suppress LPS stimulated production of IL-1β, IL-5 and TNFα. Subjects demonstrating GCR were at higher risk of developing a cold following rhinovirus exposure (Cohen et al., 2012).

GC in adipose tissue

In adipose tissue, GCs and therefore GR exert a two-faced, depot-specific effect: in subcutaneous depots, GCs increase lipolysis by activating transcription of related genes, while in central fat they boost adipogenesis, lipogenesis and adipocyte hypertrophy. GC treatments additionally interfere with insulin signaling by downregulating IRS1 and IRS2 protein levels, PI3K activity and Akt phosphorylation, as well as glucose uptake by GLUT4 (Vegiopoulos and Herzig, 2007a), leading to insulin resistance (Fasshauer et al., 2002; Masuzaki and Flier, 2003; Masuzaki et al., 2001; Viengchareun et al., 2002). GR suppresses glyceroneogenesis in adipocytes by targeting C/EBPs, which stands in contrast to its action in liver, where glyceroneogenesis is promoted. Since 3-glycerophosphate is an essential precursor for TG synthesis, this suggests a limiting role of GR in fat storage in peripheral depot adipocytes (Vegiopoulos and Herzig, 2007a). In line with this observation, ex-vivo cultures from corticosterone-treated rats lead to the finding that adipocytes from visceral, but not subcutaneous fat depots show higher lipolytic rates. Additionaly, this lead not only to increased visceral adipocyte hpyertrophy, but also to increased preadipocyte differentiation (Campbell et al., 2011). Part of the metabolic effects of GR stimulation in WAT can be attributed to ANGPTL4, an inhibitor of LPL, which was found to be a direct target of GR in adipocytes. ANGPTL4 is secreted from liver and WAT under conditions of high GC levels and fasting. It promotes lipolysis and channels lipids from adipose tissue to the liver (Patel et al., 2014).

A recent study added to the state of knowledge by comparative gene expression profiling of paired human omental and subcutaneous adipose tissue samples cultured ex vivo and

stimulated with dexamethasone for 7 days. They found common pathways (insulin signaling, glycolysis, gluconeogenesis pyruvate metabolism, FA metabolism, peroxisome and glycero(phospho)lipid metabolism) to be upregulated by Dex stimulation in both depots. In contrast, steroid biosynthesis and the pentose phosphate pathway were upregulated by Dex in omental but not subcutaneous WAT, both of which potentially feed into steroid biosynthesis pathways. Furthermore, low concentrations of Dex shifted gene expression significantly in subcutaneous, but not omental fat, which required higher concentrations to achieve clustering of gene expression away from the non-stimulated control (Pickering et al., 2016).

GC-GR molecular action

On a molecular level, GCs bind to the glucocorticoid receptor (GR), a transcription factor belonging to the nuclear receptor superfamily. GR is encoded by the NR3C1 gene and exists in two isoforms, GRα and GRβ, with differing properties concerning dimerization, DNA binding and transcriptional activation (Vegiopoulos and Herzig, 2007a). Human and murine GR is produced from exons 2-8 of the 9 exon gene NR3C1, 50 amino acids added from exon 9α to yield GRα, while addition of 15 amino acids from exon 9β yields GRβ. GRα represents the classical receptor that regulates gene transcription upon GC binding. GRβ lacks the ligand-binding domain, but seems to inhibit GRα function. Intriguingly, it has been found that GRβ but not GRα levels increase upon insulin stimulation in mice and rats, leading to the speculation that the state of GC resistance in humans (characterized by increased GR protein levels but decreased GC sensitivity) might be caused by a change in the GRα:GRβ ratio (John et al., 2015). GR whole body KO mice die at birth (Cole et al., 1995), but transgenic mice carrying a GR lacking the DNA-binding function survive, which underscores the significance of not only its properties as a transcription factor, but also the importance of GR protein-protein interactions (Reichardt et al., 1998).
Upon GC binding, GR is released from a complex containing HSP-90 and HSP-70 and translocates into the nucleus to transcriptionally regulate target genes (Patel et al., 2014; Tata, 2002). Most GR binding sites are not found in typical promoter regions, but rather in intragenic regions that can be more than 25kb away from the actual TSS (Kuo et al., 2012).

Recent studies have given a more detailed insight into the regulation of GR transcription factor activity. Chromatin accessibility at GR binding sites, crucial to transcription factor action, had previously been shown to be modulated by AP1, an early example of transcription factor cooperativity (John et al., 2011). Further studies showed that chromatin accessibility was a prerequisite for GR binding in up to 95% of loci, and that therefore cell- and tissue-specificity of GR action might arise from predetermined chromatin accessibility patterns (John et al., 2011). Additionally, chromatin areas harboring genes transcriptionally regulated by GR were found to be actively remodeled upon GC treatment, further indicating the importance of the epigenetic state of chromatin for GR action (Grøntved et al., 2013). The same study also found that 83% of GR binding sites in liver are unique, which can be extrapolated to assume a high tissue-specificity of GR action in general. Importantly, in liver, C/EBPβ seems to have a crucial

priming function for GR binding, since 62% of GR-binding sites are co-occupied by C/EBPβ (Grøntved et al., 2013). Negative transcriptional regulation of genes by GR may also depend more on epigenetic regulators than on binding site sequence specificity (Uhlenhaut et al., 2013).

Super-enhancers are large regions in the genome characterized by a high density of transcription factor occupation and high levels of Mediator of RNA polymerase II transcription subunit 1 (MED1). Epigenetic analysis has revealed that omission of dexamethasone from the adipogenic cocktail had a stronger negative impact on recruitment of MED1 to GR binding sites within super-enhancers compared to those outside of super-enhancers. This indicates that cooperation between constituents of super-enhancers is particularly sensitive to GC modulation. In contrast, hotspots activated upon adipogenic induction are less sensitive to omission of GC stimulation than GR binding sites where only a few other factors bind. This might suggest that in hotspot regions, loss or perturbation of GR can be compensated for by cooperative binding of other transcription factors (Siersbæk et al., 2014a). Additionally, at GR binding sites where many factors bind as well, sequence-specifications for binding of GR seem to be more relaxed, while binding sites for C/EBP and AP1 resemble the canonical motifs more strictly, which substantiates the claim to transcription factor cooperativity as crucial to GR-mediated effects (Siersbæk et al., 2014b). All in all, these data indicate that the interplay with other, nearby transcriptional regulators as well as the epigenetic state of chromatin affects regulation of transcription by GR.

GR in adipogenesis

During the recent decades, there was an ongoing scientific discussion of the role of GR in adipogenesis, fueled by the partly contradictory evidence discussed above. Briefly, GC-bound GR regulates C/EBPβ activity via acetylation or interaction with HDAC1 (Park and Ge, 2017; Wiper-Bergeron et al., 2003, 2007). Additionally, it is known that GR binds cooperatively with CEBPβ directly to DNA at transcriptional hotspots in early adipocyte differentiation of 3T3-L1 cells, and together act as transcriptional enhancers (Steger et al., 2010). However, it remained unclear whether GR or the mineralocorticoid receptor prevailed in its impact on adipogenesis, and whether GR had a functional role in adipogenesis *in vivo* (John et al., 2015). Additionally, one should consider the potential role of the two major isoforms, GRα and GRβ, in effects on adipogenesis, since in MEFs it was found that GRβ levels increased during adipogenesis, while the classical GRα protein was maintained at a consistent level throughout differentiation (Hinds et al., 2011).

Two recent publications have shed some more light on the role of GR in adipogenesis: Park and Ge have found that GR-deficient preadipoyctes showed adipogenesis that was not truly impaired, but merely delayed, and lack in differentiation could be compensated for by longer differentiation time. The boost in early adipogenesis that preadipocytes experience upon stimulation with dexamethasone was demonstrated to be fueled by GR-activated expression of C/EBPα, -β, -δ, KLF5, KLF9 and PPARɣ. Activated GR accomplished this via recruitment of the histone H3K27 acetyltransferase CBP, which promoted enhancer-activation of early genes in adipogenesis (Park and Ge, 2017). These

results were demonstrated in murine immortalized brown preadipocytes and the 3T3-L1 cell line, as well as primary murine brown and white preadipocytes. *In vivo*, the same group showed that GR was dispensable for BAT development, while the second recent study showed that adipocyte-specific GR deficiency impairs the transition from a fed to a fasted state, but contradictorily, alleviates obesity and its accompanying metabolic defects in HFD-fed and aged mice (Mueller et al., 2017). These findings underscore the pertinence of GR signaling not only to adipocyte metabolism, but to systemic metabolic health in diverse physiological states.

Obesity

Obesity: scale and consequences of the pandemic

In 2013, the American Medical Association recognized the extent of the negative impact that extreme overweight exerts on the systemic metabolic health of human individuals, as well as the disease burden at the population level, and classified obesity as a disease. The World Health Organisation defines overweight as a body mass index (BMI), defined as kg/m^2, of >25 and obesity as a BMI >30. In 2014, of all adults worldwide over the age of 18, 39% (almost 2 in 5 people) were overweight and 13% were obese. Strikingly, as of 2016, most of the world's population live in countries where overweight and obesity kills more people than underweight (World Health Organisation, 2016). In the European region, estimates dating back to 2008 held that more than 50% of men and women were overweight, and over 20% were obese, leaving a diminutive 30% (one in three) people classified as normal weight or below – however, newer estimates increase these numbers to 30-70% for overweight and 10-30% for obesity. Women are generally affected in higher numbers than men. In high-income countries, almost every second woman was estimated to be insufficiently physically active, which was cited as a potential contributing factor (World Health Organization, 2017).

Reduced to thermodynamics, overweight and obesity are the result of energy intake that chronically exceeds the energy expenditure of an individual. Initial excess is at first stored in subcutaneous fat, as follows from the first law of thermodynamics (law of conservation of total energy in an isolated system). Healthy normal weight individuals have been shown to have adaptable total energy expenditure, which decreased by ~10% upon acute caloric restriction, and increased upon caloric excess (Ravussin et al., 2014). However, when granted access to food ad libitum, humans tend to overeat on average 150% of their daily intake needs, explaining the human propensity to excess lipid accumulation (Ravussin et al., 2014). When storage capacity reaches its limits, lipotoxicity can occur, leading to expansion of visceral fat depots, low-grade inflammation and metabolic dysfunction (Gross et al., 2017; World Health Organization, 2017). Hypoxia, fibrosis and inflammation resulting from the adipocyte overloading then contributes to adipocyte dysfunction, with a detrimental effect on systemic metabolic health (Brestoff and Artis, 2015; Trayhurn, 2014).

Despite the pragmatic underlying principle of energy intake versus energy expenditure, twin pair studies of 8-11 year olds in the UK have shown that there is 77% heritability for BMI and waist circumference (Wardle et al., 2008a). Similar results have been found in

studies of mono- and dizygotic twins growing up together or apart, and studies on adopted children, whose tendency towards obesity was more similar to that of their biological parents than to their adopted ones (Allison et al., 1996; Sørensen et al., 1989). The first SNP locus identified from genome-wide association studies associated with fat mass and obesity was the FTO locus, variants of which have been associated with larger BMI and changes in eating behavior (Cecil et al., 2008; Wardle et al., 2008b). However, loci identified by GWAS typically give only modest effect sizes and explain less than 5% of variability in BMI (Van Der Klaauw and Farooqi, 2015).
These findings indicate that in individuals, the tendency towards weight gain in sustained situations of excess energy intake may depend on genetic predisposition; however, the underlying thermodynamic assumption are nonetheless valid.

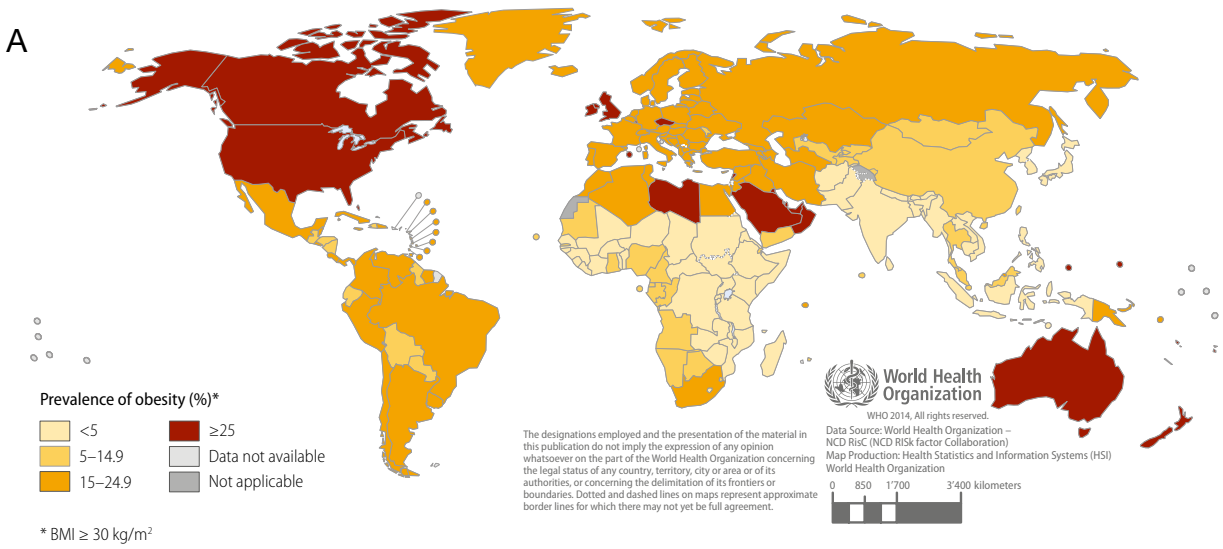

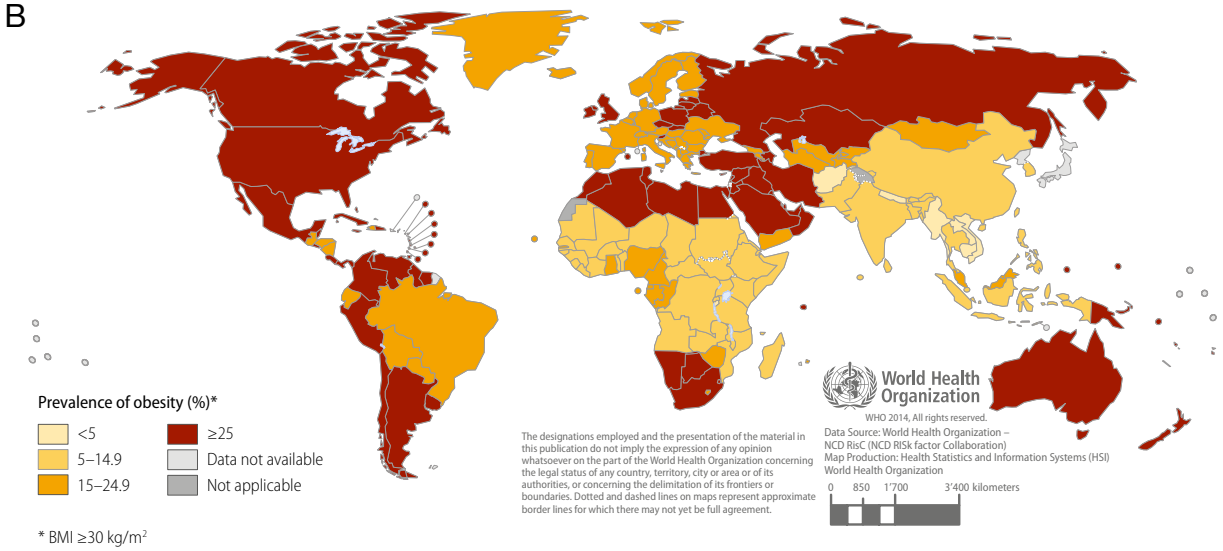

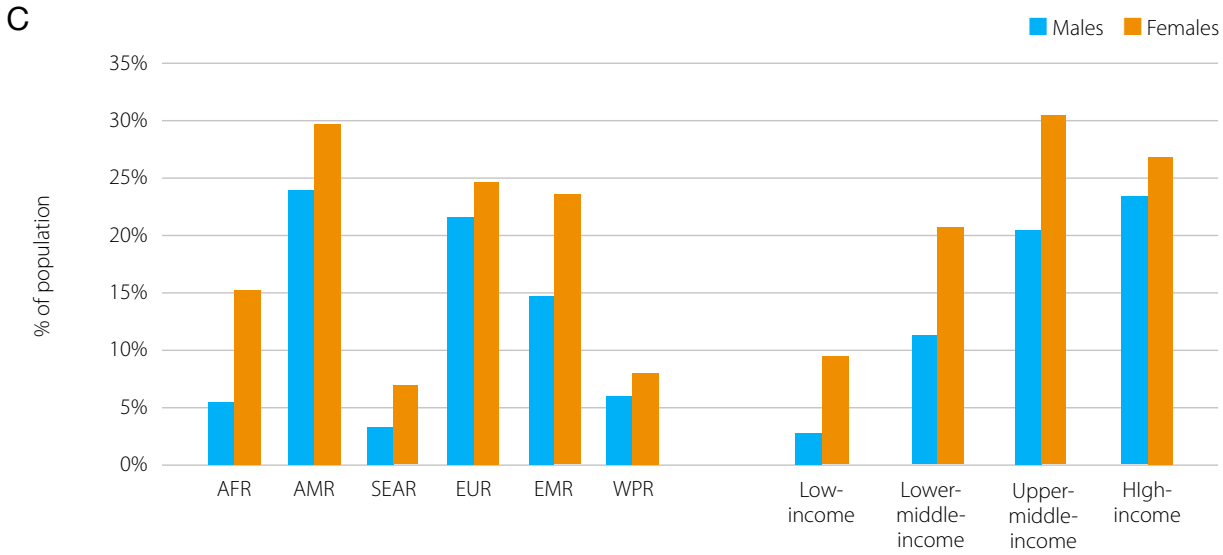

Figure 1: Worldwide prevalence of obesity for men (A) and women (B) aged over 18 in 2014. (C) shows the distribution of obesity among different regions and income strata. Figures obtained from the global status report on non-communicable diseases 2014. (c) WHO, 2014.

PPARɣ, the master regulator of adipogenesis, as well as its family members PPARα, with a pronounced role in brown adipose tissue, and PPARβ, have been targeted for therapeutic approaches. However, due to either limited potency or adverse side effects of individual compounds, no PPAR-targeting therapy has been established yet (Gross et al., 2017).

As of 2014, the only drug currently approved for long-term use in Europe and the US is Orlistat, a compound reducing energy intake by limiting intestinal lipid absorption by targeting pancreatic lipase. Centrally acting drugs targeting cannabinoid signaling, noradrenergic and serotonin signaling produced moderate effects offset by unspecific neural side effects. Hopes for the future lie in the development of gene-targeted personalized medicine, as well as cell-based biosynthetic gene circuits that combine sensing of metabolic parameters and levels of metabolites with a reaction that self-sufficiently restores metabolite homeostasis (Van Der Klaauw and Farooqi, 2015). An example tested in mice is a lipid sensor which induces dose-dependent expression of the appetite-suppressing peptide pramlintide (Rössger et al., 2013).

Several types of bariatric surgery have been employed as successful interventions in obesity and T2DM: Roux-en-Y gastric bypass, adjustable gastric band, duodenal switch and gastric sleeve gastrectomy, the currently most performed bariatric surgery worldwide. For reasons that require further investigation, bariatric surgery is the only intervention that yields short-term as well as long-term weight loss and improvement of obesity comorbidities, such as hypertension, sleep apnea and T2DM. However, to date mortality is still 3 in 1000 patients, and bariatric surgery is only indicated for severe obesity (Nguyen and Varela, 2016).

miRNAs, especially ones targeted to increase brown fat activity or facilitate browning of white adipose tissue, provide another potential line of offense in the battle against obesity and diabetes (Scheideler et al., 2013). However, limitations of this approach are discussed later in the text under “miRNAs as therapeutics”, and to date, not a single miRNA based approach against diabetes or obesity has reached the clinical trial stage.

As evidenced by the abundance of approaches targeting fat in the fight against obesity as described above, excessive weight gain and its negative side effects on systemic metabolic health have brought into focus investigations regarding regulators of adipose tissue metabolism and development.

MicroRNAs

miRNA biogenesis and function in mammalian cells

Adipose tissue, and thereby, overweight, obesity and metabolic disturbances have been shown to be controlled not only by protein-coding genes, but also by a type of regulator that has gained notoriety in mammals only in recent years: non-coding RNAs, and in particular, microRNAs (miRNAs). miRNAs are small, non-coding, nucleic acid regulators of gene expression that derive their name from their short length of approx. 22 nt (Lagos-quintana et al., 2001; Lau, Nelson C.; Lim, Lee P.; Weinstein, Earl G.; Bartel, 2001; Lee et al., 2001). miRNA genes can be located within a host gene (intragenic/intronic) or interspersed as stand-alone genes (intergenic) with their own promoters (Inui et al., 2010). Transcription of a miRNA gene by RNA polymerase II or III creates a primary transcript of up to several kilobases in length, called primary miRNA, or pri-miRNA. This primary transcript is then processed by an enzyme called Drosha in complex with various other proteins, such as DGCR8 and TRBP, yielding a ~70 nt hairpin RNA construct termed precursor miRNA, or "pre-miRNA" (Han et al., 2006). Some pre-miRNAs called "mirtrons", however, bypass this processing step since they are directly produced by splicing from short introns (Krol et al., 2010). The pre-miRNA is exported from the nucleus to the cytoplasm to be finally processed by the Dicer in a facultative complex with TRBP, which cuts the hairpin to yield a duplex of complementary, linearized, mature miRNAs (Jinek and Doudna, 2009). Dicer cleaves close to the hairpin loop, about 22 nt away from the base of the stem, with its major unannotated region acting as a molecular ruler (Yates et al., 2013). Members of the Argonaute protein family, in human cells AGO1-4, support Dicer and are physically associated with the mature miRNA (Jinek and Doudna, 2009). In contrast, some miRNAs like e.g. pre-miR-451 are cleaved by AGO2 but processed independently of Dicer (Krol et al., 2010). This endonuclease activity is, among the Argonaute proteins, unique to AGO2 and can lead to "slicing", direct miRNA-guided mRNA cleavage (Lingel and Izaurralde, 2004). The nomenclature of the mature miRNAs reflects on which end of the hairpin (3' vs. 5') they originate on, with the addition "-3p" referring to … and "-5p" to the other. It is currently assumed that only one of these pairs, called the guide strand, carries out most of the regulatory functions, as it is preferentially incorporated into the miRNA-induced silencing complex (miRISC), while the remaining "passenger strand" is degraded. Generally, the strand that has the least stably basepaired 5' end(Krol et al., 2010) becomes the guide strand.

MiRNA maturation can be regulated at several points, the two cleavage steps being the most obvious occasions. Proteins like Lin28B and hnRNPA1 are known to modulate nuclear processing of pri-miRNAs by Drosha. Dicer processing can be regulated by 3' mono- or polyuridylylation of pe-miRNAs, which can affect maturation efficiency or lead to creation of miRNA isoforms with differing seed regions and target specificities (isomiRs) (Yates et al., 2013). Mature miRNAs sometimes undergo shortening at their 3' end, but while recently the exonuclease Nibbler has been described to do this in *Drosophila* (Han et al., 2011; Liu et al., 2011a), in mammals the responsible exonuclease has yet to be identified (Juvvuna et al., 2012).

The mature miRNA incorporated in the miRISC leads the associated protein complex to target mRNAs by basepairing to their miRNA recognition element (MRE), which is

commonly located within the 3'UTR of target genes (Bartel, 2009). Essential for the recognition of the target MRE are bases 2–7 starting at the miRNA's 5' end, which has been named the miRNA "seed region". Watson-Crick basepairing of the seed region to the respective sequence in the MRE, aptly named "seed match", can be supplemented by further pairing with the 3' region of the miRNA, and sometimes even compensate for imperfect pairing in the seed region. Moreover, besides the canonical 2–7 "7mer" seed match, there are variation on this theme that also vary in miRNA efficacy. 8mer sites, which consist of an A at the first position, the 2–7 nt seed match plus an additional matching basepair at position 8, are more efficacious than 7mer sites, while 6mer matches reduce miRNA effect to only a bit above no match at all. Even the canonical 7mer sites are further distinguished into 7mer-m8, which feature the additional matched base at position 8 (more efficacious) and 7mer-A1 sites, which have no match at position 8 but offer an A at position 1 (less efficacious). Reviewed in (Bartel, 2009) Even though 6mer sites typically mediate only limited repression (Friedman et al 2008 most mammalian) and are considered "marginal sites", there is evidence that some of these still confer functional miRNA action. One example of this is a so-called offset 6mer site in the LIN28 3'UTR, which receives the prefix offset because it basepairs from position 3 to position 8, instead of the common position 2–7 for 6mer seed matches. Reviewed in (Bartel, 2009) It follows that despite the high dependability of miRNA target prediction algorithms, which give a direction to the search for miRNA effectors, we must still rely on functional evaluation *in vitro* in order to uncover miRNAs relevant to human physiology and disease.

miRNAs in pathophysiology

Deregulation of miRNAs has been implicated in various diseases, e.g. Alzheimer's (Wang et al., 2008c), myocardial diseases (Carè et al., 2007; Dangwal and Thum, 2013; Thum et al., 2008), many types of cancer (Chen et al., 2014; Ventura and Jacks, 2009; Zeng et al., 2014), and also obesity (reviewed in Hilton et al., 2013; Klöting et al., 2009; Xie et al., 2009). Most of these publications in the field of obesity research and miRNAs focus on the influence of miRNAs on fat cell development or metabolic phenotype in mice and/or humans by determining differentially regulated miRNAs, and how their specific targets mediate their effect (Karbiener et al., 2014; Kornfeld et al., 2013). Other studies aim to find interesting players by correlational analysis, like Klöting and colleagues, who showed that miRNAs expressed in human adipose tissues correlate with metabolic parameters of diabetes and obesity (Klöting et al., 2009).

The presence of extracellular miRNAs in human serum, plasma, saliva and amniotic fluid is another aspect of the relevance of these small RNAs to disease. Levels of several circulating miRNAs have been correlated to disease states, such as presence of tumors and early detection of cancer, cardiovascular disease, and obesity and diabetes **(see below)** (Cortez et al., 2011; Di Stefano et al., 2011; Tijsen et al., 2010). An example particularly relevant to this thesis is that miR-29a levels have been shown to be elevated in serum and urine of T1DM and T2DM patients (Dai et al., 2016; Dooley et al., 2016; Kong et al., 2011; Ru et al., 2015), which is in line with findings associating this miRNA with diabetes in rats and insulin resistance in murine cell lines (He et al., 2007a).

In addition to dysregulation of particular miRNAs in disease states, alterations in miRNA recognition elements (MREs) can be responsible for miRNA-mediated pathophysiological phenotypes. Since the number of miRNA targets exceeds the actual number of known miRNAs, it follows that the number of pathogenic mutations in miRNA genes should logically be outstripped by the number of functional alterations in target. About 20.000 SNPs in target MREs have been catalogued, and these target site variations have been linked to complex genetic phenotypes (Mendell and Olson, 2012). One of the starkest examples is a variant of the Myostatin (MSTN) 3'UTR, which is associated with muscle mass in sheep (Clop et al., 2006). Several MRE polymorphisms have been linked to breast cancer, hypertension, asthma and Parkinson's disease (Sethupathy and Collins, 2008). A SNP in the seed match for let-7 in the KRAS 3'UTR has been associated with non-small-cell lung cancer, ovarian cancer risk, and survival in oral cancer patients (Mendell and Olson, 2012).

miRNAs as therapeutics

There is great interest in treating various maladies with miRNA mimics or antagonists of some type (Bader, 2012; Janssen et al., 2013; van Rooij et al., 2012). As for metabolic diseases, our group has recently filed a European patent application that was further extended to all PCT countries for the clinical use of several microRNA candidates, including miR-26a (Scheideler et al., 2013).

Therapeutic approaches using miRNAs and inhibitors are very attractive since miRNA dysregulation in healthy tissues is tolerated well, while still having an impact on cells in stress or pathological conditions (Mendell and Olson, 2012). This comparatively large therapeutic window can be exploited, at least theoretically, in several ways: one can lower endogenous miRNA levels or their effects by applying LNA-modified antisense nucleotides, which can be delivered intravenously with little toxicity, as is being explored for miR-122 against HCV infection (Lanford et al., 2010). Conversely, miRNA levels can be raised by delivering miRNA mimics in lipid nanoparticle duplexes, or using adeno-associated viruses (AAVs). However, for all of these variants, tissue-specific targeting of miRNAs can still presents experimental challenges (Mendell and Olson, 2012).

Nevertheless, systemic delivery of miR-33 to obese and insulin resistant African green monkeys was rewarded with promising results, since its effects were concentrated on live, and have been reported to successfully increase circulating HDL cholesterol in obese and insulin resistant African green monkeys without major adverse effects (Rayner et al., 2011).

Regarding the applicability of miRNA therapy in humans, as of 2014, antimiRs against miR-122 against HCV were in Clinical Phase I and II trials by two different companies, while miR-34 mimics targeting unresectable primary liver cancer had reached Clinical Phase I (Rooij and Kauppinen, 2014). However, Mirna Therapeutics announced to have halted phase 1 clinical trials of MRX34 in September 2016 due to adverse immune-related effects (Beg et al., 2016). As for miR-122, the antisense medication Miravirsen by the previous Santaris Pharma, acquired by Roche, was being tested in a clinical long-term extension study that ended in November 2016, but development was ceased as published in the same year (van der Ree et al., 2016). Continued development on a chemically different variant of miR-122 antagonist seems to be in process (Van Der Ree et al., 2015).

miRNAs as regulators of complex physiological balances

Loss of miRNA function usually does not strongly affect the development of an organism (Mendell and Olson, 2012), even though discovery of the first miRNA, *lin-4*, in *C. elegans* is an iconic counter example (Lee et al., 1993). The diminutive effect of the loss of single miRNAs in development might be attributed to the fact that a single miRNA targets many mRNAs, which dilutes its potency, and that miRNAs have a rather subtle effect of typically a 2-fold change in target protein levels (Mendell and Olson, 2012). However, this does not apply to disturbances of general miRNA processing, since the synergistic effect of miRNAs regulating complex, interconnected systems is illustrated by the profound effects of Dicer KO mice (Bernstein et al., 2003). While miRNAs do not seem to have a strong impact on tissues formation, miRNAs have been shown to strongly affect the response of mature tissues to pathophysiological and stress situations (Mendell and Olson, 2012). as well the effect of adipose tissue-specific Dicer knockout on BAT development

Examples of miRNAs that show little baseline effect on the phenotype, but whose deletion gives a pronounced effect in response to stress conditions are miR-208a, which allows cardiac remodeling in response to stress (van Rooij et al., 2007), the miR-143/145 cluster, which affects reaction to vascular injury (Xin et al., 2009) and miR-375, which allows for pancreatic β-mass expansion in states of insulin resistance (Poy et al., 2009).

A diverse array of the way a miRNA might act in stress situations is reviewed by Mendell and Olson, 2012. The role of miRs as regulators of the cellular stress response was categorized in different functions: miRNAs might a) mediate a stress response, b) modulate the stress response by titrating a critical component of the signaling pathway, c) prevent hyperactivation of a pathway under stress conditions via a negative feedback loop, d) drive phenotypic switching under stress conditions by driving the signaling pathway it is activated by (positive feedback), or e) buffer signal variation to offset transient high level activation of pathways in stress states (Mendell and Olson, 2012). All of these variations have been described in pathophysiological circumstances, e.g. in the context of tumorigenesis in sequence corresponding to the categorization made above for a) miR-34 and the miR-17-92 cluster, which act as signal transducers for the oncogenic p53 and Myc pathways, (O'Donnell et al., 2005), b) miR-16, which simultaneously downregulates multiple cell cycle regulators to prevent cell cycle progression (Linsley et al., 2007), c) miR-146a which inhibits the pathway that induces it in a negative feedback loop (Taganov et al., 2006), d) let-7, whose repression by NF-kB induced Lin-28b increases IL-6 levels, which in turn activate NF-kB signaling even more, while low let-7 levels additionally derepress Myc, leading to stable transformation (Iliopoulos et al., 2010), and e) miR-26, which represses both pro- and anti-tumorigenic targets (Ji et al., 2009; Kota et al., 2009).

miRNAs in obesity, diabetes and adipogenesis

The necessity of miRNAs for adipocyte differentiation was demonstrated in 3T3-L1 preadipocytes and human BM-MSCs (Oskowitz et al., 2008; Wang et al., 2008a), in which knockdown of Drosha, and Dicer, respectively, impaired adipogenesis. Expression of non-functional dicer in MEFs and mouse primary adipocytes similarly impaired adipogenesis (Mudhasani et al., 2010). In line with these findings, abolishment of Dicer

via the aP2-Cre transgene lead to massive developmental defects in WAT formation, as well as impairment of BAT thermogenic gene expression of UCP1, PGC1A and COX8B (Mudhasani et al., 2011). These results argue for a crucial role of miRNAs in adipocyte development.

The first screen showing differential expression of miRNAs during 3T3-L1 adipocyte differentiation (Kajimoto et al., 2006) was followed by innumerable *in vitro* studies demonstrating the role of miRNAs in murine adipogenesis, an overview of which is given here. Overexpression of the miR-17-92 cluster promoted adipogenesis via targeting of the cell cycle regulator RB2/p130 (Wang et al., 2008b). The BMP-2-induced miR-24 and miR-31 have opposing functions on the differentiation of mesenchymal stem cells into adipocytes, with the first one enhancing it through an unknown mechanism, and the latter impairing it by targeting C/EBPα (Sun et al., 2009a). Let-7 negatively affected the same process, probably via targeting HMGA2, a transcription factor that was known to control cellular growth and proliferation, and revealed later to promote adipogenesis by activating C/EBPβ (Sun et al., 2009b; Xi et al., 2016). miR-448 attenuated adipogenesis by targeting KLF5 (Kinoshita et al., 2010), a key regulator of adipogenesis (Oishi et al., 2005). miR-27a and –b were down-regulated during adipogenesis and inhibited differentiation of both 3T3-L1 and OP9 cell lines (Lin et al., 2009). miR-204 and miR-211 control differentiation of murine mesenchymal stem cells by targeting Runx2, a transcription factor that promotes osteogenesis over adipogenesis by inhibiting PPARɣ (Wu et al., 2011). miR-375 was described to be upregulated during 3T3-L1 differentiation and repress adipogenesis, possibly by indirectly affecting ERK1/2 phosphorylation, whose activity is known to enhance PPARɣ and C/EBPα expression (Ling et al., 2011).

In human *in vitro* systems, miRNA expression profiling of human preadipocytes during adipogenesis revealed differentially expressed candidates, and follow-up experiments made miR-143 the first miRNA with an experimentally documented function in human adipocyte differentiation. Inhibition of miR-143 impairs human adipocyte differentiation, possibly by targeting ERK5, which is drawn into question since it was not validated by reporter assays, and considering that a study in 3T3-L1 cells revealed inhibition of adipogenesis upon ERK5 silencing (Esau et al., 2004; Sharma and Goalstone, 2005). Thus, the actual target of miR143 in adipogenesis still awaits discovery.
miR-27b was identified in 2009 as the first anti-adipogenic miRNA in human adipocyte differentiation *in vitro*, directly targeting PPARɣ as confirmed by Luciferase reporter assays (Karbiener et al., 2009) which was complemented by a subsequent study for the murine counterpart (Jeong Kim et al., 2009). Briefly, miR-27b had been found to be downregulated during adipogenesis, and impaired adipocyte accumulation by blunting PPARɣ and, indirectly, CEBPβ expression.
Further studies showed that miR-21 overexpression decreased human adipocyte differentiation of adipose-derived MSCs by targeting TGFBR2 and thus inhibiting the anti-adipogenic TGFβ signaling, while miR-130a and –b were found to be downregulated during adipogenesis and act anti-adipogenically by targeting PPARɣ, the master regulator of adipogenesis (Jeong Kim et al., 2009; Lee et al., 2011). miR-335 was

described to decrease both adipogenic and osteogenic differentiation of human bone marrow-derived MSCs as well as impair proliferation, partially via targeting of Runx2 (Tome et al., 2011).

In summary, in recent years miRNAs have clearly emerged, alongside protein-coding genes, as important regulators of adipose tissue health and physiology, impacting not only fat cell expansion but also systemic metabolism.

Aims of the study

miRNAs have been demonstrated to be potent players in the regulation of metabolism, as well as have great potential to be exploited for therapeutic purposes. Our own preliminary studies had found miR-29a to be differentially regulated in the adipogenesis of human cells. The miR-29 family has been described previously to be implicated in diabetes, insulin resistance and related comorbidities, making it a highly interesting candidate for further investigation (Dai et al., 2016; Dooley et al., 2016; He et al., 2007b; Kong et al., 2011; Peng et al., 2013; Zampetaki et al., 2010). However, none of the studies published have examined the effect of miR-29 in the context of adipocyte differentiation, which we know can contribute greatly to systemic metabolic health and insulin sensitivity. It is yet unknown if, and how, i.e. via which target, miR-29 can influence lipid accumulation in adipocytes. Additionally, most of the studies examining miR-29 in the context of metabolism and diabetes utilize murine models, leaving uncertainty as to whether their findings hold true in human physiology. Biomarker studies make it clear that miR-29 could be an interesting predictor for factors associated with T1DM and T2DM, however, we only know that miR-29 seems to be regulated under those physiological circumstances, while the mechanisms of regulators upstream of miR-29 have yet to be elucidated.

In this study, we aim to investigate the effects of the miR-29 family on adipocyte differentiation of human cells, utilizing the hMADS cell model for in vitro studies. By identifying the direct miRNA binding target that mediates a potential effect on adipogenesis, we want to gain insight in the molecular players in human adipocyte differentiation involved. Additionally, we will investigate potential regulators of miR-29 to identify upstream pathways that miRNA's effect depends on, in order to gain an understanding of the physiological and pathophysiological circumstances miR-29 plays a role in. To expand this understanding, we will analyze prevalence of the miR-29 in human samples in the context of obesity and diabetes. From these investigations we hope to increase our understanding of how miR-29 could affect systemic metabolism via its role in the adipose tissue, and potentially be relevant in combatting the rising pandemics of obesity and diabetes.

Results

miR-29a as a player in human adipocyte differentiation

Expression profiling of hMADS cells during adipocyte differentiation had revealed that mRNAs that harbored miRNA seed matches were significantly over-represented in the differentially expressed transcripts (Scheideler et al., 2008). As this insinuates a role for miRNAs in regulating adipogenesis, a microarray expression profiling of miRNAs differentially regulated during hMADS cell adipogenesis was generated prior to the start of this thesis project. Differential expression analysis had exposed hsa-miR-29a-3p (henceforth shortened to miR-29a) among the 38 identified miRNAs as one of the most strongly and consistently downregulated candidates (Figure 2).

MiR-29a was deemed particularly interesting since it had been published to be upregulated in muscle of diabetic rats and induce insulin resistance in 3T3-L1 adipocytes (He et al., 2007a). Later studies added increased levels of miR-29a in the serum and urine of T1DM and T2DM patients to our knowledge of potential metabolic effects of miR-29a (Dai et al., 2016; Kong et al., 2011; Peng et al., 2013). A knockout mouse model presented with an insulin secretion defect traced to the pancreas, but whole body improved insulin sensitivity (Dooley et al., 2016).

However, the role of miR-29a in adipose tissue and adipocytes, especially in humans, had not been explored prior to the start of this thesis. Since adipose tissue is one of the major metabolic organs, next to liver and muscle, and considering that human adults turn over 10% of their fat cells each year (Arner et al., 2011), we aimed to evaluate the effect of miR-29a on adipocyte differentiation.

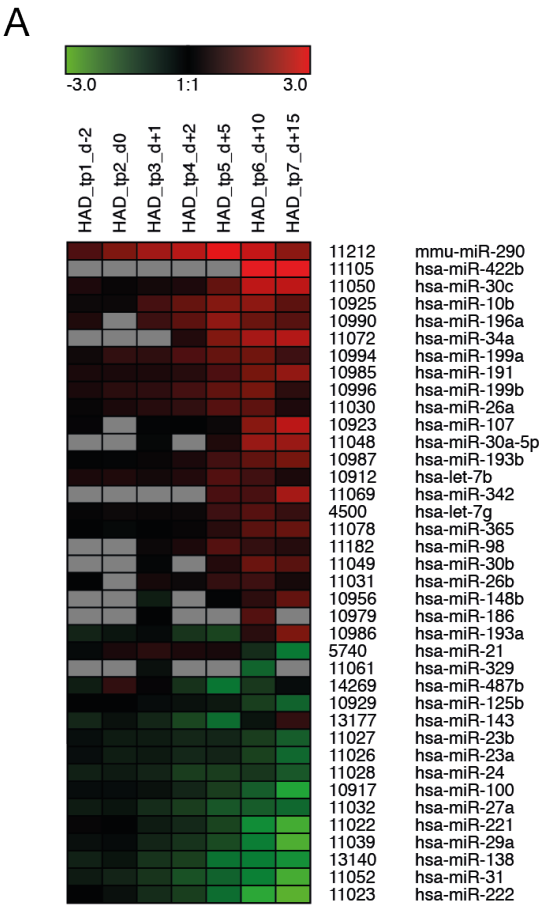

Figure 2: miRNA differential expression analysis in hMADS subjected to adipocyte differentiation. hMADS-2 cells were stimulated at d0 to undergo adipocyte differentiation. RNA was extracted at indicated timepoints (d-2, d0, d1, d2, d5, d10, d15) and analyzed using an in-house miRNA gene expression microarray. Differentially expressed miRNAs were filtered for candidates that were detected at minimum 2 timepoints and sorted by relative expression value, using a cut-off of a 2-fold differential expression fold change. Grey fields designate missing values due to quality control restrictions of the raw data.

miR-29a is downregulated during human adipogenesis

The miR-29 family consists of 3 family members, namely a, b, and c, which share the same seed motif but vary slightly in their full sequence. The downregulation of miR-29a observed in the microarray gene expression study (Figure 2) were confirmed for selected time points by RT-qPCR (Figure 3 B). Additionally, RT-qPCR showed that miR-29b showed a similar expression profile to miR-29a but without reaching statistical significance, while miR-29c expression was more homogeneous throughout the course of adipogenesis.

The family's mature miRNAs result from processing of two distinct transcripts encoded on different chromosomes, as shown in Figure 3 A. Since miR-29b showed a regulation profile similar to miR-29a but is encoded on two separate primary transcripts, we assessed expression of the two primary miRNA transcripts in the same samples (Figure 3 D). Curiously, the primary transcript henceforth named pri-miR-29ab (giving rise to miR-29a and miR-29b-1) was downregulated, thus tracing the expression profile of the mature miR-29a, while pri-miR-29bc (encoding miR-29b-2 and miR-29c) even trended upwards during adipogenesis, which is more reflective of miR-29c expression levels.

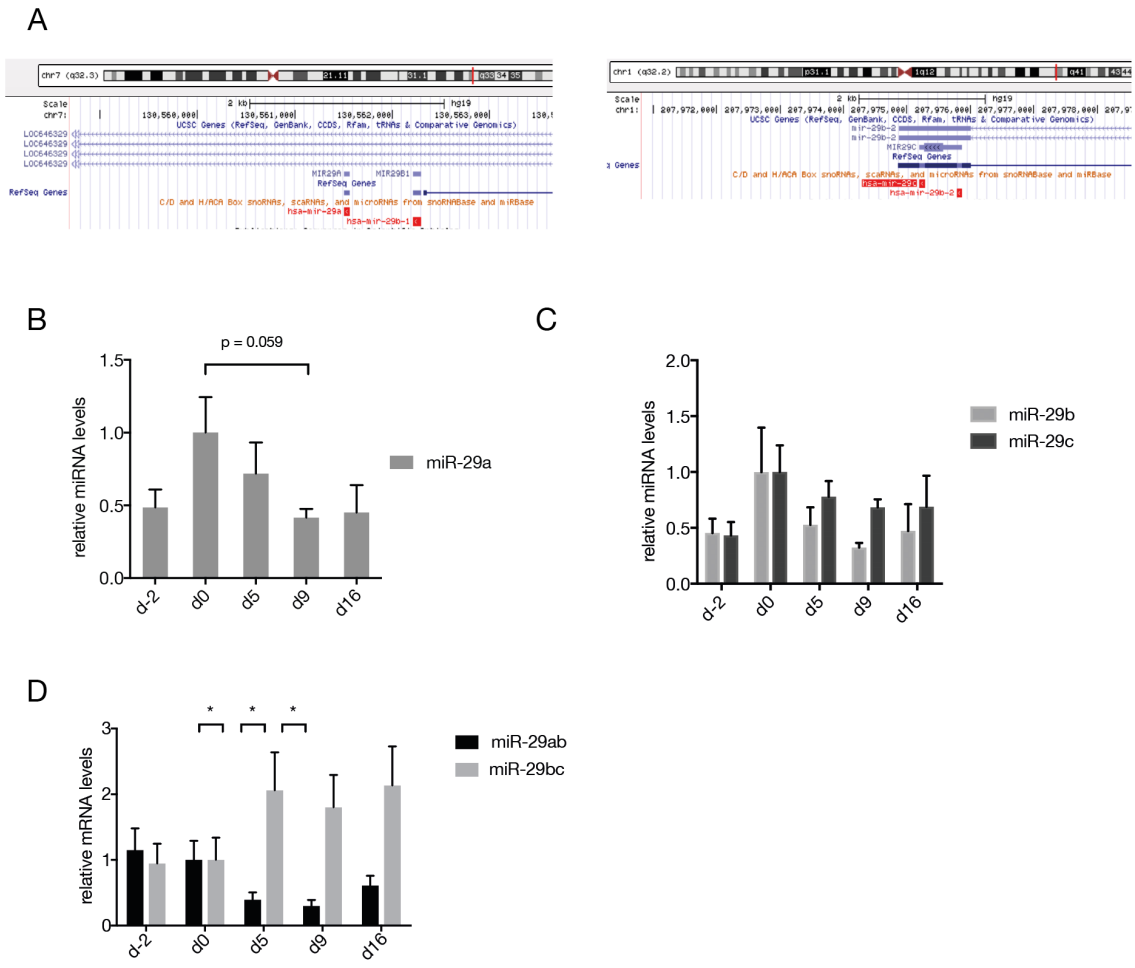

Figure 3: Expression analysis of mir-29 family members during adipogenesis (A) miR-29 family members are transcribed from two distinct loci in the human genome, located on chromosome 7 and chromosome 2. Screenshots are taken from the UCSC Genome Browser. B) miR-29a is downregulated during hMADS adipogenesis, in line with results from the previous microarray gene expression screen. miRNA levels were quantified by RT-qPCR normalized to the housekeeping gene and to d0. n=4 (C) Quantification of miR-29b and –c expression patterns throughout adipogenesis. miRNA levels were quantified by RT-qPCR normalized to the housekeeping gene and to d0. n=3-4 (D) Quantification of primary miRNA transcript (pri-miRNA) levels during adipogenesis. mRNA levels were quantified by RT-qPCR normalized to the housekeeping gene and to d0. n=4 Unless otherwise indicated, replicates are biological and data are mean ± SEM. * $P < 0.05$, ** $p < 0.01$, *** $p < 0.001$

miR-29a inhibits human adipogenesis

In order to discover the function of miR-29a in adipogenesis, we artificially increased its abundance by transfecting hMADS cells with miR-29a mimics in a gain of function experiment (Figure 4 A). This resulted in marked attenuation of adipocyte differentiation: Triglyceride accumulation was decreased as measured visually by Oil Red O staining as well as quantitatively using an assay kit (Figure 4 B, C). Expression of adipogenic marker genes was significantly reduced for 6 out of 8 genes analyzed (Figure 4 D).
Cells transfected with miR-29b and –c mimics reacted similarly, but to a much lesser extent compared to miR-29a-transfected counterparts (Figure 5).

Inhibition of miR-29 enhances adipogenesis

Complementing the study by a loss-of-function experiment, we transfected hMADS cells with LNA-modified power antisense oligonucleotides against miR-29a (pASO-29a), as

well as a miR-29 family inhibitor (pASO-29FI). Since a decrease in miR-29 family members could not be measured reliably via RT-qPCR, mRNA expression levels of known target genes that had been validated by Luciferase reporter assays in the literature were chosen as a readout for successful miR-29 inhibition (Figure 4 E). Transfection with pASO-29 lead to slightly increased triglyceride accumulation as measured by Oil Red O staining as well as a triglyceride assay kit (Figure 4 F, G). Adipogenic marker genes slightly trended upwards without reaching statistical significance (Figure 4 H).

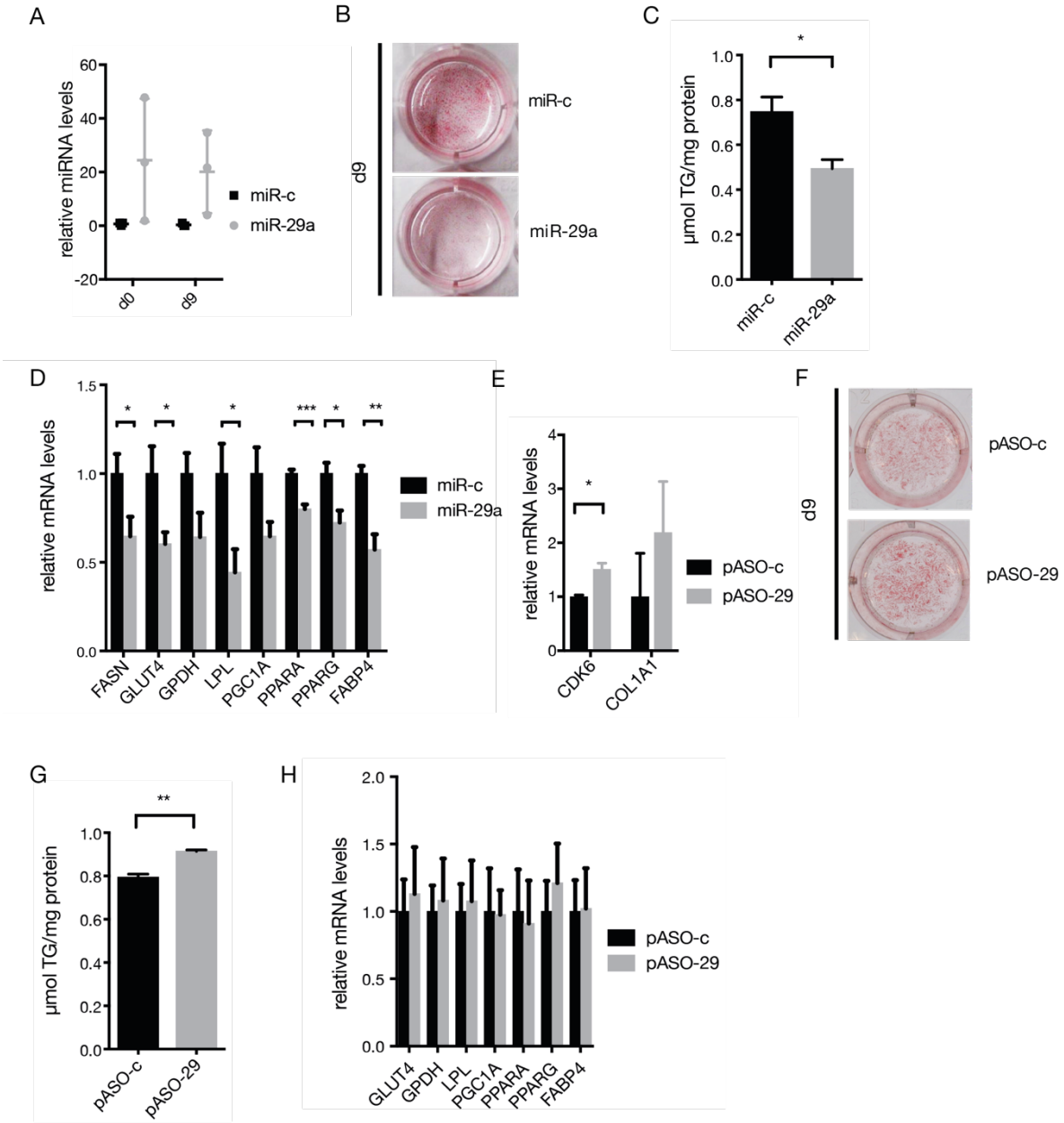

Figure 4: Modulation of miR-29a levels affects hMADS adipogenesis. A-D) Gain-of-function experiments were conducted by transfection of hMADS cells with miR-29a or control mimics (miR-c) at confluence. 48 hours later, cells were stimulated to undergo adipocyte differentiation. A) The increase in miRNA levels was quantified by RT-qPCR normalized to the housekeeping gene and the miR-c control. n=3 B) Oil-Red O staining of cells treated as in A. One representative out of at least 3 comparable experiments with similar results is shown. C) TG accumulation of cells treated as in A. n=3 D) mRNA levels of adipogenic marker genes of cells treated as in A. Data are normalized to the housekeeping gene as well as to miR-c, the control mimic. n = 6-7 E-H) Loss-of-function experiments were conducted by transfection of hMADS cells at confluence with LNA-modified power antisense oligo inhibitors against miR-29

(pASO-29) or a non-targeting control (pASO-c). E) mRNA levels of miR-29 target genes of cells transfected with paso-c or paso-. n=2-3 F) Oil-Red O staining of cells transfected either with paso-c or -mir29. One representative out of at least 3 comparable experiments with similar results is shown. G) TG accumulation of cells normalized to protein amount. n=3 H) mRNA levels of adipogenic marker genes were quantified using RT-qPCR. Data are normalized to the housekeeping gene as well as to miR-c, the control mimic. n=4 Unless otherwise indicated, replicates are biological and data are mean ± SEM. * P < 0.05, ** p < 0.01, *** p < 0.001

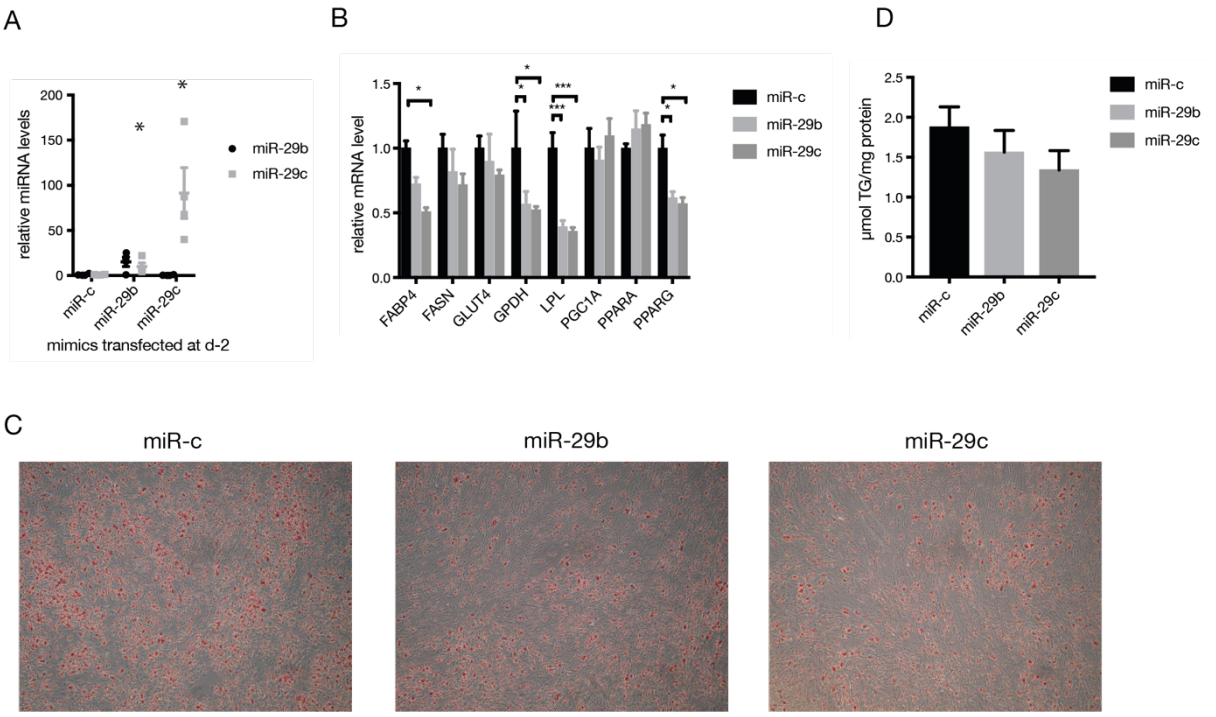

Figure 5: miR-29b and -c decrease triglyceride accumulation to a lesser extent than miR-29a. A-D) Gain-of-function experiments were conducted by transfection of hMADS cells with miR-29b or -c or control mimics (miR-c) at confluence. 48 hours later, cells were stimulated to undergo adipocyte differentiation. A) miRNA expression levels in cells transfected with miR-29b or –c mimics or miR-c controls 48 hours after transfection, quantified by RT-qPCR normalized to the housekeeping gene and the miR-c control. n=3 B) mRNA levels of adipogenic marker genes in cells transfected as in A on d9. Data are normalized to the housekeeping gene as well as to miR-c, the control mimic. n = 6-7 C) Oil-Red O staining of cells as in B. One representative out of at least 3 experiments is shown. D) TG accumulation was quantified and normalized to protein amount. n=3 Unless otherwise indicated, replicates are biological and data are mean ± SEM. * P < 0.05, ** p < 0.01, *** p < 0.001

Identification of direct miR-29a targets

Since miRNAs effect phenotypical changes by silencing one or more mRNA targets, we next screened for potential direct miR-29a targets in the hMADS cell system by transfecting cells with miR-29a mimics at d-2, harvesting RNA 48h later and performing a microarray analysis to analyze mRNA gene expression. Since miRNAs are known to inhibit their direct targets, we consecutively sorted the resulting list by the extent of downregulation, considering only those mRNAs that had been detected in at least 3 out of 4 biological replicates. These candidates were then further screened for presence and number of different types of miR-29a seed matches (including the canonical 7mer-A1 and 7mer-m8 seed matches, plus 6mer and 6mer offset seed matches), potential for being a strong regulator owing to the type of protein (e.g. transcription factors) and published literature that pointed at a role in the broad area of adipose tissue, adipogenesis, metabolism and diabetes.

The resulting list had been narrowed down to 8 candidates shown in Figure 6 A, including the number of predictions out of 10 online target prediction tools and the amount and type of seed matches for miR-29a. For these candidates, we designed and

cloned Luciferase assay vectors to investigate direct binding of the miR-29a to the seed match harboring regions (in this case, 3'UTRs). These vectors were then co-transfected with miR-29a mimics into HEK293T cells. For 5 out of 8 candidates, we found that the Luciferase signal in co-transfected cells compared to vector-only controls was significantly decreased, indicating (potentially direct) regulation (Figure 6 B and C). This reduction in Luciferase signal was observed for miR-29a co-transfection with reporter vectors harboring the 3'UTRs of S100A16, XBP1, SIAH2 and NR3C1.
Consequently, in order to assess whether these direct targets of miR-29a have a functional role in adipogenesis, we transfected hMADS cells with siRNAs against these target mRNAs. All of the transcript variants that harbored miR-29a seed matches were targeted by the employed siRNA mixtures. After transfection, adipogenesis was allowed to proceed until day 14 in order to maximize potential emerging differences between the silenced targets and the controls. Out of the 4 remaining candidates, only silencing of one candidate mimicked miR-29a transfection effects: NR3C1, the gene encoding glucocorticoid receptor (Figure 6 D)[1].

NR3C1, the glucocorticoid receptor gene, is a direct target of miR-29a that affects adipogenesis

Confirming the visible phenotype in the Oil Red O staining (Figure 6 D), hMADS transfected with siRNAs against NR3C1 accumulated less triglycerides during adipogenesis (Figure 6 E). In line with these results, adipogenic marker genes were significantly reduced (Figure 6 F), phenocopying the effect of transfection with miR-29a mimics. Additionally, we could confirm the specificity of miR-29a binding, since direct binding of the mRNA to the NR3C1 3'UTR could be abolished by mutating the miR-29a seed matches (Figure 6 G). According to these results, the second seed match between the start of the 3'UTR and the start codon seems to be essential for miRNA function, as mutation of this single seed match reconstitutes the Luciferase signal of miR-29a transfected cells as much as mutation of all three seed matches.

Overexpressing the NR3C1 CDS partially rescues impaired TG accumulation by miR-29a

Silencing of NR3C1 in hMADS cells before adipocyte differentiation impairs TG accumulation and adipogenesis, which is phenotypically similar to transfection with miR-29a mimics. Together with the evidence that miR-29a directly binds to the NR3C1 3'UTR *in vitro*, this strongly indicates that NR3C1, the glucocorticoid receptor gene, mediates the effects of miR-29a on adipocyte differentiation. However, in order to bolster this claim, we attempted to rescue the miR-29a gain-of-function phenotype by transducing hMADS cells with lentiviral particles carrying the NR3C1 coding sequence (CDS), thus lacking the 3'UTR necessary for miR-29a binding. Preliminary results are shown in Figure 7. TG accumulation, as visualized by Oil-Red O staining, could be partially rescued upon forced NR3C1 CDS expression by transduction 1 or 2 days before transfection with miR-29a mimics. However, these results will need to be replicated to ensure their robustness.

[1] Silencing of MEST, another direct target of miR-29a, yielded the complete opposite phenotype. See p. 46, "MEST in human vs mouse"

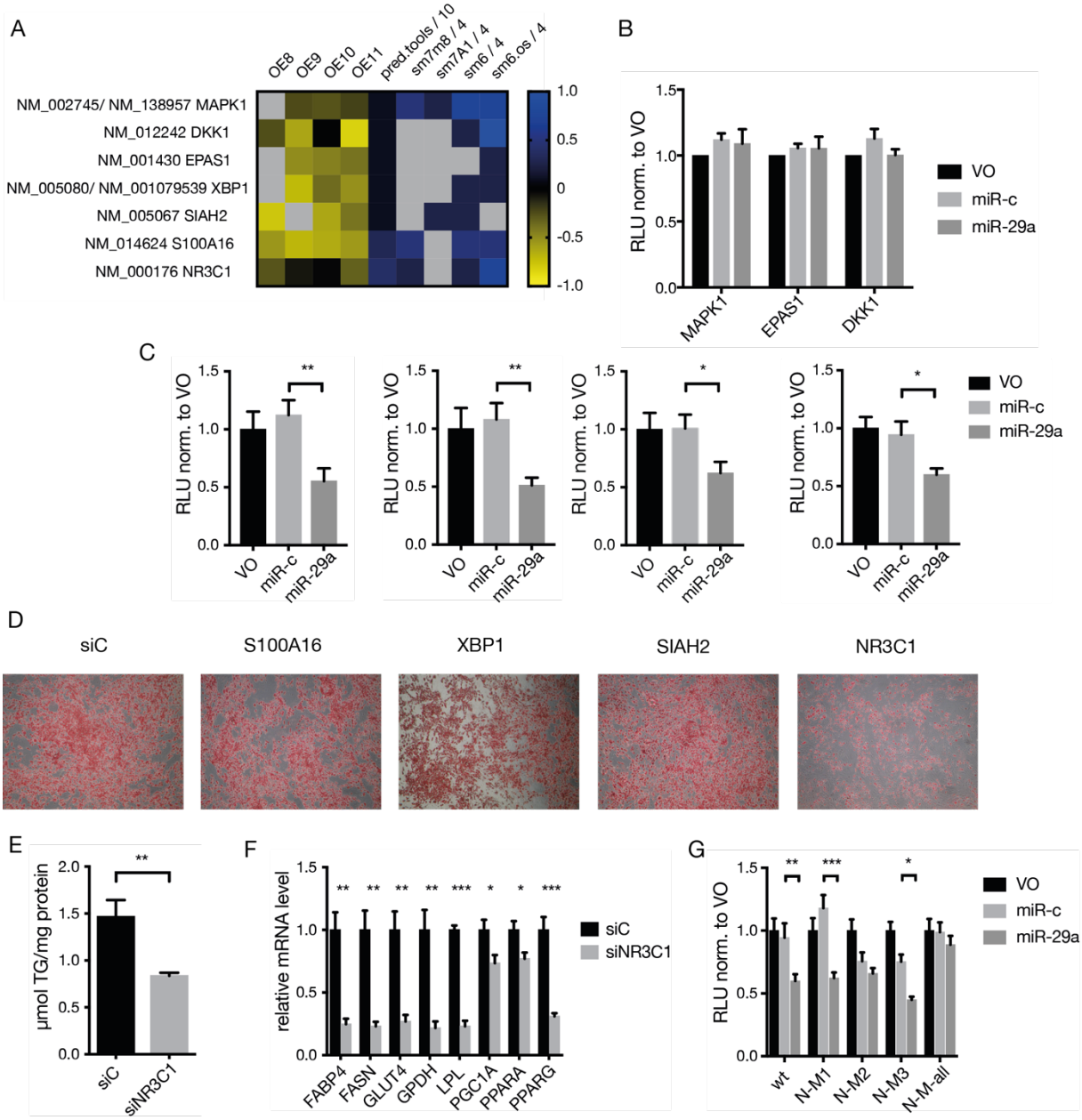

Figure 6: NR3C1 is a direct target of miR29 and mediates its effect on adipogenesis A) Gene expression microarray of hMADS cells transfected with miR-29a mimics at d-2. RNA was harvested 48h later and subjected to microarray analysis, normalized to hMADS cells transfected with control mimics (miR-c). The leftmost four columns show results for the chosen target candidates. The middle column gives the number of online target prediction tools used that predicted the specific transcript as a miR-29a target, divided by the number of prediction tools used (10). The rightmost four columns give the number of different types of seed matches present in the 3'UTR of these transcripts (7mer-m8, 7mer-A1, 6mer, 6mer offset as described in the introduction), divided by 4. n=4 B) Luciferase assay results for candidates that did not a reduction of Luciferase signal. HEK293 cells were co-transfected with miR-29a or miR-c mimics and a Luciferase reporter vector with the target 3'UTR. Cells were harvested and assayed for Luciferase activity 48 hours later. Relative Luciferase Units (RLU) are normalized to the vector only (VO) control. n=3 C) Luciferase assay results for candidates that showed reduction of Luciferase signal. The assay was conducted as in B). n=3-4 D-F) hMADS were stimulated to undergo adipogenesis until d14. hMADS cells were transfected at d-2 with siRNAs against the candidates shown in C). D) Oil-Red O staining of hMADS cells at d14. One representative out of at least 3 experiments is shown. is shown. E) TG accumulation was quantified and normalized to protein amount. n=4 F) mRNA levels of adipogenic marker genes were quantified using RT-qPCR. Cells were transfected and differentiated as in D). Data are normalized to the housekeeping gene as well as to miR-c, the control mimic. n=4 G) Mutation of miR-29 seed matches in the NR3C1 3'UTR abolishes direct binding *in vitro*. Luciferase assays were conducted as in C) with the intact NR3C1 3'UTR (wt), or having mutated one of the three seed matches for miR-29a (N-M1 to N-M3), or all of them mutated in one construct (N-M-all). n=3-4 Unless otherwise indicated, replicates are biological and data are mean ± SEM. * $P < 0.05$, ** $p < 0.01$, *** $p < 0.001$

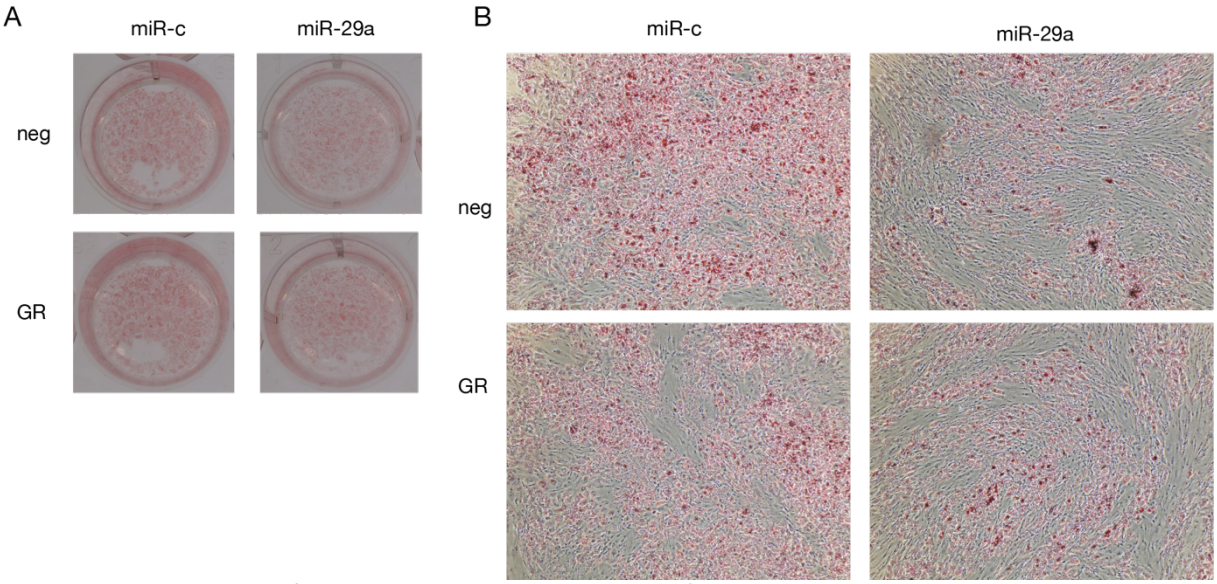

Figure 7: Overexpression of a GR lacking the 3'UTR necessary for miR-29a binding partially rescues the miR-29a overexpression phenotype. A) Whole well photographs of Oil-Red O stained differentiated hMADS cells at d9. Cells were transduced at d-3 (one day before reaching confluence) with either lentiviral particles forcing GR-CDS expression, or lentiviral particles produced with an empty control plasmid. Consecutively, cells were transfected with either miR-29a mimics or control mimics at d-2. B) Microscopy photographs of Oil-Red O stained differentiated hMADS cells at d9 from a different experiment, 40x magnification. Conditions as in A) except cells were transduced at d-4.

miR-29a and its target, NR3C1, form an incoherent feed-forward loop

Since NR3C1 is a direct target of miR-29a and seems to play a role in hMADS adipogenesis, we wanted to confirm that miR-29a affects NR3C1 expression levels in our cell system. RT-PCR analysis of NR3C1 in hMADS cells transfected with either miR-29a mimics or the miR-29 LNA inhibitors show a modest effect on the target mRNA levels (Figure 9 A, D). However, this effect is amplified at the protein level, as evidenced by Western blotting (Figure 9 B-C, E-F), which shows that after transfection with miR-29a mimics, GR protein levels are markedly reduced, but increase following transfection with the miR-29 inhibitor.

To investigate what controls miR-29a expression, an exploration of the ENCODE ChIP-Seq data available online in the UCSC Genome Browser (Euskirchen et al., 2007; Hudson and Snyder, 2006) revealed multiple peaks for TCF7L2, CEBPβ and NR3C1 upstream of the miR-29a gene (Figure 9 G). First, we investigated TCF7L2, which as part of the TCF/LEF transcription factor family participates in the anti-adipogenic Wnt signaling pathway. After testing several Wnt signaling activators (LiCl, BIO) (Visweswaran et al., 2015) and an inhibitor (sFRP-4) (Visweswaran et al., 2015) as well as recombinant Wnt-7a, which individually did not affect hMADS adipogenesis (data not shown), we achieved impairment of hMADS adipocyte differentiation by applying the canonical Wnt protein Wnt-3a (Clevers and Nusse, 2012) (Figure 8 A). However, despite the effect on adipogenesis, miR-29a expression was not affected, leading us to abandon further investigations of Wnt signaling as a potential upstream modulator of miR-29 expression (Figure 8 B). Since dexamethasone is a known activator of GR activity (Miller et al., 1978; Rubin et al., 1978), we treated hMADS preadipocytes with 5 μM dexamethasone, which increased levels of the mature miR-29a and miR-29b four- to six-fold. Simultaneous equimolar addition of RU486, an inhibitor of GR activity, abolished the effect (Figure 9 H).

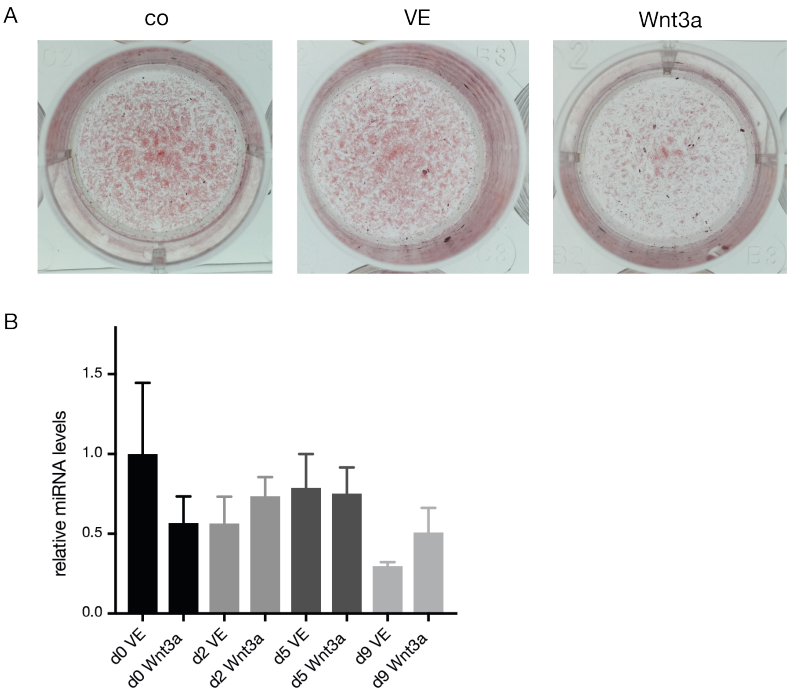

Figure 8: Wnt signaling does not seem to regulate miR-29a expression. hMADS cells were differentiated to adipocytes until d9 while 50µg/ml recombinant Wnt3a protein were added to the media starting at d0. A) Oil-Red O staining at d9 of untreated cells (co), cells treated with vehicle (VE) and Wnt3a. B) miR-29a levels were quantified by RT-qPCR normalized to the housekeeping gene and the VE control at different timepoints throughout differentiation. n=3 Replicates are biological and data are mean ± SEM. * $P < 0.05$, ** $p < 0.01$, *** $p < 0.001$

Since dexamethasone induces miR-29a and activates GR, we were interested in whether GR directly regulates miR-29a transcriptionally. Potential transcriptional regulation could be mediated by direct binding of GR to the DNA regions upstream of the miR-29a gene locus. ChIP-qPCR revealed a 3.5-4-fold increase of signal for GR in two of the miR-29a upstream loci assayed. The same loci also gave increased signals for H3K9ac pulldown, a marker of open chromatin (Figure 9 I) (Bannister and Kouzarides, 2011). As positive controls, we included two genes that are known to be regulated by dexamethasone in preadipocytes, ZBTB16 and FKBP5, to ascertain that dexamethasone treatment was effective (Pereira et al., 2014). Combined, the positive ChiP-qPCR results and the induction of miR-29a upon dexamethasone stimulation indicate the existence of a feedback loop where not only miR-29a regulates its target, but also the target NR3C1 regulates miR-29a expression. One model of action might be that glucocorticoids (in this case, dexamethasone) activate GR, which then presumably binds to the miR-29a upstream region to promote its transcription. Consequently, higher levels of miR-29a lead to increased binding of miR-29a to the NR3C1 3'UTR, dampening GR activity by reducing its expression levels. This type of feedback loop is typical for situations where miRNAs need to balance or counteract situations of (patho)physiological stress (Mendell and Olson, 2012).

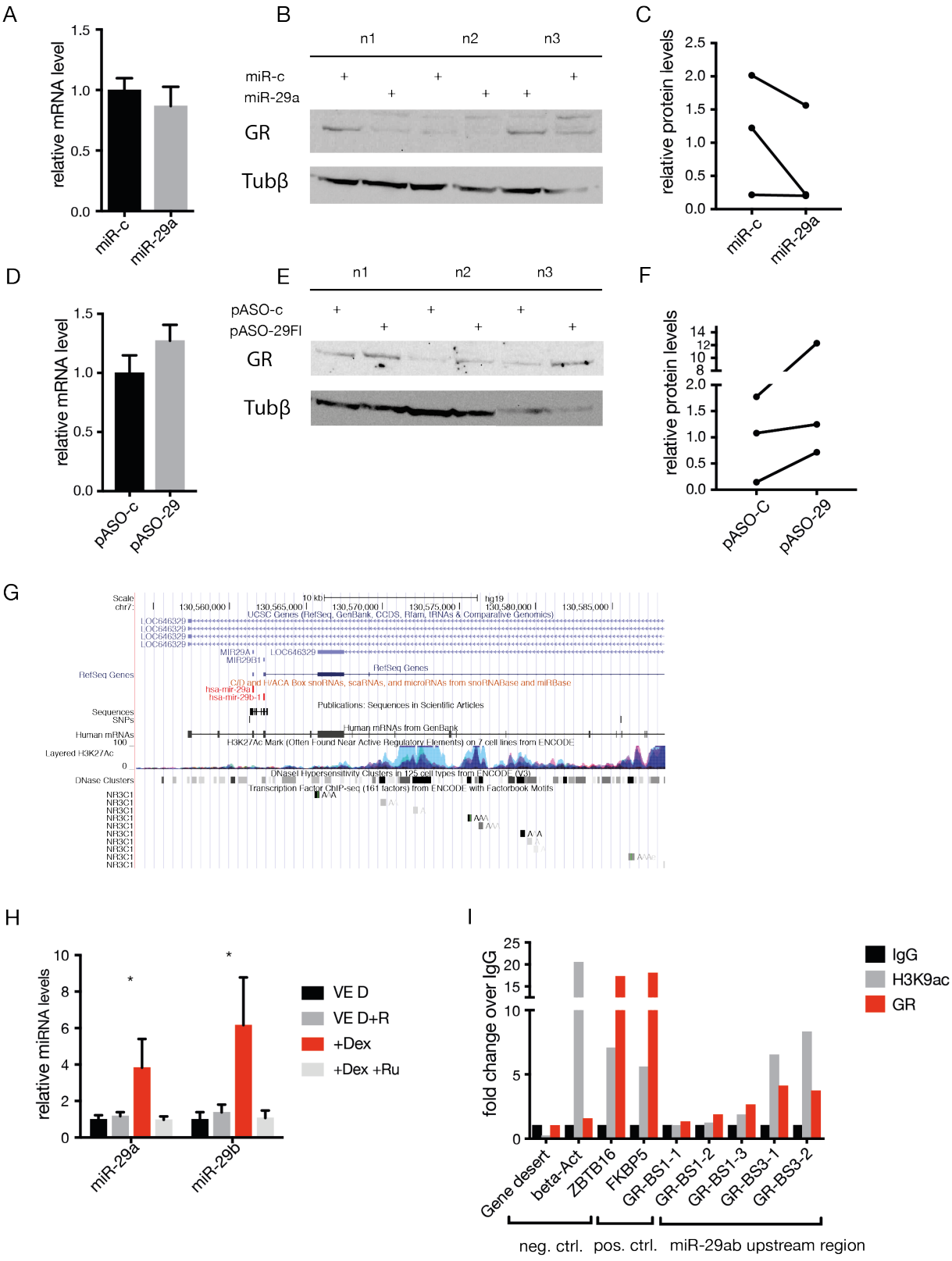

Figure 9: miR-29a affects protein levels of GR, which regulates miR-29a levels via a negative feedback loop. miR-29a directly targets NR3C1, the glucocorticoid receptor (GR) gene. A-F) hMADS cells were transfected with miR-29a or control (miR-c) mimics (A-C), or with LNA power antisense oligo inhibitors against miR-29 (pASO-29) or controls (pASO-c) (D-F) at confluence. Cells were induced to undergo adipogenesis 48h later, and RNA and protein lysates were harvested another 2 days later. A) Quantification of NR3C1 mRNA levels in miR-29a mimic-transfected cells by RT-qPCR normalized to the housekeeping gene and the miR-c control. n=3 B) GR protein levels of cells treated as in A). n=3 C) Quantification of B). D) Quantification NR3C1 mRNA levels in pASO-29-transfected cells quantified by RT-qPCR normalized to the housekeeping gene and the pASO-c control. n=3 E) GR protein levels of cells treated as in E. n=3 F) Quantification of E). G) Screenshot of the upstream region of the miR-29ab gene in UCSC Genome

browser, showing the ENCODE ChIP-Seq data peaks for NR3C1. H) Quantification of miR-29a levels in hMADS preadipocytes treated with dexamethasone (+Dex) compared to vehicle-treated control (VE D), or upon equimolar addition of the GR inhibitor, RU486 (+Dex +Ru) compared to control (VE D+R). n=3-7 I) ChIP-qPCR of the miR-29ab gene upstream region. hMADS cells were grown to confluence, harvested and directly subjected to the ChIP procedure. Results show fold increase in qPCR signal over the IgG control when pulled down with the anti-GR antibody. Additional pulldown signals for the H3K9-acetylation antibody (H3K9ac), a marker of open chromatin, are shown. A gene desert region, as well as β-Actin, a constitutively transcribed gene in all cells, serve as negative control loci. ZBTB16 and FKBP5 are genes that are known to be induced by dexamethasone treatment and thus served as positive controls for the GR pulldown signal. The representative result of 3 experiments is shown. Unless otherwise indicated, replicates are biological and data are mean ± SEM. * P < 0.05, ** p < 0.01, *** p < 0.001

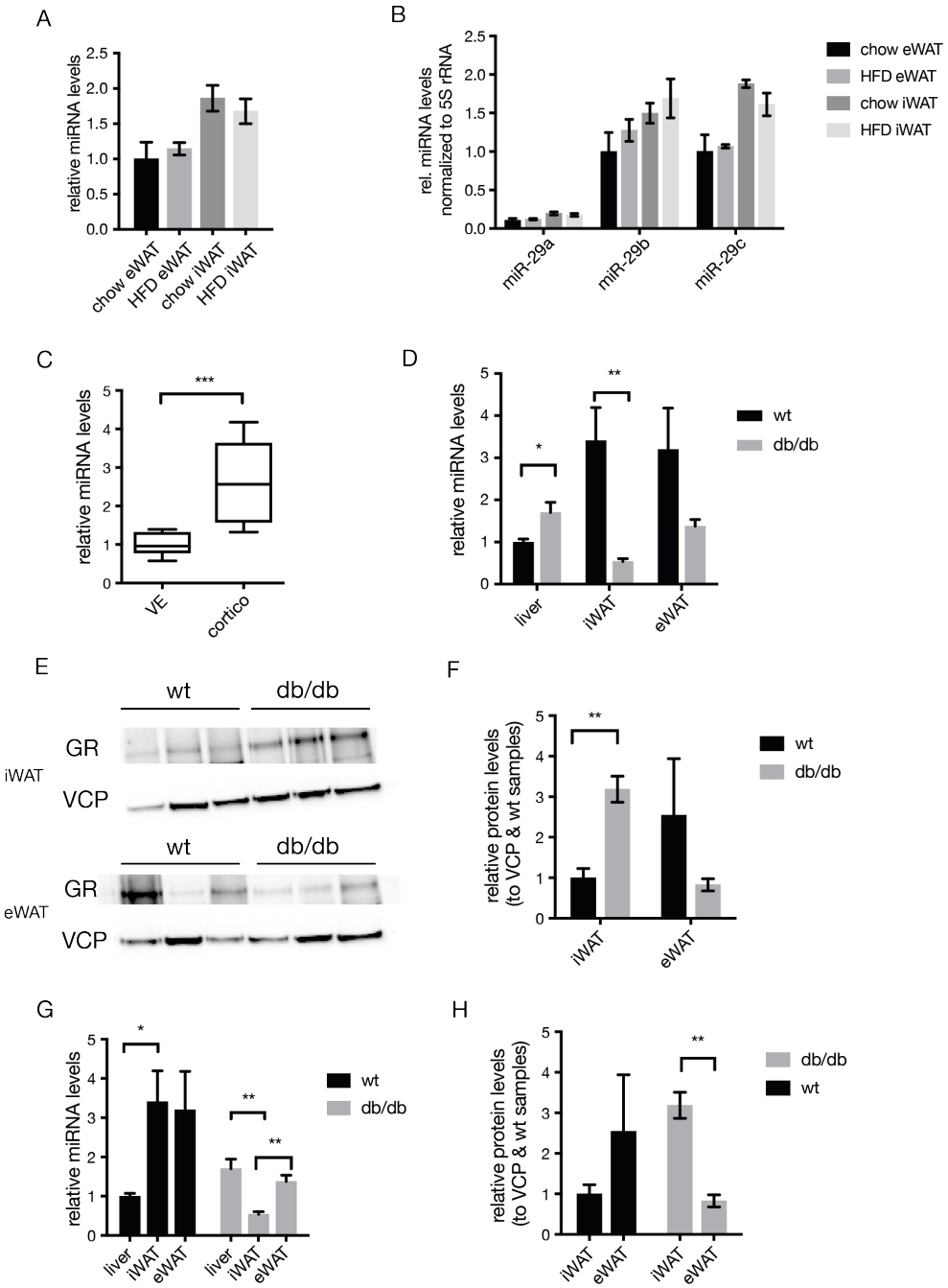

Figure 10: The interplay of miR-29a and GR in vivo: miR-29 seems to regulate GR in high GC level environments. A-B) C57BL/6J mice were fed a HFD for 15 weeks. Adipose tissues were harvested and RNA was extracted. A) miR-29a expression levels were quantified by RT-qPCR normalized to the housekeeping gene and the chow eWAT sample. n=3-6 B) miR-29a, -b and -c expression levels were quantified by RT-qPCR normalized to the housekeeping gene. C)

Mice were supplied with corticosterone in their drinking water for 4 weeks, then the eWAT was harvested and RNA extracted) miR-29a expression levels were quantified by RT-qPCR normalized to the housekeeping gene and the chow eWAT sample. n=9 D-F) eWAT, iWAT and liver of *db/db* mice were harvested for RNA and protein lysates. n=5 D) miR-29a expression levels were quantified by RT-qPCR normalized to the housekeeping gene and the wt liver sample. Statistical significance is shown for wt vs. *db/db* comparisons only. E) GR protein levels of iWAT and eWAT samples. F) Quantification of E) normalized to wt iWAT. Statistical significance is shown for wt vs. *db/db* comparisons only. G) Same date as in D) but rearranged to facilitate comparison of depot-specific expression differences of miR-29a. Statistical significance is shown for tissue comparisons only. H) Same date as in F) but rearranged to facilitate comparison of depot-specific expression differences in GR protein levels. Statistical significance is shown for tissue comparisons only. Unless otherwise indicated, replicates are biological and data are mean ± SEM. * $P < 0.05$, ** $p < 0.01$, *** $p < 0.001$

miR-29a seems to regulate GR *in vivo* in high GC level environments

The potential importance of the miR-29a-GR axis in stress situations, as evidenced by the incoherent feedforward loop described in Figure 9 G-I, lead us to investigate the regulation of the miRNA and its target in in vivo conditions of stress and/or high GC levels. miR-29a is 100% conserved between humans and mice as apparent from the miRbase entries (Kozomara and Griffiths-Jones, 2014), so moving to the analysis of mouse tissue was a viable option.

A common type of physiological stress that can be applied to mice in metabolic research is the feeding of a HFD. In the adipose tissue of mice fed a HFD for 15 weeks, miR-29a is not differentially regulated compared to chow-fed mice, neither in the eWAT nor the iWAT. miR-29a levels tend to be a bit higher in the latter depot in both conditions (Figure 10 A). Noticeably, when one does not normalize levels of each miRNA to a control sample (as is usual in the ΔΔct method), but only to the housekeeping gene (5S rRNA), one can appreciate that miR-29a levels are much lower compared to the other family members, b and c, in all conditions and all fat depots examined (Figure 10 B). This fits the hypothesis that for adipogenesis to work correctly, miR-29a must not be present in high levels.

As the involvement of GR hints at potential importance of GC levels in activating the incoherent feedforward loop, we next looked at the eWAT of mice supplied with corticosterone in their drinking water for 4 weeks. In line with our in vitro data, levels of miR-29a were significantly increased in these mice compared to vehicle-treated controls by ~2.5 fold (Figure 10 C), further underscoring the initial hypothesis.

Since GR activation by GCs points toward a possible relevance of the feedback loop in conditions of hypercorticoidism, we also investigated its regulation in *db/db* mice. The *db/db* mouse, a genetic mouse model of diabetes and obesity deficient in the leptin receptor, is known to have elevated GC levels (Liu et al., 2005; Livingstone et al., 2009). For this reason, we assayed miR-29a levels in liver, iWAT and eWAT as well as GR protein levels in both fat depots these mice (Figure 10 D-F). miR-29a was significantly higher in the liver of *db/db* mice compared to wt, however, the effect size was rather small. In contrast, miRNA levels were decreased compared to wt in iWAT, while no statistical significance could be obtained for a tendential decrease of the miRNA in eWAT. As opposed to miRNA levels, protein levels of GR were increased in the iWAT of *db/db* mice compared to wt. For easier comparison of the *db/db* vs. the wt phenotype,

Figure 10 G and H show the same data as Figure 10 D and F, respectively, with a different bar arrangement. This visualization underscores that while in wt, there is no significant difference of either the GR protein levels or the miR-29a levels between the iWAT and the eWAT depot, their expression seems to be dysregulated in the depots of the *db/db* phenotype.

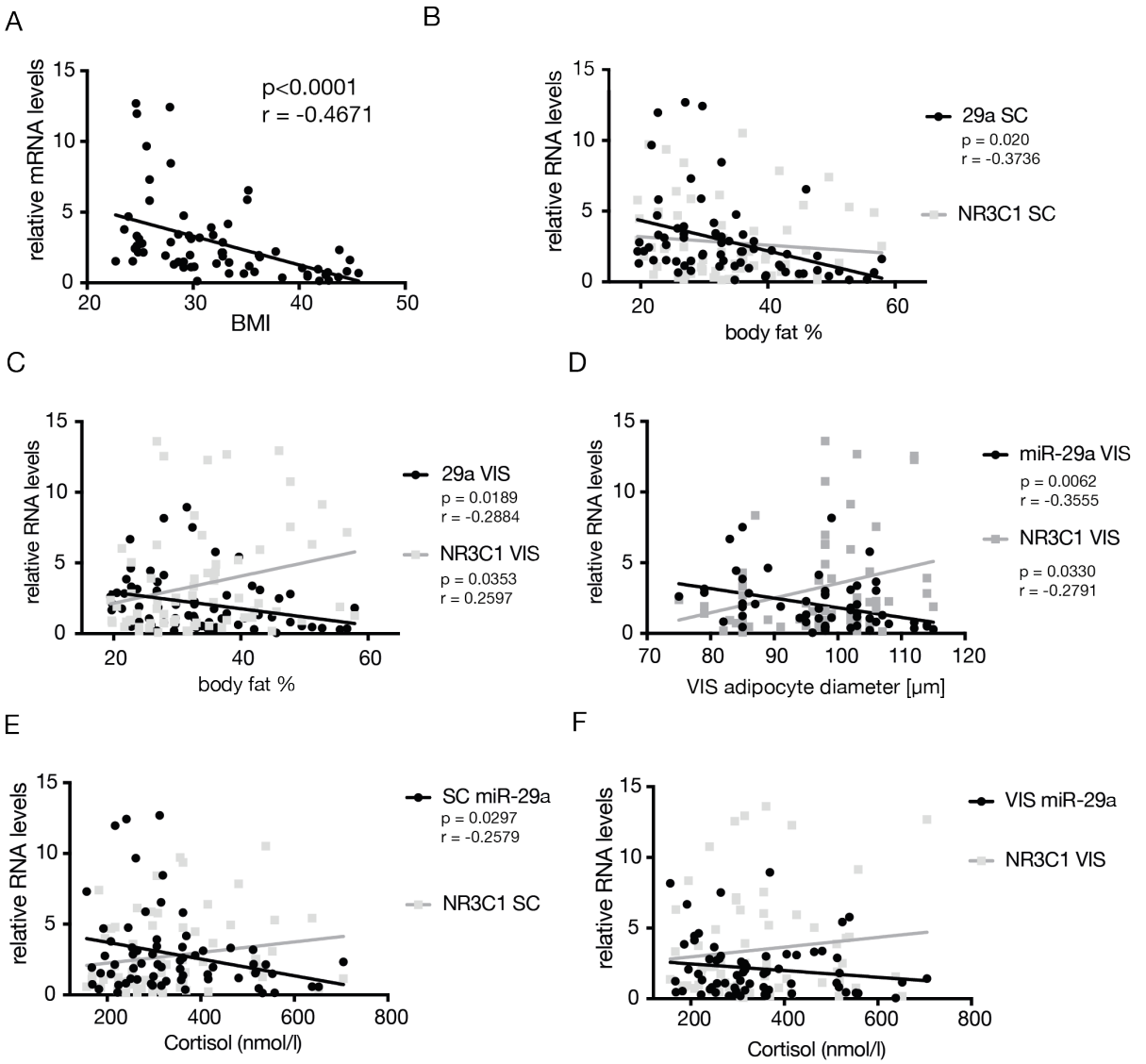

Figure 11: miR-29a and NR3C1 mRNA levels are anti-correlated in human adipose tissue *in vivo*. Levels of miR-29a and NR3C1 mRNA were measured in a well-characterized cohort of 66 patients. miR-29a levels anti-correlate with BMI, body fat %, adipocyte diameter and cortisol levels. A) miR-29a levels are strongly and highly significantly anti-correlated with BMI. B) C) miR-29a levels are anti-correlated with body fat percentage in B) subcutaneous (SC) and C) visceral (VIS) fat depots, while NR3C1 mRNA levels correlate positively. D) miR-29a levels correlate negatively with adipocyte diameter in visceral fat depots, while NR3C1 mRNA levels correlate positively. E) F) miR-29a levels are negatively correlated with systemic cortisol levels in the E) subcutaneous and F) visceral fat depots, while NR3C1 levels correlate positively with cortisol levels. If no significance is specified, correlations are statistically n.s.

In humans, miR-29a and its target correlate with characteristics of obesity

To examine the relevance of the miR-29a-GR axis in humans, we analyzed a cohort of 66 patients that had been extensively characterized regarding obesity, adipose tissue distribution and metabolic phenotype graciously provided and processed by Matthias

Blüher. In human subcutaneous and visceral fat depots, gene expression analysis of miR-29a revealed that miR-29a correlates negatively with BMI in a surprisingly strong and highly statistically significant manner ($p<0.0001$, Figure 11 A). In accordance with this finding, miR-29a correlates negatively with body fat percentage in both the subcutaneous and the visceral fat depot, while NR3C1 shows the opposite trend, which is especially pronounced in the visceral depot (Figure 11 B+C). Interestingly, miR-29a is also negatively correlated with adipocyte diameter in the visceral, but not the subcutaneous fat depot (Figure 11 D).
In line with previous results concerning the miR-29a-GR axis and feedback loop, miR-29a expression in both adipose tissue depots correlates negatively with systemic cortisol levels, while NR3C1 mRNA levels trend upwards (Figure 11 E-F). Even though only the correlation with miR-29a in scWAT is statistically significant, this and the trends for the other variables recapitulate the findings in *db/db* mice and underscores the idea that after reduction of GR levels by a GC-induced miR-29a, miR-29a levels fall again, allowing for a slight increase in NR3C1 mRNA. Since cortisol levels in this cohort correlate significantly with BMI, one might consider that the increase in NR3C1 levels observed with high cortisol levels may present either a conspiring factor contributing to the cause of metabolic changes in obese patients, or an adaptation brought about by the physiological circumstance of overweight or obesity. Significant interaction of weight with the miR-29a to cortisol correlation has been confirmed by linear modelling and ANOVA testing in R for visWAT ($p = 0.0296$), while no interaction was found in scWAT. Additionally, one has to keep in mind that GR protein levels under the regulation of miR-29a do not correlate tightly with the mRNA levels, as demonstrated in Figure 9. Interestingly, neither the diabetes status (yes/no) nor glucose tolerance interacted with the miR-29a to cortisol correlation in either fat depot.

In conclusion, miR-29a seems to be an important player in human adipogenesis. Its regulation of NR3C1, the target mRNA, affects GR levels and, as an incoherent feedforward loop induced by high GC conditions, is relevant in vivo in mice and humans.

MEST is a negative regulator of human adipogenesis

While screening for potential direct targets of miR-29a, Mesoderm-specific transcript (MEST) emerged as a direct target of miR-29a binding as determined by Luciferase assays (Figure 12). However, contrary to existing literature which had found MEST to be a positive regulator of adipogenesis in murine cells, applying siRNAs against MEST in our hMADS cell model lead to a marked increase of triglyceride accumulation (Figure 13). This surprising result lead us to disregard MEST as a potential mediator of miR-29a's effects on adipogenesis in human cells, and instead prompted us to investigate the effect of MEST on adipogenesis independently.

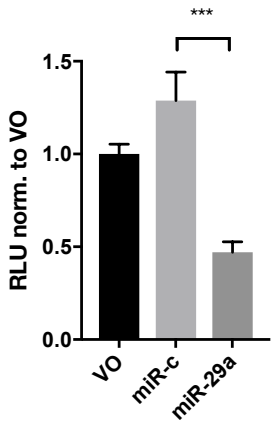

Figure 12: miR-29a directly binds to the 3'UTR of MEST in vitro. HEK293 cells were co-transfected with miR-29a or miR-c mimics and a Luciferase reporter vector with the target 3'UTR. Cells were harvested and assayed for Luciferase activity 48 hours later. Relative Luciferase Units (RLU) are normalized to the vector only (VO) control. n=3 data are mean ± SEM, *** $p < 0.001$

Subsequent data are an excerpt from the manuscript published in the International Journal of Obesity in 2015 and focus on the data I was personally involved in producing. The full story can be found in the original article (Karbiener et al., 2015).

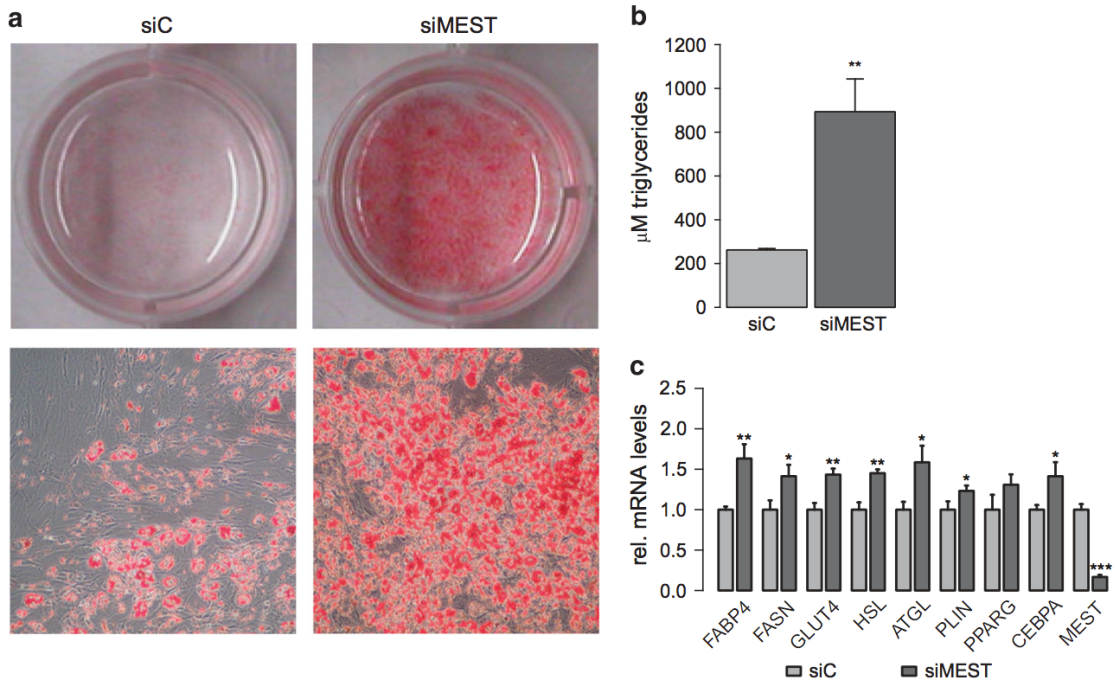

Figure 13: Silencing of MEST promotes human adipocyte differentiation. hMADS cells were transfected with siRNAs against MEST or control (siC) at confluence and induced to undergo adipogenesis 48h later, until d9. A) Oil-Red O staining shows a marked increase in TG accumulation upon transfection with siMEST siRNAs compared to controls (siC). Upper row shows photos of whole wells, lower row shows TL microcopy pictures taken at 40x magnification. One representative out of at least 3 experiments is shown. is shown. B) TG accumulation was quantified and normalized to protein amount. n=4 D) mRNA levels of adipogenic marker genes, as well as of MEST itself to validate knockdown efficiency, were quantified using RT-qPCR. Data are normalized to the housekeeping gene as well as to the siC control. n = 3-64 Unless otherwise indicated, replicates are biological and data are mean ± SEM. * P < 0.05, ** p < 0.01, *** p < 0.001

As mentioned above, silencing of MEST in hMADS cells surprisingly lead to increased triglyceride accumulation, instead of the anticipated decrease, as visible from Oil-Red O staining and quantification using a triglyceride assay kit (Figure 13 A-B). Correspondingly, marker genes for adipogenic differentiation were significantly decreased in siMEST transfected cells compared to controls (Figure 13 C).

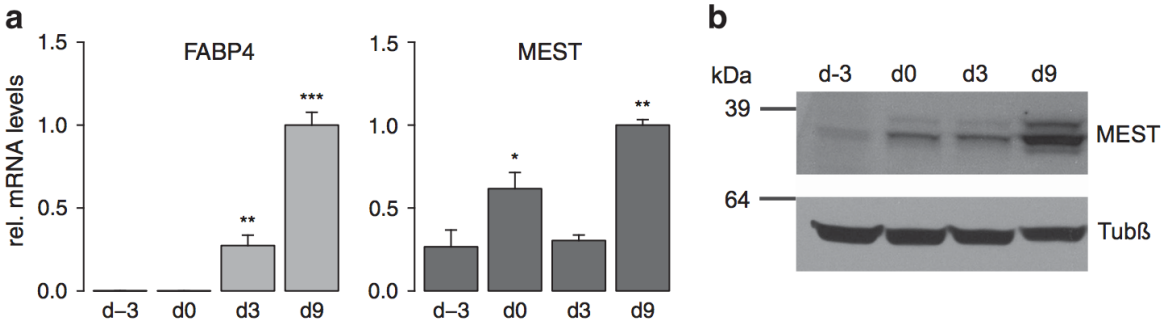

Figure 14: Endogenous MEST mRNA and protein levels increase during hMADS adipogenesis. hMADS cells were grown to confluence (d-2) and after 48h (d0) induced to undergo adipocyte differentiation until d9. At several timepoints, cells were harvested as protein lysates and for RNA isolation. A) mRNA levels of FABP4, an adipocyte marker gene, and MEST, as quantified by RT-qPCR normalized to the housekeeping gene and d9. n=3 B) Western blot analysis of the MEST protein, with an anti-β-Tubulin antibody as loading control. One representative out of at least 3 experiments is shown. is shown. Unless otherwise indicated, replicates are biological and data are mean ± SEM. * P < 0.05, ** p < 0.01, *** p < 0.001

Since decreasing MEST transcript levels before inducing adipocyte differentiation facilitated triglyceride accumulation in hMADS cells, we examined the endogenous expression of MEST during adipocyte differentiation. Following the pattern of FABP4, a classic marker for adipocyte differentiation, MEST was upregulated between d-3 and d0, as well as d3 and d9 of differentiation, at the mRNA as well as the protein level (Figure 14 a and b). One could hypothesize that because MEST seems to negatively impact adipocyte differentiation, it is high in the differentiated condition where recruitment of preadipocytes to the differentiation process is decreased.

Loss of MEST can substitute for IBMX as an inducer of adipogenesis

Gene expression analysis of hMADS cells transfected at d-2 with siRNAs against MEST compared to a control siRNA showed a marked change in PPAR signaling and glycolysis pathways already 48 hours after transfection (Karbiener et al., 2015). This, in addition to the observation that siMEST transfected preadipocytes were morphologically different from siC-transfected controls already at d3 of differentiation, lead us to suspect that MEST triggers events in early adipogenesis (Figure 15 a). Since in the induction phase of differentiation several *in vitro* models of adipogenesis, including hMADS cells, are exposed to dexamethasone and IBMX, we decided to investigate whether silencing of MEST could render either of these compounds superfluous.

hMADS cells transfected with siMEST or siC were differentiated with the induction cocktail lacking either IBMX or dexamethasone. As expected, control cells failed to differentiate well without these compounds – however, siMEST transfected cells could compensate for the lack of IBMX in the medium, as evidenced by Oil-Red O staining and TG accumulation assays (Figure 15 b-c). The increase in adipogenic marker genes in the siMEST cells lacking IBMX in their differentiation medium compared to siC-transfected controls confirms these results (Figure 15 d-e).

In summary, we found MEST to be a positive regulator of human adipogenesis, which stands in stark contrast to its published role in murine cells. The unknown molecular function and detailed regulation of MEST in adipocytes opens up fertile ground for future investigations.

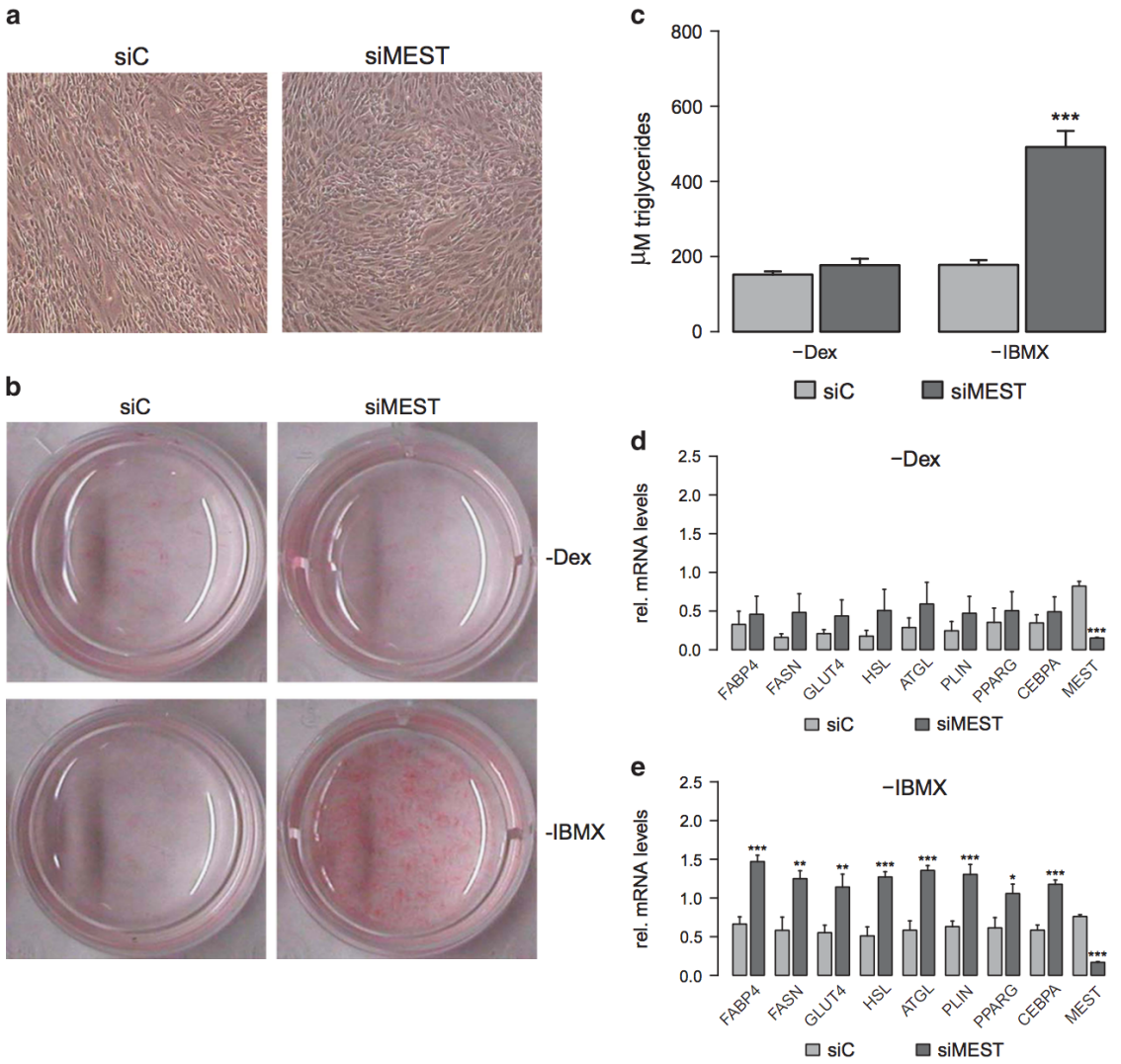

Figure 15: Silencing of MEST compensates for lack of BMX as an inducer of hMADS differentiation. hMADS cells were transfected at confluence with siRNAs against MEST (siMEST) or control (siC), and induced to undergo adipocyte differentiation 48h later using a suboptimal adipogenic cocktail, lacking either dexamethasone (-Dex) or IBMX (-IBMX). A) Representative TL microscopy images of cells at d3 shows slight morphological changes in siMEST samples. B) Oil-Red O staining of cells at d9 of differentiation visualizes TG accumulation. One representative out of at least 3 experiments is shown. is shown. C) TG accumulation was quantified and normalized to protein amount. n=4 D-E) mRNA levels of adipogenic marker genes were quantified using RT-qPCR in D) –Dex and E) –IBMX samples. Data are normalized to the housekeeping gene and presented relative to siC-transfected cells that were differentiated in full adipogenic differentiation medium. n=4 Unless otherwise indicated, replicates are biological and data are mean ± SEM. * $P < 0.05$, ** $p < 0.01$, *** $p < 0.001$

Discussion

MiR-29a is involved in metabolism and associated with diabetes

One criterion for selecting miR-29a for investigation was that it was one of the most strongly downregulated miRNAs through the course of adipogenesis in the gene expression microarray of differentiating hMADS cells. However, additional factors played into this decision: i) the miR-29a sequence is perfectly conserved between mouse and humans, which opens up the possibility of further *in vivo* investigation, ii) miR-29a was associated with metabolic disturbances in mice and rats, and iii) the role of miR-29a in adipocyte differentiation and, expanding the scope, in obesity, was yet undescribed.
As alluded to in point ii), He and colleagues had found the miR-29 family to be upregulated in a gene expression array comparing muscle tissue from healthy and diabetic rats (He et al., 2007a). miR-29a expressed in muscle, fat and liver of diabetic rats, and overexpression of the whole family lead to insulin resistance in 3T3-L1 adipocytes. Both miR-29a and b were induced by incubation of 3T3-L1 cells with high glucose and insulin concentrations. Inhibition of miR-29 increased Akt phosphorylation, but did not affect insulin-stimulated glucose uptake. Though it downregulates Akt, this was not found to be a direct target of miR-29 (He et al., 2007a). This shows a role of the miR29 family in regulating glucose metabolism, although the mechanism of action still seems unclear.

Over the last years, additional findings showed that miR-29a can be detected in human serum and is increased in samples from T1DM patients (Dai et al., 2016; Kong et al., 2011) Additionally, miR-29a in the urine of T2DM patients was found to be associated with albuminuria (Peng et al., 2013). In contrast, miR-29b was found to be lower in T2DM patient serum compared to controls (Zampetaki et al., 2010). A whole body knockout mouse model of the miR-29a and -b gene cluster demonstrated an insulin secretion defect, which was traced to originate in the pancreas but simultaneously had improved systemic insulin sensitivity, a reason for which was not given by the study authors (Dooley et al., 2016). It is tempting to speculate that improved insulin sensitivity in miR-29 knockout mice might originate from the muscle or the adipose tissue.

miR-29a inhibits adipogenesis in hMADS cells

Confirming the findings of the preliminary microarray gene expression study, downregulation of miR-29a during hMADS adipocyte differentiation was confirmed via RT-qPCR. Since miR-29a belongs to a family of three miRNAs, miR-29a, -b and c-, and because miRNAs of the same family share the same seed region, and therefore might mediate similar effects, we analyzed expression of all family members and found that miR-29a and miR-29b have a similar expression profile.

The miR-29 family is encoded in two distinct loci in the human genome. The first locus on chromosome 7 gives rise to the miR-29a and miR-29b1 precursors (we named this precursor pri-mir-29ab), while the second is transcribed to miR-29b2 (identical to miR-29b1 in sequence) and miR-29c from chromosome 1 (named miR-29bc). Within each locus, the two precursor-encoding sites are more than 1 kb apart, but are nonetheless transcribed as one polycistronic pri-mirNA (Ślusarz and Pulakat, 2015).

MiR-29b showed a similar expression profile to miR-29a. Interestingly, although miR-29b is encoded in both pri-mir-29ab and pri-mir-29bc, only pri-mir-29ab followed an expression pattern similar to miR-29a and miR-29b, while pri-mir-29bc behaved differently. This leads to the open question if i) the two loci encoding the precursors are differentially induced in a manner specific to the tissue or the physiological circumstances, or if ii) miR-29b is processed preferentially from one primary transcript over the other, or if iii) other influences can dynamically shift the production ratio of mature miR-29a vs miR-29b, or miR-29b vs miR-29c from either of the two primary transcripts. One may use these as a starting point for further investigation into the molecular details of transcriptional regulation of the miR-29 family.

Transfection of confluent hMADS cells with miR-29a mimics 2 days before the induction of adipogenesis strongly impaired several aspects of adipocyte differentiation: triglyceride accumulation, as assessed optically by Oil-Red O staining and quantified via a colorimetric assay, was reduced by about 40% compared to cells transfected with a non-targeting control oligo; and mRNA expression of major adipogenic marker genes was correspondingly lowered. The marker genes significantly repressed were fatty acid synthase (FASN) and glycerol-3-phosphate dehydrogenase (GPDH), which are essential for TG storage, glucose transporter type 4 (GLUT4) which facilitates insulin-stimulated glucose uptake into adipocytes, lipoprotein lipase (LPL) which both hydrolyses TGs and facilitates lipoprotein uptake from the bloodstream, adipocyte protein 2/fatty acid binding protein 4 (FABP4) which serves as a carrier for fatty acids and marker of TG accumulation, as well as peroxisome proliferator-activated receptor alpha (PPARα) and peroxisome proliferator-activated receptor gamma (PPARɣ), two transcription factors essential for adipocyte differentiation. PPARɣ is known as the master regulator of adipogenesis in general (Farmer, 2006), while increased PPARα levels are viewed as indicating more specifically a brown/brite adipocyte phenotype (Gross et al., 2016). Additionally, PGC1A expression showed a non-significant downwards trend. These results fit with our hypothesis and the expectations following from the downregulation of miR-29a during hMADS adipogenesis.

Vice versa, inhibition of the miR-29 family by transfection of an Exiqon LNA power inhibitor antisense oligonucleotide, herein called "pASO-29", expedited hMADS adipogenesis, with a ~10% increase in triglyceride accumulation at d9 of differentiation. The corresponding increase in most of the marker genes was, however, small and not statistically significant.

It is important to point out that in contrast to transfection with miRNA mimics, it was not feasible to validate successful inhibition via RT-qPCR. LNA-modified antisense oligonucleotides are known to bind to endogenous miRNAs, but not necessarily lead to their degradation, which makes quantification by RT-qPCR unreliable (Torres et al., 2011). Therefore, we resulted to quantifying the increase of published direct target genes (validated by reporter gene assays in the literature) upon miR-29 inhibition. This might even surpass Northern blotting in quality as a functional readout because it quantifies the effect of the miRNA rather than just its amount, though it is subject to other factors

influencing the miRNA-target interaction. Since we can see a plausible effect on adipogenesis in line with our hypotheses, we can, however, assume that inhibition worked sufficiently for our purposes.

Since the inhibition of the miRNA likely removes a repressor of adipogenesis, the small size of the effect is not unexpected, as the differentiation process can be controlled by several negative regulators, such as for example the anti-adipogenic Wnt signaling (Ross et al., 2000), or, as described in this thesis and a published manuscript, mesoderm-specific transcript (MEST) (Karbiener et al., 2015). Thus, the removal of one of these negative regulators is not likely to override the other controlling factors.
Alternatively, one might ask, since miR-29a inhibits the process of adipogenesis, what does it actually promote instead? miR-29a has been published to promote osteoblast differentiation in a human cell model (Kapinas et al., 2009, 2010). Osteoblasts and adipocytes are believed to arise from the same precursors (Kapinas et al., 2010), and hMADS are also capable of differentiating into osteoblasts and osteocytes when stimulated with a different hormonal cocktail (Elabd et al., 2007). An interesting approach would be to measure marker genes for osteoblast differentiation in cells transfected with a miR-29 inhibitor - one might expect to find an increase in osteoblastic markers over the control transfected cells. Another option would be to directly study the miRNA's effect on osteoblast differentiation in hMADS cells.

In our cell system, out of the 3 family members, miR-29a seemed to exert the greatest negative impact on adipocyte differentiation. Therefore, we focused on its anti-adipogenic nature rather than the effects of miR-29b and -c. It is, however, conceivable that the other family members play a greater role in the regulatory context of other tissues, possibly even by targeting the same transcripts. As an example, miR-29b has been described to target the GR as well as the norepinephrine transporter in a rat pheochromocytoma cell line (Deng et al., 2016).

One limitation of our study is that we did not investigate the role of miR-29 in mature adipocytes, which would possibly have increased the pertinence of our results to *in vivo* situations. Nevertheless, we have elucidated the impact of the miR-29 family on human adipogenesis. Since it is believed that about 10% of fat cells are renewed in adult humans each year (Spalding et al., 2008b), this knowledge may contribute to our understanding of its relevance to diverse disease states such as diabetes and obesity.

Identification of the target that mediates miR-29's effect on adipocyte differentiation

In order to find possible direct targets of miR-29a in the hMADS cell system, we used a microarray screen to assay global mRNA expression 48 h after transfecting with miR-29a or control mimic. Since miRNAs usually decrease mRNA levels of their direct targets, we first filtered the downregulated mRNAs by presence in at least 3 out of 4 biological replicates, then sorted by fold change using a cut-off of at least -0.3x (~19% downregulation). This unbiased screen was then complemented by a heuristic approach to narrowing down potential targets: i) we determined which of the downregulated mRNAs harboured miR-29 seed matches, and sorted by presence and number of these, ii)

we screened for predictions by online miRNA target prediction tools (miRanda miRbase (Betel et al., 2008; Kozomara and Griffiths-Jones, 2014), PITA (Kertesz et al., 2007), PicTar (Krek et al., 2005) and TargetScan (Lewis et al., 2005)) iii) we employed literature search to highlight genes that have been previously implicated to affect metabolism, adipocyte differentiation, or were associated with diabetes, iv) we highlighted genes that encoded powerful regulators such as transcription factors, since they were likely to have a strong effect on the differentiation process. The latter two criteria were used to give preference to candidates but lack thereof was not an exclusion criteria, in order not to bias against unexpected new findings.

Using the criteria described above, we chose 8 promising candidates to investigate further: mitogen-activated protein kinase 1 (MAPK1), also known as ERK2, was known to mediate CREB activation (Reusch et al., 2000), which induces C/EBPβ (Rosen and MacDougald, 2006), a crucial player in early adipogenesis (3 seed matches); dickkopf homologue 1 (DKK1) is an inhibitor of the anti-adipogenic canocial Wnt signaling pathway (1 seed match) (Clevers and Nusse, 2012; Cristancho and Lazar, 2011) endothelial PAS domain protein 1 (EPAS1) is a transcription factor published to promote 3T3-L1 adipogenesis (Rosen and MacDougald, 2006); x-box binding protein (XBP1) had been published to be required for adipogenesis (1 seed match) (Sha et al., 2009), seven in absentia homologue 2 (SIAH2) is a ubiquitin ligase that regulates PPARɣ activity in adipocytes (1 seed match) (Kilroy et al., 2012); S100 calcium binding protein A16 (S100A16) promotes adipogenesis in 3T3-L1 adipocytes (Liu et al., 2011b) (2 seed matches); mesoderm-specific transcript homologue (MEST) had been published to enlarge adipocytes and correlate with adipocyte size (Jung et al., 2011; Kadota et al., 2012) (1 seed match); nuclear receptor subfamily 3 group C member 1 (NR3C1) encodes the glucocorticoid receptor gene (3 seed matches), which was a prime candidate due to the implications of GCs in Cushing's disease with visceral expansion of adipose tissue (Shibli-Rahhal et al., 2006), as well as the fact that most adipogenic cocktails to induce adipogenesis *in vitro* include some kind of GR agonist, e.g. dexamethasone (Miller et al., 1978; Rubin et al., 1978).

For these 8 candidates, we designed 3'UTR Luciferase reporter vectors that were co-transfected with the miR-29a into HEK293 cells in order to confirm direct binding *in vitro*. This experiment ruled out MAPK1, EPAS1 and DKK1 as direct targets since co-transfection of the miRNA with the reporter vector did not decrease the Luciferase signal. For the remaining 5 potential targets, we conducted a phenotypical screen to see if siRNA-mediated knockdown of these genes in hMADS cells would attenuate adipogenesis and thus phenocopy transfection with miR-29a mimics. Interestingly, though silencing of SIAH2 was published to inhibit adipogenesis in 3T3-L1 cells (Kilroy et al., 2012), this was not the case in hMADS cells. Only silencing of NR3C1, the glucocorticoid receptor gene, achieved a marked reduction in triglyceride accumulation and gene expression of adipogenic genes by d9 of hMADS adipogenesis, which made it the obvious candidate for mediating the miR-29a effect in developing adipocytes. Additionally, the amount of reduction of TG accumulation in siNR3C1 samples was ~30-40%, similar to the results achieved by transfection with miR-29a mimics.

Mutations of the three seed matches in the NR3C1 3'UTR as well as one construct harbouring mutations in all three seed matches simultaneously showed that the second seed match seemed to be most important for miR-29 binding, as its mutation abrogated the decrease of Luciferase signal usually accomplished by miR-29a co-transfection. Mutation of all three seed matches at once yielded the same result. All in all, this confirms direct binding of miR-29a to the NR3C1 3'UTR *in vitro*.

Thus, the results so far show that miR-29a directly targets NR3C1 by binding to its 3'UTR, and that silencing of NR3C1 by siRNAs phenocopies the miR-29a effect on adipogenesis. These data are already a strong indication that NR3C1, the gene encoding the GR, is the target that mediates a considerable part of the miRNAs impact on adipocyte differentiation. However, to conclusively demonstrate this, one would need to show that reconstitution of GR function would rescue the miR-29a effect, as it would negate the miRNA-mediated silencing of NR3C1. Therefore, we produced lentiviral particles from a vector encoding only the GR coding sequence (CDS), which lacks the 3'UTR essential for miRNA binding. By transducing proliferating hMADS cells with these particles, we forced expression of an NR3C1 transcript that, other than the endogenous variant, cannot be knocked down by miR-29a. At confluence, we transfected these cells with miR-29a mimics and induced adipogenesis 48 hours later. Indeed, at d9 of adipocyte differentiation, we observed a partial rescue of the impaired TG accumulation as visualized by Oil-Red O staining at d9 for two distinct experiments. However, these differences could not be quantified using the TG assay normally employed.

Additionally, technical problems hamper the robustness of these results, which is why thus far they have not been reproduced. hMADS cells do not seem to be suited to efficient production of proteins the size of GR (97 kDa). Even without co-transfection of miRNA mimics, transduction was problematic, since even at the highest multiplicity of infection (MOI) the cells could tolerate without differentiation being impaired in the GR-CDS transduced cells, we could not see a clear increase in GR protein (data not shown). Given the same MOI, GR-CDS-transduced cells also tended to differentiate worse than eGFP-transduced controls, which in turn differentiated worse than empty vector-transduced controls. In line with this observation, successful overexpression of proteins in hMADS cells has been published only for small proteins below 50 kDa (Goudenege et al., 2009; Karbiener et al., 2015; Roux et al., 2013). Besides lentiviral transduction, different transfection methods as well as nucleofection have been tested to no avail, thus excluding that the effect is due to an adverse reaction to the pseudoviral particles, and more probably due to the stress of ectopic protein expression.

An alternative approach to demonstrate that GR mediates the miR-29a effect could be an indirect rescue via C/EBPβ. Induction of C/EBPβ is among the earliest events in adipocyte differentiation and might be a prerequisite to GR function, since upon adipogenic induction, GR and other transcription factors have been found to be recruited to adipogenic transcriptional hotspots that are already occupied by C/EBPβ, and which are vital for adipogenic induction (Steger et al., 2010). Vice versa, and more pertinent to

this issue, GCs are known to encourage C/EBPβ activity by inducing removal of an inhibitory HDAC1 complex (Wiper-Bergeron et al., 2003, 2007). More recent studies have shown that GR is recruited to and binds CEBPβ gene loci already 4 hours into early adipocyte differentiation (Park & Ge 2016). Hence, if part of the miR-29a phenotype is caused by loss of induction of C/EBPβ due to GR repression, reconstituting C/EBPβ activity might be a way to rescue the loss of GR activity. Moreover, as with GR, ENCODE ChIP-Seq data available in the UCSC Genome Browser also indicate binding of C/EBPβ to the upstream region of miR-29a- and -b gene cluster, in regions overlapping with GR ChIP-Seq signals. Most importantly, a recent study has found that in 3T3-L1 cells, ectopic CEBPβ expression can rescue impaired adipogenesis caused by silencing of GR (Park and Ge, 2017). Thus, given the above evidence, one might speculate that C/EBPβ overexpression in hMADS cells might suffice to partially rescue the negative impact of miR-29a on differentiation, and might be more successful technically due to the smaller (36 kDa or 18 kDa for different isoforms) size of the protein.
Another option would be to circumvent the technical hindrances by switching to a different cell system. The basic phenotype of miR-29a in the context of adipogenesis has been confirmed in 3T3-L1 cells (data not shown); however, as differences in the effect of GCs on murine vs. human preadipocytes have been demonstrated (Lee et al., 2014b), the transferability of knowledge gained in a murine model regarding miR-29a and GR is as yet unclear.

Additionally, recent studies suggest that GR only has a mild impact on adipogenesis *in vitro* (Park and Ge, 2017) and *in vivo* (Mueller et al., 2017).
The *in vitro* study shows that in 3T3-L1 cells, differentiation to mature adipocytes is impaired in GR-depleted preadipocytes at d7, but given enough time, differentiation catches up to wt cells at d21. The same was shown for differentiation of murine primary white preadipocytes. A clear limitation of this study, however, is that all the results use murine cell models to examine adipogenesis, which is closely related to, but not necessarily an exact mirror image of the human adipocyte differentiation process. To date, there is knowledge of several factors that impact adipogenesis differentially in humans vs. mice, for example mesoderm-specific transcript (MEST) and lim domain only 3 (LMO3) (Karbiener et al., 2015; Lindroos et al., 2013). Additionally, there are indications from other *in vitro* studies that GCs have a diverging effect on murine vs. human preadipocyte cell models (Lee et al., 2014b). Alternatively, we can suspect that species-specific regulatory circuits might be the reason why MEST plays different roles in murine vs. human adipogenesis, as is the case for example for the lim domain only 3 (LMO3) gene (Lindroos et al., 2013)
In vivo findings show that adipocyte-specific GR knockout does not impair formation of white adipose tissue in mice. However, the authors do find that GR KO reduces bodyweight gain during aging and 20 week HFD feeding. Thus, the miR-29a-GR axis might be relevant not in the developmental stages, but during adipose tissue expansion/turnover in the adult stage of life (e.g. described by (Spalding et al., 2008a), as well as upon diet-induced obesity (see also: "miR-29a and NR3C1 in human samples"). Therefore, further study is required before discounting the glucocorticoid receptor as a

player in adipocyte differentiation.

Clearly, a successful rescue experiment would strengthen the findings described above. Nevertheless, considering that miR-29a directly binds to the NR3C1 3'UTR has a negative effect on NR3C1 protein levels, and that silencing of NR3C1 phenocopies miR-29a's detrimental impact on adipogenesis, there is strong evidence that the GR mediates a substantial part of miR-29a's function in impairing adipocyte differentiation.

GR activity regulates miR-29a through a negative feedback loop

Next, we wanted to find out what controls miR-29a expression in hMADS. Explorations of the miR-29a-encoding upstream region showed that according to the ENCODE ChIP-Seq dataset available online in the UCSC Genome browser, the ChIP-Seq signal peaked for TCF7L2, CEBPB and, counterintuitively, GR.

TCF7L2 is part of the TCF/LEF transcription factor family, which mediates the effects of the anti-adipogenic Wnt signalling pathway, making it a good candidate for potential regulation of miR-29a. Mutations in the TCF7L2 gene, specifically, have been implicated in T2DM (Clevers and Nusse, 2012). Additionally, miR-29 had already been published to modulate Wnt signalling in human osteoblasts (Kapinas et al., 2010), and Dkk1 was one of the putative targets we considered when searching for the direct miR-29a target that mediates its effect in adipocytes. However, while adding different concentrations of the canonical Wnt3a (Davis et al., 2008) proteins to the differentiation medium did impair adipogenesis in hMADS, this failed to modulate endogenous miR-29a expression.

dexamethasone, however, a potent selective GR agonist, unexpectedly increased levels of the mature miR-29a and miR-29b 3- to 5-fold at a final concentration of 5 µM, which is 5x higher than used for induction of adipogenesis. This increase could be abolished by equimolar addition of RU486 (Mifepristone), an inhibitor of GR activity.

Thus, since GC stimulation induces miR-29a, which targets and knocks down GR/NR3C1 protein levels, there is evidence for a negative feedback loop, where the target of a miRNA, GR, induces the miRNA that in turn reduces its own protein levels. These findings are in line with a study showing that Dex stimulation downregulates GR mRNA and protein in hepatoma cells as well as in rat liver *in vivo*. The decrease in GR protein was found to be most pronounced after 24 h but was restored to the original level after 48 h (Dong et al., 1988). Similar experiments showed that the GR receptor number in HeLa cells was reduced after 24 h of Dex treatment, but not before (Cidlowski and Cidlowski, 1981). Indeed, in hMADS preadipocytes, Dex stimulation of at least 24 h was necessary to robustly induce miR-29a levels (data not shown). We did not investigate the protein levels of GR after this treatment. This would be an interesting follow-up experiment. In contrast to our findings, one of these studies found a marked decrease in NR3C1 mRNA levels (Dong et al., 1988), which we could not observe at any timepoint after Dex stimulation, as well as a decrease in GR protein half-life from 25 h to 11 h, which might indicate a different mechanism contributing to the negative effect on protein levels than miRNA-related RNAi. Another study added that the downregulation of GR mRNA levels was most likely independent of protein synthesis, since it was also observed in the presence of cycloheximide, an inhibitor of the same. They even found a slight increase in GR mRNA levels upon cycloheximide addition (Okret et al., 1986).

which we also observed in preliminary experiments that included cycloheximide (data not shown). Taken together with the report that GR protein stability was decreased upon Dex stimulation, one might speculate that protein synthesis is involved in mediating the negative effect on GR mRNA levels, e.g. by inducing proteins of the RNAi response, or via synthesis of an unknown protein factor that further destabilizes the GR mRNA in addition to miR-29a targeting.
ChIP-qPCR of miR-29a in dexamethasone-stimulated, confluent hMADS cells showed a ~4-fold increased pulldown with an anti-GR antibody over the IgG control in two regions upstream of the miR-29a and -b encoding gene cluster. The pulldown was also increased ~3-4-fold over two negative control regions (a gene desert, which by definition lacks transcriptional activity, and β-Actin, a constitutively expressed, typical "housekeeping" gene), indicating that GR binds the DNA regions upstream of the miR-29a and -b gene cluster.

These results made a very potent case for GR activating miR-29a expression, which at first seems counterintuitive. Why would the target of a miRNA that is subject to its posttranscriptional knockdown effect increase the levels of the miRNA when active?
Firstly, reciprocal regulation of miRNAs and their targets is emerging as a common theme, adding another multilayer of complexity to the gene regulation network. Pasquinelli described several other mechanisms besides direct transcriptional induction of the miRNA by its target, by which targets can affect miRNA function or expression levels: Targeting of the miRISC complex, as demonstrated by LIN41, which antagonizes Argonaute stability while itself being regulated by the let-7 family of miRNAs; pseudogenes acting as endogenous miRNA sponges: competing endogenous RNAs (ceRNAs); and RNA binding proteins such as HuR, which under stress conditions translocates from the nucleus to the cytpolasm to protect certain mRNAs from miRNA degradation (Pasquinelli, 2012) .
Functionally, as suggested by Mendell and colleagues, this type of negative feedback might serve the purpose of "signal resolution": if the pathway, in this case, GR, is excessively activated under certain stress conditions, the miRNA-mediated negative modulation of GR expression might be necessary to prevent hyperactivation or to restore homeostasis after return to normal physiological conditions (Mendell and Olson, 2012).
Another possible interpretation is that miR-29 titrates GR activity to a specific, blunted level under certain stress conditions, as in this situation, normal GR expression levels would be maladaptive (Mendell and Olson, 2012). A third possible purpose would be ensuring signal stability by buffering GR levels to safeguard against strong short-term fluctuations in GR-activating signals (probably acutely high GC levels).

However, if one disregards the evidence suggesting that GR directly increases miR-29a expression, one would, instead of a negative feedback loop, be looking at an incoherent feedforward loop: The case when induction of a signal transducer, in this case GR, coincides with parallel induction of its inhibitor (Ebert and Sharp, 2012). This induction might be caused by other transcription factors activated by dexamethasone. One could examine the direct effect of GR on miR-29a expression more closely by reporter gene assays, e.g. with a Luciferase construct including the supposed GR binding site. However,

this would still not conclusively prove GR's induction of miR-29a, since it might be that GR only facilitates binding of other transcription factors, as suggested by Siersbaek and colleagues (Siersbæk et al., 2014b), or that transcription factor cooperativity is essential for miR-29a induction. Additionally, since adipogenic hotspots have been found to be more robust concerning GR perturbance or lack of activation by GC (Siersbæk et al., 2014a), binding of other transcription factors might ensure miR-29a induction even without dexamethasone stimulation and subsequent GR binding. In this case, GR would enhance induction speed rather than determining whether GR is expressed.
These trains of thought could be explored further by pulling down the wider GR binding region upstream of the pri-mir-29ab gene locus in order to determine which other proteins are involved, and then silencing these transcription factors or co-factors to see if dexamethasone can still induce miR-29a expression in their absence. Conversely, if silencing of NR3C1 would abrogate miR-29a induction, this would indicate that GR is indeed the main effector of miR-29a induction by dexamethasone.

Referring back to the ChIP-qPCR experiment mentioned above, another layer of evidence adds to our results: Since GC treatment induces massive chromatin remodelling at GR binding loci (Grøntved et al., 2013), and chromatin accessibility was found to be a prerequisite for GR binding in up to 95% of loci (John et al., 2011), one could read the increase in pulldown with the anti-H3K9ac antibody as an additional indication that GR binding is indeed happening. The C/EBPβ binding site found in the ENCODE ChIP-Seq data set upstream of the miR-29a locus is another indication bolstering the hypothesis that GR binds to the miR-29a upstream region, if one assumes that the observation made in liver that almost two thirds of GR binding sites are co-occupied by C/EBPβ (Grøntved et al., 2013), holds true for preadipocytes.

It would be interesting to see if GR activation leads to an induction of other miRNAs. Consecutive pathway analysis of these and their known targets might lead to a greater understanding of the physiological circumstances where GR regulation of miRNAs plays a role.
Another aspect from which one may consider the feedback loop is through the lens of the recently published evidence that GR is not necessary for adipogenesis, but does speed up the process (Park and Ge, 2017). In this case, does miR-29a ensure that GR enhances adipogenesis, but that expression does not debauch? Conversely, one would expect that inhibition of miR-29 (which relieves GR repression) might lead to enhanced or faster adipogenesis. This might explain why we observe a slight increase of TG accumulation in pASO-29 transfected hMADS, but almost no change in adipogenic marker genes at day 9 of differentiation: pASO-29 transfected adipocytes do not necessarily hypertrophy as an end result, but may just reach their target differentiation state more quickly than control cells. The fact that in hMADS cells, there is almost no difference in the expression level of adipogenic marker genes between d9 and later days in white adipogenic differentiation, fits with this idea. In order to substantiate this line of thought, it would be useful to identify marker genes that do change in the late stage of differentiation, or preferentially, that are expressed exclusively at late stages, and inquire whether these changes in gene expression signatures happen earlier in the pASO-29 transfected cells.

miR-29a regulates GR *in vivo*

miR-29a and GR in mouse models of obesity and diabetes

MiRNAs often play a crucial role in determining an organism's response to stress and pathophysiological circumstances (Mendell and Olson, 2012). Since we had found GR, the nuclear receptor that reacts and binds to GCs, to be one of the direct target of miR-29a in adipocyte differentiation, and the GC-GR axis plays a role in mediating stress responses in mammals, we investigated *in vivo* models that might elucidate the role of miR-29 and its target in stress responses.

A common metabolic stressor, a 12 week high fat diet (HFD) has been shown to induces hypercorticoidism in rats as well as in C57BL/6 mice (Mueller et al., 2017; Sharma and Fulton, 2013; Underwood and Thompson, 2016). Additionally, in adipocytes, GR downregulates PEPCK, a prominent enzyme in glyceroneogenesis, which is important for triglyceride (TG) synthesis. In mice fed a HFD, overexpression of PEPCK in adipocytes leads to exaggerated fat gain (Vegiopoulos and Herzig, 2007b), raising curiosity as to whether miR-29a would be modulated in these animals.
Thus we fed C57BL/6 wt mice a HFD for 15 weeks and analyzed levels of miR-29a, b and c in both the inguinal (subcutaneous) (iWAT) and the epididymal (visceral) WAT (eWAT). We did not find a significant difference in the levels of any of the miR-29a family members between neither the chow and the HFD fed mice, nor between the fat depots, though there was a tendency for miR-29c to be slightly higher in the iWAT compared to the eWAT. Interestingly, miR-29a levels were much lower in both fat depots of all mice when compared to the other two family members. Since we have found miR-29a to inhibit adipogenesis much more strongly than miR-29b or -c do, this result re-emphasizes the anti-adipogenic role of this specific family member. All in all, these results suggest that the miR-29 family is not regulated, and probably does not play a role in the context of HFD-induced metabolic stress. How the elevated GC levels might affect miRNA expression levels in this model is hard to assess, since we did not measure ACTH secretion or serum corticosterone levels.

High GC levels are a major symptom in the pathophysiology of Cushing's disease, where GR function is disturbed. To produce similar conditions in mice, we supplied mice with corticosterone in their drinking water for 4 weeks to then analyze eWAT miR-29a levels. We have no information on the resulting systemic GC levels, but it is known that at the end point of the experiment, the mice were highly insulin resistant. Levels of mature miR-29a were upregulated ~2.5 fold in mice supplied with corticosterone compared to vehicle controls, confirming the induction of miR-29a by GCs *in vivo*. We can assume that the negative feedback loop of high systemic GC levels to reduce the activity of the HPA axis results in less endogenous GC production, which is overshadowed by the exogenously administered corticosterone. In order to illuminate whether the feedback loop between miR-29a and GR is intact in this system, and to elucidate the kinetics of this interaction, it would be interesting to measure mRNA and protein levels of GR to see the effect of long-term hypercorticoidism on receptor expression. Given our previous data, we would expect GR protein levels to be lower in corticosterone-supplied mice than in controls, since the induction of miR-29a would decrease GR expression in the

WAT. An alternative, faster approach would be to inject wt mice with dexamethasone and after 24h measure miR-29a levels as well as GR protein levels. However, GC resistance might take longer than 24h to develop, and dexamethasone is an artificial GC that in contrast to corticosterone selectively stimulates only GR, not MR. For these reasons, supplying corticosterone in the drinking water of mice is to be preferred for its closer mimicry of pathophysiological circumstances.

Db/db mice are a genetic model of T2D. These mice develop obesity, insulin resistance and are known to have aberrant steroid metabolism: They show higher 11β -HSD1 activity in visceral WAT compared to wt, while in contrast, 11β -HSD1 mRNA was decreased in scWAT (Livingstone et al., 2009). Since 11β -HSD1 reduces the precursor cortisone to the active hormone cortisol in humans, and the precursor 11-dehydrocoticosterone into active corticosterone in mice, it is presumed that higher activity of this enzyme leads to higher local cortisol concentrations, potentially acting on the GR. Moreover, *db/db* mice have elevated levels of circulating corticosterone as well as liver 11β -HSD1, and part of their phenotype could be reversed by administration of RU486, a glucocorticoid receptor antagonist (Liu et al., 2005). As these findings insinuate a dysregulation of GR in *db/db* mice, in order to gain more insight on the miR-29a-GR feedback loop, we examined the levels of miR-29a and GR in *db/db* liver, iWAT and eWAT.
Our results show that miR-29a levels in wt are low in liver and high in both adipose tissue depots, with no significant difference between the depots. Concerning the liver, the low miR-29a levels might explain why corticosterone has been found to induce GR in hepatocytes (Liu et al., 2005) rather than leading to a reduction via the GR-induced miR-29a, as would be expected due to the GR-miR-29a feedback cycle. While miR-29a levels are quite high in wt iWAT and eWAT, we found them to be starkly reduced in both adipose tissues of *db/db* mice, indicating that the dysregulation of miR-29a levels in the adipose tissue might be related to the diabetic phenotype the mice display.

Taking a closer look at the results from *db/db* mice, divergent from wt mice where there was no difference between depots, we can see that in *db/db* mice miR-29a is significantly lower in iWAT compared to eWAT. In line with this finding, in *db/db* mice the protein levels of GR, which again were about the same in wt, were drastically and highly significantly increased in the iWAT compared to the eWAT. Vice versa, eWAT demonstrated the opposite anti-correlation. This adipose depot-specific regulation that occurs in *db/db* mice but not in wt mice indicates that miR-29a might reduce GR levels in these tissues, but for some reason, the feedback loop where GR activity induces miR-29a expression is inactive. Thus, one could argue that loss of the GR-miR-29a feedback loop function might contribute to the pathophysiological phenotype of *db/db* mice.
If we leave behind the adipose depot-specific results and focus on comparing miR-29a and GR levels of *db/db* mice to wt mice, it is apparent that miR-29a levels are elevated in liver, but strongly and highly significantly reduced in the iWAT of *db/db* compared to controls. Unfortunately, we lack information on GR protein levels in the liver. However, in the iWAT of *db/db* mice, GR protein levels are about 3x higher than in wt mice. This shows that firstly, the reduction of miR-29a in *db/db* iWAT is accompanied by a

corresponding increase in GR protein as would be expected if miR-29a targets GR in this tissue. Secondly, as mentioned above, the GR-miR-29a feedback loop seems to be inactive. There is no sig. difference in either miR-29a or GR levels in the eWAT of *db/db* mice compared to wt, although there is a trend towards a reduction of both. These results indicate that surprisingly, despite the more prominent role of GCs in the visceral fat depot, the miR-29a-GR axis and especially the GR-miR-29a feedback loop are dysregulated mainly in the iWAT depot of *db/db* mice.

In summary, there are several points of knowledge gained from these investigations. Firstly, miR-29a levels are significantly lower in the subcutaneous adipose tissue of *db/db* mice compared to wt mice, with the visceral adipose tissue only showing a trend towards reduction. Secondly, miR-29a levels in *db/db* iWAT conceivably lead to the observed significant 3-fold increase in GR protein levels in the same depot, compared to wt mice. Moreover, if one examines the depot-specific regulation of miR-29a vs. GR levels within each genotype, it is striking that while both miR-29a and GR levels are about equal in both WAT depots of wt mice, these levels are significantly anti-correlated in both depots of *db/db* mice. This indicates an intact miR-29a-GR target axis, but also a loss of GR-miR-29a feedback regulation. Thus, one can conclude that while in wt mice, the GR-miR-29a feedback loop keeps levels of miR-29a and GR protein in a tight physiological balance, the dysregulation of these levels due to loss of the feedback loop might contribute to the detrimental metabolic phenotype of *db/db* mice.

In order to fully understand why the GR-miR-29a feedback loop is defective in *db/db* mice, however, one would need to evaluate systemic, and preferably, local corticosterone levels or 11β -HSD1 activity in the WAT of *db/db* mice. Possible explanations would be differing feedback loop kinetics in *db/db* mice, another yet unknown repressor of miR-29a induction, or lowered local GC levels in *db/db* iWAT leading to no miR-29a induction.

In part, a difference in local GC levels due to increased local production of GCs in the visceral depot by 11β-HSD1 may conduce the differential regulation of miR-29a and GR between wt and *db/db* mice (Lee et al., 2014b), as touched upon below: Since *db/db* mice have higher circulating corticosterone levels, this might induce the positive feedforward loop that activates 11β-HSD1 to locally increase GC levels even more, which perhaps is sufficient to activate the GR-miR-29a feedback loop in the visceral WAT depot of *db/db* and thus balance miR-29a and GR levels. Nevertheless, this explanation does not clarify why the feedback loop seems to be disrupted in *db/db* iWAT.

In conclusion, even though more detailed experiments with higher time resolution are necessary to decode the reciprocal regulation of miR-29a and GR in different adipose depots in health vs. metabolic disease states, our results provide an interesting starting point for further investigation.

miR-29a and NR3C1 in human samples

In an effort to analyze whether our findings in mice hold true in humans, we examined levels of miR-29a and NR3C1 mRNA in a well-characterized cohort of patients in various metabolic states. The most striking observation we made is that, even when not correcting for any other phenotypical variation, miR-29a is strongly ($r = -0.4671$) and highly significantly negatively correlated with BMI in both the subcutaneous and the

visceral fat depot. Since low BMI individuals thus have higher miR-29a levels in their adipose tissue, the crucial question to pose is whether miR-29a is contributing causally to leanness, or whether low miR-29a levels are an effect of leanness. One might speculate that in the first case, miR-29a somehow contributes to keeping body weight low and loss of miR-29a expression in adipose tissue facilitates the development of obesity, while in the second scenario, miR-29a is downregulated by conspiring factors in overweight and obesity. Concerning the first scenario, a recent study has found that adipose-specific GR KO mice fed a HFD for 20 weeks show reduced weight gain, lower WAT tissue weight and volume, and smaller adipocyte diameter (Mueller et al., 2017). Assuming that miR-29a expression truly anti-correlates not only with NR3C1 mRNA but also GR protein levels in human WAT, these findings indicate that a role for miR-29 in restricting the development of obesity is indeed conceivable.
In line with the negative correlation with BMI, miR-29a in the subcutaneous as well as the visceral human WAT is anti-correlated with body fat percentage, while NR3C1 mRNA levels trend in the opposite direction, indicating that the miR-29a-GR axis is probably functional in human adipose tissue. Curiously, while NR3C1 mRNA levels are significantly positively correlated with body fat percentage in the visceral fat ($p = 0.0353$), this tendency is not apparent in the subcutaneous depot, where there seems to be almost no variation in the mRNA levels. Of course, one has to keep in mind that for the GR, the mRNA levels do not correlate perfectly with protein levels, as evidenced by our own data (see Fig. 6). However, this illustrates the first aspect of the differential reaction of the subcutaneous and the visceral fat depots to different physiological circumstances, more of which will be discussed below.

The second layer to this dimension of depot-specific regulation is that miR-29a is strongly and significantly negatively correlated with adipocyte diameter in the visceral adipose tissue, but not in the subcutaneous one. In the scWAT, there is no emergent trend for expression levels of either miR-29a or NR3C1 in relation to adipocyte size. Assuming that corticosterone induces miR-29a expression, these observations fit with a study where a wax ball with a fixed dose of corticosterone was implanted subcutaneously in Sprague-Dawley rats for 10 days, followed by ex vivo culture of the adipose tissues. The visceral adipose depot was found to have smaller adipocytes, which had increased in number, which the authors attributed to enhanced adipogenesis (Campbell et al., 2011). Similar results were obtained by a study where C57BL/6J mice were administered with corticosterone in their drinking water, which led to an increase in epidydimal fat accumulation but decreased eWAT adipocyte size (Yu et al., 2014). Thus, high (local) levels of corticosterone would be associated with high miR-29a levels and smaller adipocyte diameter in the visceral WAT.
On the other hand, Cushing's disease, which is characterized by chronically elevated levels of circulating GCs is characterized by an increase in abdominal fat mass, which, intriguingly, affects visceral as well as abdominal subcutaneous fat in humans (Lee et al., 2014a) This increase of 2-5x adipose tissue mass in the abdominal area, both in subcutaneous and visceral depots, is accompanied by a slight but non-significant increase in sc and vis abdominal adipocyte size. In contrast, femoral subcutaneous adipocyte size was reduced, perhaps due to wasting of peripheral scWAT as described for Cushing's

syndrome. (Lee et al., 2014a; Rebuffé-Scrive et al., 1988). These findings contradict the hypothesis described above that GCs lead to decreased visWAT adipocyte size.
The discrepancy might originate in species-specific metabolic differences, since studies described in the first paragraph were conducted in rodents, whereas the last paragraph treats findings in humans. Regardless, these findings suggest that in states of hypercorticoidism, e.g. in Cushing's disease, the anatomic location (abdominal/central vs. peripheral) of the adipose depot might be more predictive of its behavior and function than it being of visceral or subcutaneous origin.

Taken together, these two results might suggest that the miR-29a-GR axis is more important in visceral than in subcutaneous adipose tissue, since the anti-correlation of miR-29a and GR seems more pronounced in visWAT than in scWAT. However, this predicates that the relationship between miR-29a levels and adipocyte size in the visWAT is truly functional, instead of merely correlational, which is of course a speculation. One way to verify this idea would be to inject young mice with miR-29a mimics in order to assess the effect on adipogenesis and adipocyte size after a few weeks or months.

With regards to the negative feedback cycle between GR and miR-29a that we had found *in vitro*, where induction of GR activates transcription of miR-29a, which in turn reduces GR protein levels by directly targeting its 3'UTR, we have found that miR-29a correlates quite profoundly and significantly negatively with systemic cortisol levels in subcutaneous adipose tissue, while NR3C1 expression levels are anti-correlated with miR-29a. In the visceral, there is no significant correlation for either parameter, albeit the correlations trend in a similar direction. Again, it is striking that there seems to be a distinction in how the GC-GR-miR-29a axis is regulated in different fat depots.

One explanation for the diverging responses of subcutaneous and visceral WAT to high GC levels is given by a study that showed that in organ culture, human adipose tissue derived from the visceral depot treated with dexamethasone increased expression of 11β -HSD1, forming a feedforward cycle; these results could not be replicated in subcutaneous adipose tissue culture (Lee et al., 2014b). Another study contributes to this line of argument, showing that adipose-specific overexpression of 11β -HSD1 results in preferential fat accumulation in the visceral over the subcutaneous depots, promoting adipocyte hypertrophy. The resulting higher local availability of GCs in the visWAT but not the scWAT would conceivably lead to higher GR activity, and might tip the scales towards more fat accumulation in the visWAT over the scWAT (Giordano et al., 2013). This is supported by findings that GC turnover in WAT is rather low and possibly unaffected by fluctuations in systemic GC levels (Lee et al., 2014b), putting a greater emphasis on the importance of local tissue GC levels, primarily influenced by biochemical balances. Additionally, despite the short term lipolytic effect of GCs on adipose tissue, GCs seem to promote adipose tissue expansion and adipogenesis in the long term (Lee et al., 2014b). This has a preferential effect on the visceral adipose tissue, which might be explained by the higher GR protein levels that we observed in eWAT of wt mice compared to iWAT. One might speculate that the dysregulation of this ratio in *db/db* mice could contribute to the metabolic defects, for example the insulin resistance

of this T2DM model.

Regarding the effect of the miR-29a-GR feedback loop, it is interesting to note that if one separates the patients by BMI into three groups of lean, overweight and obese, the correlation of miR-29a with cortisol still holds true, but is lost for the obese cohort. This insinuates that the correlation of miR-29a with GC levels, and thus, possibly, the feedback loop of GR to miR-29a, are a marker of healthy weight and somehow get disturbed in the pathological state of obesity.

As a caveat, when comparing results obtained from human adipose tissue and hMADS cells with results of studies in rodents or murine cell models, one should keep in mind that there is some evidence for deviating effects of GCs between the species. *In vitro*, GCs induce lipolysis in murine adipocytes, but have no effect on lipolysis in human cells. Moreover, GCs are required for cell survival during the clonal expansion phase preceding differentiation in 3T3-L1 preadipocytes, while the same is dispensable for human preadipocytes (Lee et al., 2014b). One should also keep in mind that in cell culture, GCs are usually applied in order to induce differentiation of precursor cells into adipocytes, and therefore part of an adipogenic cocktail that commonly includes insulin. GCs have been shown to act synergistically with insulin by shifting away from their sometimes reported lipolytic effect to instead upregulate lipogenesis, a finding that might confound pure *in vitro* results, when comparing to *in vivo* studies.

In summary, there are several dimensions along which the effect of GCs on adipose tissue metabolism and function can vary: depot specificity (visceral vs. subcutaneous WAT), time (acute vs. long-term exposure), species specificity (human vs. mouse) and systemic effects (*in vitro* vs. *in vivo* experiments). These should be kept in mind when interpreting results pertaining interplay of GCs, GR and the miR-29a.

miR-29a and glucocorticoid resistance

Above we had discussed the possible mechanistic details of the miR-29a-GR negative feedback loop. Focusing now on consequences rather than causes, we can ask the question: What is the consequence of this feedback regulation under pathophysiological circumstances?

One might extrapolate from our findings in *db/db* mice as well as measurements in human patients, that under conditions of hyperelevated GC levels, the otherwise delicate balance between miR-29a expression and GR protein levels might be disturbed. At a certain activity of GR, miR-29a could reach such a high level that the balance tips, leading to a reduction of GR. Speculatively, simultaneous repression of putative miR-29a repressors by the miRNA itself or by GR might contribute to this gain in momentum. As an end result, high miR-29a levels would lead to GR reduction, leading to low miR-29a levels due to lack of induction by GR activity. Conceivably, this lack of GR activity could confer defective GC responsiveness, which is one definition of GC resistance (Schlossmacher et al., 2011).

Definitions of GC resistance vary from one pathological context to another; however,

they do share the suspected underlying mechanisms. The most notorious form of GC resistance is perhaps generalized familial GC resistance, also called Chrousos syndrome. This is a rare genetic condition, where tissue GC insensitivity as well as compensatory HPA hyperactivation arise from mutations in the GR gene (Evangelia Charmandari, Tomoshige Kino, 2007).
In cancer, GCs provoke apoptosis in in some entities, most effectively in acute lymphoblastic leukaemia, osteosarcoma and small-cell lung carcinoma. However, there are also cases of GC resistance in these cancers, which are caused by mutations in the GR gene, downregulation of GR at the transcriptional, posttranscriptional or protein level, or alterations in the expression levels of the different GR isoforms and their ratios to each other (Schlossmacher et al., 2011). The ratio between isoforms, especially GRα and GRβ, have additionally been suggested to determine the inflammatory response in adipocytes (Hoppmann et al., 2010). The same mechanism may well be involved in GC resistance in the context of metabolism.
Tissue-specific GC resistance occurs in patients treated chronically with GCs for asthma, rheumatoid arthritis, osteoarthritis, Crohn's disease, ulcerative colitis and asthma (Lu et al., 2007). In asthma, cases defined by decrease in GC receptor number as well as cases with no changes in that number but instead defective DNA binding ability of GR have been observed. Additionally, the ratio between GRα and GRβ isoforms has been discussed as in the context of cancer mentioned above (Szefler and Leung, 1997). For rheumathoid arthritis, all the molecular reasons implicated in cancer-related and asthma-related GC resistance have been suspected, and additionally the phosphorylation status of GR, cross-talk with other signalling pathways like NF-κB, STAT, MAPK and AP-1, as well as changes in the cytokine milieu (Chikanza and Kozaci, 2004). In Chron's disease and ulcerative colitis, the main mechanism as currently understood seem to be reduced intracellular availability of GCs, as well as the inflammatory signalling pathways and reduction of GR protein discussed above (Maltese et al., 2012).
GR protein reduction upon GC treatment has been demonstrated several times *in vitro*, and was described for the first time in 1981: Treatment of HeLa S_3 cells with dexamethasone has been shown to reduce GR receptor number by 70% (Cidlowski and Cidlowski, 1981). Since miR-29a is constitutively expressed in HeLa cells (Kriegel et al., 2012), one may speculate that it could be mediating this effect. A more detailed description of this effect is discussed under "GR activity regulates miR-29a through a negative feedback loop".

Relating back to the mice supplied with corticosterone in their drinking water, as mentioned in "miR-29a and GR in mouse models of obesity and diabetes", if GR receptor number was indeed reduced in these mice, the next logical step would be to administer a dexamethasone suppression test as described by Evangelia Charmandari, Tomoshige Kino, 2007. This test assesses whether a rise in cortisol levels (either physiological as determined by circadian rhyhm, or induced by acute stress) can be suppressed by preceding dexamethasone administration, thus showing whether the HPA-axis feedback to suppress cortisol production is working. Such a test would ascertain whether the GC-miR-29a-GR axis could potentially be involved in mediating a GC resistance phenotype, and help evaluate if miR-29a modulation could potentially represent a promising new

approach to treat clinical GC resistance.

Furthermore, another hint that the relationship between miR-29a and GC resistance might be worth investigating are the findings of Melo and colleagues, who found that patients with systemic lupus erythematosus react less during a dexamethasone suppression test, i.e. show GC resistance (Melo et al., 2013). Strikingly, one of the pathways that emerged from the GSEA analysis at d3 of hMADS cells transfected with miR-29a mimics at d-2 was KEGG_SYSTEMIC_LUPUS_ERYTHEMATOSUS, with an FDR q-value of 0.31, bolstering the link between miR-29a and GC resistance (data not shown).
Conversely, thinking more broadly about the effect of miR-29a on GR levels, it might be valuable to consider that Liu et al. found that transgenic mice overexpressing 11β-HSD1 in adipose tissue have increased local corticosterone levels and GR expression, and develop visceral obesity as well as other negative metabolic side effects on a HFD (Liu et al., 2005). Considering the repressive effect of miR-29a on GR, one might consider exploring whether miR-29a could be used as an antagonist to ameliorate the metabolic state of these animals.

Even though from our current results we cannot conclusively answer the question whether miR-29a can confer GC resistance, these results build a solid base for further exploration of the miR-29a-GR axis in broader metabolic circumstances and systemic metabolic dysfunctions.

Outlook

In summary, our study has found a new role for miR-29 in the adipocyte differentiation in humans, as well as identified a direct target, the GR, which mediates some of its effects. Most intriguingly, we have discovered a previously undescribed negative feedback loop between miR-29a and its target, where the target induces the miRNA that leads to its own repression. Our functional and mechanistic investigations of the miRNA-target interplay as well as descriptive analysis in metabolically challenged mouse models and as human patient samples provide a framework for further investigation of the physiological and pathophysiological impact of the GC-GR-miR-29a axis on metabolism. This could potentially lead to the development of new therapeutic approaches to combat metabolic diseases such as GC resistance, diabetes, and obesity.

MEST in human vs mouse

Our findings that MEST has a negative effect on adipocyte differentiation contrast with the results of Jung et al., who found that MEST enhances adipogenic differentiation of 3T3-L1 cells (Jung et al., 2011). Using an siRNA approach to knock down MEST expression in these cells, they observed enhanced adipogenesis, which they attributed to MEST functionally inhibiting the anti-adipogenic Wnt pathway by blocking maturation of low density lipoprotein receptor-related protein 6 (LRP6). In our study, we did not find upregulation of the Wnt signaling pathway in the gene expression profile of hMADS cells transfected with the siMEST siRNA. On the contrary, we saw a 2-fold increase in DKK1 mRNA levels, an inhibitor of Wnt signaling (data not shown).

This diverging effect on adipocyte development between humans and murine cells may be associated with the stage of commitment of the respective cell system. 3T3-L1 cells are commited to the preadipocyte lineage, while hMADS cells are mesenchymal stem cells still at the multipotent stage. Thus, we cannot exclude that MEST might play a role in preadipocyte commitment rather than differentiation.

Alternatively, we can suspect that species-specific regulatory circuits might be the reason why MEST plays different roles in murine vs. human adipogenesis, as is the case for example for the lim domain only 3 (LMO3) gene (Lindroos et al., 2013)

Mechanism of MEST action

Perhaps the most remarkable aspect of the role of MEST in human adipogenesis may be its yet unidentified enzymatic function. According to UniProt (The UniProt Consortium, 2015), MEST features 3 helical transmembrane regions, as well as, most curiously, a predicted alpha-beta hydrolase fold. This type of domain is commonly associated with hydrolytic enzymes, such as esterases, and importantly, lipases. Thus, the molecular function of MEST might potentially be related to lipolytic activity, and it would be highly interesting to further investigate this potential function in adipocytes by biochemical assays, such as investigating lipolytic activity in siMEST vs. control cells.

MEST as a miR-29a target

As for the discrepancy between the effects of MEST knockdown (increased adipogenesis) and transfection with miR-29a mimics (impaired adipogenesis) in hMADS cells, it is crucial to keep in mind that a miRNA normally targets several mRNAs, and the overall effect may not be determined by a single target. The effect of MEST silencing by miR-29a may be overridden in the context of adipocyte differentiation by simultaneous silencing of other targets, such as NR3C1, which powerfully inhibits adipogenesis. One way to investigate if this is the case would be to ascertain whether the anti-adipogenic miR-29a overexpression phenotype could be rescued by simultaneous silencing of MEST. If not, one can assume that other targets of miR-29a mediate the net negative effect of miR-29a gain of function on human adipocyte differentiation. A similar dominance of one miRNA target over another has been described in the context of leukemia, where miR-196b was published to on the one hand target the oncogenes Hoxa9/Meis1, but on the other hand also directly bind to Fas, a known tumor suppressor. *In vivo*, miR-196 was found to act in an oncogenic way despite simultaneous targeting of the oncogenes, whose levels were still high enough in the pathophysiological situation to permit (in

addition to repression of the tumor suppressor) cancer development (Li et al., 2012). Another point to consider is that not all targets of one miRNA are relevant in one and the same tissue, or developmental/physiological state. It is conceivable that under certain (patho)physiological circumstances, or at certain stages of development, the balance between MEST silencing and NR3C1 silencing by miR-29a would be shifted towards the pro-adipogenic effect, possibly by interference of additional regulators(Bartel, 2009; Mendell and Olson, 2012).

MEST can compensate for lack of IBMX in adipocyte differentiation

The pro-adipogenic effect of MEST on human adipocyte differentiation seems to be particularly germane to early differentation, as silencing of MEST can overcome lack of IBMX in the adipogenic induction medium for hMADS cells, and IBMX is added only from d0 (start of differentiation) to d2. IBMX as a phosphodiesterase inhibitor prevents the degradation of cAMP and cGMP, second messengers that are known to activate protein kinase A (PKA) and G (PKG), which phosphorylate cAMP response element-binding protein (CREB). Ectopic CREB expression is sufficient to induce adipoyte differentiation in 3T3-L1 cells (Reusch et al., 2000). Accordingly, upon investigation of these signaling pathways, our group found that hMADS transfected with siRNAs against MEST showed increased phosphorylation of CREB, as well as increased cGMP levels. Surprisingly, cAMP levels were reduced in siMEST-transfected cells. For these reasons, it was hypothesized that siMEST-induced CREB phosphorylation might be effected via pathways distinct from PKA activation, such as via mitogen-activated protein kinase (MAPK) (Ginty et al., 1994; Reusch et al., 2000), Ca2+/calmodulin-dependent protein kinase (CAMK) (Sheng et al., 1991) or protein kinase C (PKC) signalling (Guo et al., 2012), all of which have been described to phosphorylate CREB in diverse cellular contexts. Further research is necessary to elucidate details of the link between CREB and MEST.

Outlook

Results have so far shown a surprising and diverging role for MEST in the adipocyte development of human in contrast to murine cells. Further experiments are necessary to elucidate the molecular function and mechanistic relationships of MEST in lipid metabolism and development of adipose tissue. Our work provides the basis for these functional investigations needed to fully understand the role and contribution of MEST to adipocyte and systemic metabolism.

Materials and Methods

Materials

Instruments

PRODUCT NAME	COMPANY
Microcentrifuge 5415r	Eppendorf
Cr 4 22 Centrifuge	Jouan
6k16 High Volume Refrigerated Centrifuge	Sigma
Ms1 Minishaker	IKA Works
Mr2001k Magnetic Stirrer & Hotplate	Heidolph
Explorer Analytical Balance	OHAUS
Dna120 Speedvac	ThermoSavant
Thermomixer Compact	Eppendorf
Shaking Incubator 3033	GFL
Water Bath	GFL
Sonopuls Uw2070	Bandelin
Ultra-Turrax T25	IKA
Spectramax Plus384 Absorbance Microplate Reader	Molecular Devices
Heraeus Function Line Incubator Type T 6	Kendro Laboratory Products
Co2-Incubator Cb210	Binder
Laminair Model 1.2	Holten
Ot340 Hotplate	Medite
Ckx41 Inverted Light Microscope	Olympus
C-4040 zoom Digital Camera	Olympus
Nanodrop Nd-1000	Thermo Scientific
Ptc-225 Pcr Cycler	MS Research
Gel Doc 2000 Gel Documentation System	BioRad
Abi Prism 7000 Sequence Detection System	Applied Biosystems
Mini Orbital Shaker Ssm1	Stuart
Genepix 4000b Scanner	Axon Instruments
Mp-300v Agarose Gel Electrophoresis Device	Cleaver Scientific
Gel Doc 2000tm Gel Documentation System	BioRad
Mini Tran-Blot Electrophoretic Transfer Cell	BioRad
Orion Ii Microplate Luminometer	Berthold
Transmitter Arpege40 Liquid N2 Tank	Air Liquide
Benchtop Microfuge 20 1	Beckman Coulter
Balance, Analytical, Entris, 2200g	Sartorius
Balance, Cubis, MSE623S-100DE	Sartorius
Balance, Kern, Plj600-2gm	Kern
Countess Ii Cell Counter	Life Technologies
Heracell™ CO^2 240i Vollkupfer	Thermo Scientific
Magnetic Stirrer Rsm-10hs	Phoenix Instruments
Microcentrifuge Myspin	Thermo Scientific
Nucleofector 4d X+Y Unit	Lonza
Trans-Blot, Turbo Blotting System	BioRad

Vortex Genie 2 G560E	Scientific Industries, Inc
Waterbath Lauda Aqualine AL 25	Lauda
Western Blot Tank Blotting System Mini Trans-Blot® cell	BioRad
ChemiDoc	BioRad
Intas Gel Imager	BioRad
TissueLyser MixerMill	Retsch

Chemicals

PRODUCT NAME	COMPANY	PRODUCT NUMBER
EDTA	Roth	R80431
Sodium dodecyl sulfate (SDS)	Merck	APPCA2263
Methanol	Roth	83885
Sodium dodecyl sulfate (SDS)	Merck	APPCA2263
Sodium Orthovanadate	Sigma	S6508
NaF	Merck	27860.231
β-Glycerophosphate	Sigma	G9891 R
Protease Inhibitor Cocktail (PIC)	Roche	11836170001
TRIS	Roth	5429.3
NaCl	Roth	3957.2
tApo-Transferrin Human	Sigma	T3705-1G
Ampicillin sodium salt	Sigma	A9518-5G
Cycloheximide	Sigma	C1988-1G
dexamethasone Cell culture	Sigma	D4902
Fibroblast Growth Factotr Basic human	Sigma	F0291
3-Isobutyl-1-methylxanthine	Sigma	I7018
LiCl	Sigma-Aldrich	L4408-100G
BIO	Sigma-Aldrich	B1686-5MG
Phenylmethanesulfonyl fluoride >=98.5% (GC)	Sigma-Aldrich	P7626-1G
Dynabeads Protein A for Immunoprecipitation-1 mL	Life Technologies	10001D
NuPAGE MOPS SDS Running Buffer (20X)-500 mL	Life Technologies	NP0001
HCl 1 mol/L	Sigma-Aldrich	35328-1L
16% Formaldehyde (w\/v\), Methanol-free 10 x 10 mL	Fisher Scientific	10321714
Glycogen	Roth	HP51.1
D-Biotin cell culture tested	Sigma	SI B4639-500MG
D-Pantothenic acid hemicalcium salt, cell culture tested	Sigma	P5155-100G
L-ASCORBIC ACID SODIUM	Sigma	SI A4034-100G

CELL CULTURE*TEST ED

Kits

Product Name	Company	Product Number
BCA Protein Assay Kit	Thermo Scientific	23227
Triglycerides Kit	Thermo Scientific	TR22203
Universal cDNA Synthesis Kit II	Exiqon	203301
QuickChange Lightning Site-Directed Mutagenesis Kit	Stratagene	210519
PureLinkTM Quick Gel Extraction Kit	Invitrogen	K2100-12
QIAquick PCR Purification Kit	QIAGEN	28106
QIAprep Spin Miniprep Kit	QIAGEN	21706
QIAamp DNA Mini Kit (50)	QIAGEN	51304
QUANTITECT REV.TRANSCRIPTION KIT (50)	QIAGEN	5000651
P1 Primary Cell 4D-Nucleofector Kit S (32 RXN)	Lonza	V4XP-1032
qPCR Lentivirus Titration (Titer) Kit	Abm	LV900

Consumables

Product Name	Company	Product Number
Cell Scrapers	Becton Dickinson	353087
MicroAmp Optical 96-Well Reaction Plates	Applied Biosystems	N801-0560
MicroAmp Optical Adhesive Film	Applied Biosystems	4311971
0.2 mL PCR Tubes	Biozym	710980
1.5 mL Microcentrifuge Tubes	Sarstedt	72.690.001
2 mL Microcentrifuge Tubes	Biozym	710190
1.5 mL Safe-Lock Tubes	Eppendorf	0030 123.328
15 mL PP Centrifuge Tubes	Corning	430791
50 mL PP Centrifuge Tubes	Greiner Bio-One	227261
10 µL Pipette Tips	Biozym	720031
100 µL Pipette Tips	Greiner Bio-One	685290
1000 µL Pipette Tips	Corning	4868
10 µL Filter Tips	Biozym	693010
100 µL Filter Tips	Biopointescientific	342-4050
1 mL SafeSeal-Tips	Biozym	691000
BIOTRACE NT 0.2UM, 30CMX3M	VWR	732-3031
Extra Thick Blot Paper, 15 x 20 cm, 30 s	BioRad	170-3960

EPPENDORF DNA/RNA LoBIND S/L TUBES,0.5ML	Sigma Aldrich	Z666521-250EA
EPPENDORF PROTEIN LoBIND S/L TUBES,2.0ML	Sigma Aldrich	Z666513-100EA
DNA LoBind Tubes, 2,0ml, PCR clean	Eppendorf	10031282

Cell culture

PRODUCT NAME	COMPANY	PRODUCT NUMBER
Phosphate Buffered Saline (PBS)	Invitrogen	10010015
Dulbecco's Modified Eagle Medium (DMEM) 1g/l Glucose Ham's F12	Lonza	BE12-707F
Ham's F12	Lonza	BE12-615F
Dulbecco's Modified Eagle Medium (DMEM) 4.5 g/l	Invitrogen	41966029
Glucose Fetal Bovine Serum	Pan Biotech	P30-3300
L-Glutamine (200 mm)	Invitrogen	25030024
HEPES Buffer Solution (1M)	Invitrogen	15630-122
Trypsin, 0.5 % (10x) with EDTA	Invitrogen	15400054
Normocin	Invivogen	ant-nr-2
Penicillin-Streptomycin	Invitrogen	15140122
Trypan Blue Solution – 0.4 %	Sigma	T8154
Hemocytometer	Neubauer	T728.1
Cellstar 100 mm Cell Culture Dishes	Greiner Bio-One	664160
Cellstar 145 mm Cell Culture Dishes	Greiner Bio-One	639160
Cell culture 6-well Multiwell Plates	Greiner Bio-One	657160 G
Cell culture 12-well Multiwell Plates	Greiner Bio-One	665180 C
Cell culture 24-well Multiwell Plates	Corning	3524
Cell culture 96-well Multiwell Plates	Corning	3596
Dimethylsulfoxide (DMSO)	Sigma	472301
2 mL Cryotubes	Lactan	E3091
Nuclease-free H2O	Exiqon	203400-02
Aqua Bidestillata Sterilis (ddH2O)	Fresenius Kabi	0698961/01A
HiPerFect Transfection Reagent	QIAGEN	301707
DharmaFECT Duo Transfection Reagent	Dharmacon	T-2010

siGENOME Non-Targeting siRNA pool #2	Dharmacon	D-001206-14-20
miRIDIAN miRNA mimic negative control #1	Dharmacon	CN-001000-01-20
SMARTpool: ON-TARGETplus SRF siRNA	Dharmacon	L-009800-00-0005
Recombinant human Wnt-7a protein	R&D systems	3008-WN-025
Recombinant human Wn-3a protein	R&D systems	5036-WN-010
TransDux Virus Transduction Reagent (200 x)	Biocat	LV850A-1-SBI
Puromycin dihydrochloride25MG	abcam	ab141453-25mg
Mifepristone (RU486)	abcam	ab120356-100mg
hsa-miR-29 miRCURY LNA™ microRNA Power family inhibitor	Exiqon	460039-1
miRCURY LNA™ Power microRNA inhibitor control, 5 nmol	Exiqon	199007-101
negative control B, miRCURY LNA™ microRNA inhibitor control, 5 nmol	Exiqon	199007-001
5 nmol hsa-miR-29a-3p mimic	Dharmacon	C-300504-07-0005
EndoFectin 1ml	Genecopoeia	EFL1001-01
Opti-MEM I Reduced Serum Medium-500 mL	Life technologies	31985047
Lenti-X GoStix, 20 tests	Takara Bio Clontech	631243
Lenti-Pac™ Lentivirus Concentration Solution (50 ml)	Genecopoeia	LPR-LCS-01

Molecular biology & biochemistry

PRODUCT NAME	COMPANY	PRODUCT NUMBER
Platinum SYBR Green qPCR SuperMix-UDG w/ROX	Invitrogen	11744500
PeqGOLD Universal Agarose	PEQLAB	35-1020
1 kb Plus DNA Ladder	Invitrogen	10787-018
100 bp DNA Ladder	Invitrogen	15628-019
6x DNA Loading Dye	Fermentas	R0611
RNASE A,DNASE&PROTEASE FREE 10MG	Thermo Fisher	EN0531
SYBR Green Master Mix, Universal RT	Exiqon	203400
ROX Reference Dye, 1 mm	Roche	04673549001
Proteinase K Solution (20 mg/mL)-1.25 mL	Life Technologies	AM2546

Dynabeads Protein A for Immunoprecipitation-1 mL	Life Technologies	10001D
10x Tris/Glycine/SDS, 1 L	BioRad	161-0732
Nonidet P40 (NP40)	Roche	13269300
Triton X-100	Roth	3051.2
TWEEN 20 Detergent, Molecular Biology Grade	Merck	655204
5S rRNA (hsa, mmu) PCR Primer Set, UniRT	Exiqon	203906
RNU5G (mmu, hsa) PCR Primer Set, UniRT	Exiqon	203908
hsa-miR-29a-3p LNA™ PCR primer set, UniRT	Exiqon	204698
hsa-miR-29b-3p LNA™ PCR primer set, UniRT	Exiqon	204679
hsa-miR-29c-3p LNA™ PCR primer set, UniRT	Exiqon	204729
Bovine serum albumin (BSA)	PAA	K45-001
LEUPEPTIN HEMISULFATE FROM MICROBIAL*SOU RCE	Sigma	SAFSL2884-.5MG
ExiLENT SYBR® Green master mix, 20ml	Exiqon	203421
ATX Ponceau S red staining solution	Fluka	09276
BioTraceTM NT Nitrocellulose Transfer Membrane	Pall	66485
Extra Thick Blot Paper	BioRad	170-3966
NuPAGE Antioxidant	Invitrogen	NP0005
NuPAGE MOPS SDS Running Buffer (20X)	Invitrogen	NP0001
NuPAGE Novex 10% Bis-Tris Gel 1.0 mm, 10 well	Invitrogen	NP0301
Restore Plus Western Blot Stripping Buffer	ThermoScientific	46430
SeeBlue Plus2 Pre-Stained Standard	Invitrogen	LC5925
SimplyBlue SafeStain	Invitrogen	LC6060
SuperSignal West Pico Chemiluminescent Substrate	Pierce	34077
Amersham Hyperfilm ECL (18 x 24 cm)	GE Healthcare	28-9068-36
High Fidelity PCR Enzyme Mix	Fermentas	K0192
PeqGOLD Universal Agarose	PEQLAB	35-1020
Ethidium Bromide Solution 1 %	Lactan	2218.1
GeneRulerTM 1 kb DNA Ladder, 250–10000 bp	Fermentas	SM0311

6x DNA Loading Dye	Fermentas	R0611 I
XhoI Restriction Enzyme	Promega	R6165
NotI Restriction Enzyme	Promega	R6435
4-CORE Buffer Pack	Promega	R9921
Bovine Serum Albumin, Acetylated	Promega	R3961
psiCHECK-2 Luciferase Vector	Promega	C8021
T4 DNA Ligase	Invitrogen	15224017
DH5αTM Competent Cells	Invitrogen	
S.O.C. Medium	Invitrogen	15544034
Select Agar	Sigma	A5054
Pepton	Roth	8986.1
Yeast Extract	Sigma	Y1625
Taq DNA polymerase (recombinant)	Fermentas	EP0402
Dual-Luciferase Reporter Assay System	Promega	E1980
Passive Lysis Buffer (PLB)	Promega	E1941
96-well Assay Plate Flat Bottom, polystyrene, non-treated, white	Costar	3912
Salmon sperm DNA sodium salt (sonified)	Biomol	54653.1
Proteinase K-100mg	Life Technologies	25530015
cOmplete(TM), Mini, EDTA-free,Protease Inhibitor Cocktail Tablets provided in a glass vial	Sigma Aldrich	11836170001

Plasmids

NAME	DESCRIPTION
ORF expression clone for NR3C1 (NM_000176.2) in Lv105, Ex-Z2515-Lv105-B	For Lentivirus production
EGFP control vector for pReceiver-Lv105, EX-EGFP-Lv105	For Lentivirus production
empty control vector for pReceiver-Lv10, EX-NEG-Lv105	For Lentivirus production
psiCHECK^{TM}-2	Promega, for Luciferase assays

Primers

RT-qPCR

GENE	FORWARD PRIMER 5'-3'	REVERSE PRIMER 5'-3'
CEBPα	CTTGTGCCTTGGAAATGCAA	GCTGTAGCCTCGGGAAGGA
CEBPβ	AACCAACCGCACATGCAGAT	GGCAGAGGGAGAAGCAGAGAGT
CEBPγ	GGTGCCCGCTGCAGTTTC	CACGTTTAGCTTCTCTCGCAGTT

		T
FABP4	TGTGCAGAAATGGGATGGAAA	CAACGTCCCTTGGCTTATGCT
FASN	TGAACTCCTTGGCGGAAGAGA	GTAGGACCCCGTGGAATGTCA
GLUT4	CGTCGGGCTTCCAACAGATA	CACCGCAGAGAACACAGCAA
GPDH	TTGTGGTGCCCCATCAGTTC	CCCAATCACTTCCGAGATGA
LPL	TGGAGGTACTTTTCAGCCAGG AT	TCGTGGGAGCACTTCACTAGCT
PGC1A	ACAACACTTACAAGCCAAACCA	GCCTGCAGTTCCAGAGAGTT
PPARA	GGCGAACGATTCGACTCAAG	TCCAAAACGAATCGCGTTGT
PPARG2	CAAACCCCTATTCCATGCTGTT	ATCAGTGAAGGAATCGCTTTCT G
CDK6	CTGCAGGGAAAGAAAAGTGCA A	CTCCTCGAAGCGAAGTCCTC
COL1A1	GTCAGATGGGCCCCCG	GCACCATCATTTCCACGAGC
pri-mir-29ab (hmiR-29a_ HGNC:31616 _F+128, hmiR-29a_ HGNC:31616_R+29)	TCATTCCATTGTGCCTGGGT	ACACCAAAAGAAATCAGTCATC
pri-mir-29bc (hmiR-29a_ ENST00000385231_F+879, hmiR-29a_ ENST00000385231_R+102 2)	TCGACACCATCAGTCTGCTC	TCGGTCAGCCTGTGTAAGAG

Cloning of Luciferase vectors

NAME	SEQUENCE	PURPOSE
DKK1_3UTR_F+0	CATCAGctcgagACCAGCTATCCAAATG CAGTG	Amplification of Dkk1 3'UTR
DKK1_3UTR_R+778	CGGATCgcggccgcTTCACTCTCATTCTG CCATGAT	Amplification of Dkk1 3'UTR
EPAS1_3UTR_F+44	CATCAGctcgagCCAGCTTCACTCTCTCC GTC	Amplification of EPAS1 3'UTR
EPAS1_3UTR_R+2037	CGGATCgcggccgcATGAAATCGTTACG TTGACAGGT	Amplification of EPAS1 3'UTR
MAPK1_3UTR_F+1833	CATCAGctcgagACCAGCTATCCAAATG CAGTG	Amplification of MAPK1 3'UTR
MAPK1_3UTR_R+3045	CGGATCgcggccgcTTCACTCTCATTCTG CCATGAT	Amplification of MAPK1 3'UTR
MEST_3UTR_F+72	CATCAGCTCGAGATGCCCAAAAGAGG TCCTGG	Amplification of MEST 3'UTR
MEST_3UTR_R+1177	CGGATCGCGGCCGCACACTTATTCCA GTTTCAAAGTTGT	Amplification of MEST 3'UTR
NR3C1_all_sm_F+294	CATCAGctcgagGGATGGCACCTAAACC A	Amplification of NR3C1 3'UTR
NR3C1_all_sm_R+2800	GCGATGgcggccgcGGGTTGGGATGGC CAGA	Amplification of NR3C1 3'UTR
g533a_t534c_g535t_c536 a_Fwd	ctgatagctaagtgccatcaggttagaatagtca acccatttcacacagatgattgatt	QuikChange Point mutation of NR3C1

		3’UTR
g533a_t534c_g535t_c536a_Rev	aatcaatcatctgtgtgaaaatgggttgactattctaacctgatggcacttagctatcag	QuikChange Point mutation of NR3C1 3’UTR
g1863a_t1864c_g1865t_c1866a_Fwd	ctattagatggtgcctttaaggatgtaatagtcaccttcctgtctcctgtttacatactt	QuikChange Point mutation of NR3C1 3’UTR
g1863a_t1864c_g1865t_c1866a_Rev	aagtatgtaaacaggagacaggaaggtgactattacatccttaaaggcaccatctaatag	QuikChange Point mutation of NR3C1 3’UTR
g2597a_t2598c_g2599t_c2600a_Fwd	aacacatacataggaaataaatctgctttcaaacatagtcaccatatagcacttaaatccacaattaaacataa	QuikChange Point mutation of NR3C1 3’UTR
g2597a_t2598c_g2599t_c2600a_Rev	ttatgtttaattgtggatttaagtgctatatggtgactatgtttgaaagcagatttatttcctatgtatgtgtt	QuikChange Point mutation of NR3C1 3’UTR
S100A16_3UTR_F+5	CATCAGctcgagCCTTTGGCCACACCTTCCAG	Amplification of S100A16 3’UTR
S100A16_3UTR_R+593	CGGATCgcggccgcAGAGGGACCAGGGGATACAA	Amplification of S100A16 3’UTR
SIAH2_3UTR_F+0	CATCAGctcgagTGTGACTTTCGTAAACCTTCAAAA	Amplification of SIAH2 3’UTR
SIAH2_3UTR_R+922	CGGATCgcggccgcAGCAAGCATATGACACACCG	Amplification of SIAH2 3’UTR
XBP1_3UTR_F+171	CATCAGctcgagTTCCGGAGCTGGGTATCTCA	Amplification of XBP1 3’UTR
XBP1_3UTR_R+965	CGGATCgcggccgcGCTGCATTGTACCTTTTAATTGC	Amplification of XBP1 3’UTR
SeqPrimer_psiCheck2_F+1503	TAAGAAGTTCCCTAACACCG	Sequencing of the psiCHECK-2 vector
SeqPrimer_psiCheck2_R+1742	CGAGGTCCGAAGACTCATTTAG	Sequencing of the psiCHECK-2 vector

ChIP-qPCR

NAME	INTERNAL REFERENCE	SEQUENCE
GR-ENC1	29a_ENCODE_1_Fwd	CCCCAGGGGAAGTGACCTTA
	29a_ENCODE_1_Rev	TGTGGCAACAGCTGAGTAGT
GR-ENC2	29a_ENCODE_2_Fwd	GCCTCAATACTCAGGTTGGGA
	29a_ENCODE_2_Rev	TGGCTTAAGGTCACTTCCCC
GR-ENC3	29a_ENCODE_3_Fwd	TACTAGTGAGCCATGGGGGT
	29a_ENCODE_3_Rev	ACATCTTGAGTTGGGTCCTTGT
GR-ENC-BS3-1	29a_ENCODE_bs3_1_Fwd	AATCAAGCAGGAAGGGGGTG
	29a_ENCODE_bs3_1_Rev	ACAAGTGCCTCTTGGGATGG
GR-ENC-BS3-2	29a_ENCODE_bs3_2_Fwd	GGTTCACCTCCTGGCTTTGA
	29a_ENCODE_bs3_2_Rev	ACCCCCTTCCTGCTTGATTG
ZBTB16	ZBTB16_Anne_Fwd	CTGCCAGCATTCCAGAGAGT
	ZBTB16_Anne_Rev	ACGGTAGTCAAGCCTGCATT
FKBP5	FKBP5_Anne_Fwd	TGCAAAACATCACTTAAACTGGA

	FKBP5_Anne_Rev	CCACATTCAGAACAGGGTGT
GD (gene desert)	GD_IFE_Fwd	AATCACCTTGCATCTGTTTGG
	GD_IFE_Rev	AAAAGGAGAAACCCAGTGGAA
B-Act	bAct_IFE_Fwd	TAGAAGTCGCAGGACCACACT
	bAct_IFE_Rev	TGGGTAGGTTTGTAGCCTTCAT

Antibodies

NAME	SUPPLIER	PRODUCT NUMBER	PURPOSE
Anti-hNR3C1 BuGR2	Thermo Fisher	MA1-510	Western Blot
Anti-β Tubulin	Sigma Aldrich	T5201-100UL	Western Blot
Anti-mNR3C1	Santa Cruz Biotechnology	sc-1004 (M-20)	Western Blot
Anti-mVCP	Abcam	ab11433	Western Blot
Secondary HRP-conjugated goat anti-mouse	Dako	P044701-2	Western Blot
Secondary HRP-conjugated swine anti-rabbit	Dako	P039901-2	Western Blot
Anti-hNR3C1	Santa Cruz Biotechnology	Sc1003-x Rb (E-20)	ChIP
Anti-H3K9Ac ChIP grade	Abcam	ab4441-50ug	ChIP
IgG isotype control (no antibody) rabbit	Thermo Fisher	26102	ChIP

Software

SOFTWARE NAME	SOURCE/SUPPLIER
GraphPad Prism 6 and 7	GraphPad
Illustrator	Adobe
ImageLab	Biorad
ND-1000	Nanodrop
Office	Microsoft
GIMP	www.gimp.org
UCSC Genome Browser	http://genome.ucsc.edu
ImageJ	https://imagej.nih.gov/ij/
R	https://www.r-project.org/

Methods

Cell culture

Culturing and differentiation of hMADS cells

hMADS cells from two different donors were used for experiments in this thesis. hMADS-1 cells were originally extracted from the umbilical area of a female ~2.5 year old donor, hMADS-3 were established from the prepubic region of a 4 month old male donor. Both cell populations have been shown to have a normal karyotype and be able to expand to over 160 population doublings *in vitro* (Rodriguez et al., 2005). hMADS cells have been shown to differentiate into viable white as well as brown/brite adipocytes in culture (Elabd et al., 2009; Pisani et al., 2011).

Cells were cultured in growth medium termed "Medium I" (Table 2) plus the human growth factor hFGF2 added as recombinant protein, in 10 to 15 cm dishes to a visible estimated confluence of 50-70%. Care must be taken to not allow hMADS cells to reach higher than 90% confluence, since this will negatively impact adipogenic differentiation potential. At the desired percentage of confluence, old medium was aspirated and cells were washed 1-2x using at least 50% of the normal medium volume in PBS. Trypsin 0.05% with EDTA in PBS was applied and cells detached during an incubation of 5-7 minutes in the CO2 incubator or on a heating plate at 37°C. The trypsinization reaction was stopped by addition of Medium I. The cell suspension was mixed by cautious pipetting and an adequate aliquot transferred to new culture dishes. The passaging ratio, depending on the growth rate of the cells as well as the starting density, was between 1:2 and 1:5.

For experiments involving differentiation, cells were usually plated in 6-well, 12-well or 24-well plates at the densities indicated in Table 1 and grown in Medium I + hFGF2 until confluence (d-2), when the hFGF2 was withdrawn from the medium for the remaining two days before induction. Medium was changed every 2-3 days, volumes being 600µl, 1ml and 2.5ml per well of 24-well, 12-well and 6-well plate.
Differentiation of hMADS cells was induced on d0, 2 days after cells had reached confluence (denoted as d-2), by changing the medium to "Medium II" (Table 3). Two days later, differentiation was continued by changing to "Medium III" + Rosiglitazone (Table 4) at a final concentration of 100nM.
This was continued until d9 of differentiation, from which point on one can either remove Rosiglitazone to obtain "late white" adipocytes, or keep it in the cocktail to induce a brite adipocyte phenotype.

To ensure viability as well as good differentiation capacity of hMADS cells, all culture media were prewarmed to 37°C in a water bath. PBS and Trypsin were equilibrated at RT before applying them to the cells.

Freezing of hMADS was accomplished by trypsinization and addition of Medium I as described above, followed by centrifugation at 600g for 7min to sediment the cell pellet. After decanting the supernatant, the cell pellet was resuspended in FBS + 10% DMSO, transferred to a cryotube and quickly put on dry ice to freeze. The vials then got transferred to -80°C for max. 1 week, whereafter they were kept in liquid N2 tanks.

hMADS were thawed by transferring them to the cell culture room on ice or dry ice to prevent premature thawing. Cells were then thawed quickly at 37°C in the water bath or by holding them. As soon as the vial content was pourable, it was decanted into 5-10ml prewarmed Medium I. 1ml of this suspension was pipetted back into the cryovial to pick up leftover cells and added back to the suspension. This was then centrifuged at 600g for 7min and the supernatant was decanted to remove any residual DMSO in the supernatant. The pellet was resuspended in Medium I and plated to 10cm culture dishes.

Cells were counted using a Neubauer improved hemocytometer. 50µl of cell suspension was supplemented with 10µl Trypan Blue solution to stain dead cells. This suspension was then filled into 1-2 chambers, of which 4-9 squares were counted. Cell concentration c per ml was determined as follows,

$$c = \frac{n_c}{n_{Sq}} * 12000$$

where n_c is the number of cells counted, n_{Sq} the number of squares that were evaluated, and 12000 is a factor accounting for the depth of the chamber as well as the volume applied.

Table 1: Cell densities plated for differentiation experiments of hMADS cells.

	24-WELL	**12-WELL**	**6-WELL**
hMADS-3	15.000	25.000	40.000
hMADS-1	25.000	40.000	95.000

Table 2:Constituents of hMADS growth medium named "Medium I". As described, hFGF2 was continually added for proliferation, except after the cells had reached 100% confluence, whereupon it was withdrawn from the medium and cells were cultured in Medium I without FGF for 2 days.

MEDIUM I:	
Ingredient	Final concentration
DMEM low glucose (1g/L), no glutamine, 500 ml	
HEPES buffer 1M liquid	10 mM
Glutamine (added freshly every month)	2 mM
Normocin	0.1 mg/ml
FBS	10%
If added: hFGF2	2.5 ng/ml

Table 3: Constituents of hMADS induction medium for adipogenic differentiation named "Medium II"

MEDIUM II	
Ingredient	Final concentration
DMEM low glucose (1g/L), no glutamine, 250 ml	50%

Ham's F12 Nutrient Mixture, no glutamine, 250 ml	50%
HEPES buffer 1M liquid	10 mM
Glutamine (added freshly every month)	2 mM
Normocin	0.1 mg/ml
Human Insulin 10 mg/ml, diluted to 0.1 mg/ml in 25 mM HEPES in PBS	58.08 ng/ml
Apo-Transferrin in H_2O, 10 mg/ml	0.01 mg/ml
T3 in Ethanol, 2µM	0.2 nM
Rosiglitazone in Ethanol, 1 mM	0.1 µM
IBMX in H_2O, single use aliquots 100 mM	0.1 mM
dexamethasone in Ethanol, 1 mM	0.001 mM

Table 4: Constituents of hMADS differentiation medium named "Medium III". As described, Rosiglitazone was added until d9 of differentiation, whereupon it was either withdrawn from the medium, resulting in "late white" adipocytes, or continually added, creating adipocytes with a "brite" phenotype.

MEDIUM III

Ingredient	Final concentration
DMEM low glucose (1g/L), no glutamine, 250 ml	50%
Ham's F12 Nutrient Mixture, no glutamine, 250 ml	50%
HEPES buffer 1M liquid	10 mM
Glutamine (added freshly every month)	2 mM
Normocin	0.1 mg/ml
Human Insulin 10 mg/ml, diluted to 0.1 mg/ml in 25 mM HEPES in PBS	58.08 ng/ml
Apo-Transferrin in H_2O, 10 mg/ml	0.01 mg/ml
T3 in Ethanol, 2µM	0.2 nM
If added: Rosiglitazone in Ethanol, 1 mM	0.1 µM

Transfection of hMADS cells

hMADS were transiently transfected with siRNAs, miRNA mimics or anti-miRNA ASOs using HiPerfect Transfection Reagent according to the manufacturer's instructions, on d-2 unless otherwise specified. Medium was changed to Medium I ~1h before transfection. Aliquots of oligonucleotides were thawed on ice and diluted in PBS or nuclease free water as needed. Transfection mixtures consisted of the appropriate oligonucleotide amount to reach a final concentration between 5 and 25 nM, a 1:1 ratio of µl HiPerfect to pmol oligonucleotides, and the amount of DMEM low glucose needed to reach a transfection volume of 106µl per 12-well or 157.5 µl per 6-well. The reactions were vortexed briefly and incubated for 10 min at RT before dropwise application onto the cells while swaying the plate.

Culture of HEK 293T cells

HEK 293T cells were cultured in growth medium termed "HEK Medium" (Table 5) in 10 cm dishes. Cells were passaged every 2-3 days at a ratio of 1:5 to 1:10. Thawing and freezing were accomplished as with hMADS cells.

Table 5: Constituents of HEK Medium, the growth medium used to culture HEK 293T cells

HEK MEDIUM

Ingredient	Final concentration
DMEM 4.5g/l glucose 500 ml	
10% FBS	10 mM
Pen/Strep	1%

Transfection of HEK 293T cells for Luciferase assays

HEK 293T cells were seeded into 96-well plates at $2^{*}10^{4}$ cells/well 16h before transfection. Cells were co-transfected with reporter vectors and miRNA mimics or inhibitor ASOs using DharmaFECT Duo transfection reagent. Transfection solutions included 100 ng vector plus 10 pmol miRNA mimics in 20 µl DMEM per condition. A second solution per condition was prepared that included 0.6 µl transfection reagent in 20 µl DMEM per well. These two solutions were combined to 40 µl of transfection solution, mixed and incubated at RT for 20-30min. Old medium was aspirated and 80 µl fresh HEK Medium added back. Slowly while swaying the plate we added 20µl transfection reaction per well (final concentration of miRNA mimics/inhibitors: 50 nM). Cells were incubated at 37°C with 5% CO_2 for 48 hours before the harvest (see Luciferase reporter assays).

Production of lentiviral particles for overexpression

HEK 293T cells were seeded at 1.5*10^6 cells per 10 cm dish 3 days before transfection, or at 4*10^6 cells per dish in the morning for transfection next evening, to reach 80-95% confluence at the time of transfection. At the day of transfection, medium was changed to 8 ml fresh HEK Medium without antibiotics per 10 cm dish. The next day, early in the morning, medium was changed to HEK Medium without antibiotics supplemented with 1.1 g/100 ml BSA. Supernatant containing the lentiviral particles was collected once ~36h after transfection, and if desired a second time 24h later at ~50h post transfection. Lentiviral supernatant was centrifuged at 2000g for 10 min at 4°C to sediment cells and debris. The supernatant was then filtered through 0,22µM PES filters. In case of a second harvest, the first supernatant was then stored at 4°C until it can be combined with the second, which was also filtered as described. The lentiviral supernatant was purified and concentrated using GeneCopoeia Lenti-Pac Lentivirus Concentration solution according to the manufacturer's manual. The final viral pellet was dissolved in 1/10 the original volume of sterile PBS and kept on ice until the transduction the same day, or aliquoted and stored at -80°C. Before use or freezing, lentiviral suspensions were titered using the abm qPCR Lentivirus Titration Kit as indicated by the manufacturer's instructions. Briefly, 2µl of the PBS-based, purified lentiviral suspension described above were taken to generate viral lysate, which was consequently subjugated to RT-qPCR using the reagents and primers provided by the kit. The titer was calculated using the formula

$$Titer\ [\frac{IU}{ml}] = 5 * \frac{10^7}{2^{3(Ctx-Ct1)/(Ct2-Ct1)}}$$

where Ct1 is the average Ct value of standard 1 (STD1, included in the kit), Ct2 is the average Ct value of standard 2 (STD2, also included) and Ctx is the average Ct value of the sample to be titered.

For transfection, Opti-MEM, the transfection reagent Endofectin Lenti and the plasmids needed were equilibrated to RT. The plasmids were diluted in Opti-MEM before adding Endofectin, mixing by tapping the tube and spinning down. After a 20 min incubation at RT, the transfection mixture was slowly added onto the cells dropwise while swaying the dish.
Reactions were scaled down by ¼ to transfect 6-well plate wells. Since we used a 3rd generation packaging system, the packaging vectors containing RRE, VSVG and REV were used in roughly equimolar amounts of 3.25 µg, 1.75 µg and 1.25 µg. Master mixes of these packaging vectors were prepared before adding an aliquot to 5-10 µg of lentiviral vector of interest per 10 cm dish, diluted in Opti-MEM.
As per the manufacturer's instructions, the transfection mixture for 1 10 cm dish was 1.5ml total volume, which was divided into 750 µl DNA-Opti-MEM dilution, plus a 750 µl Endofectin-Opti-MEM dilution. 30 µl Endofectin were used per 10 cm dish reaction. Since a transfection efficiency of 80%+ was obtained each time as observed visually by eGFP expression of the control vector, there was no need to further optimize the transfection protocol.

Lentiviral transduction of hMADS cells

hMADS cells were transduced with lentiviral particles either at d-4 or d-3, one or two days before reaching 100% confluency. At the day of transduction, medium was changed to pre-warmed Medium I without antibiotics, supplemented with Transdux (200x stock) as indicated by the manufacturer. For 12-well plates, 600µl per well, and for 6-well plates, 1 ml per well were supplied. After the medium change, the volume of lentiviral suspension necessary to reach the desired MOI (between 1 and 3), kept at 4°C, was dripped slowly unto each well while gently swaying the plate. Cells were then returned to the 37°C CO_2 incubator.
After 8-12h post-transduction, medium is filled up to 1 ml per 12-well plate well and 2.5 ml per 6-well plate well with Medium I without antibiotics.

Molecular biology and biochemistry

RNA isolation from cultured cells

TRIzol lysis reagent was used to isolate total RNA from cell culture as well as tissue samples (see next paragraph). After aspiration of the medium, cells grown in monolayer culture were lysed directly in culture plate by adding ~1 ml of TRIzol per 10 cm^2 of growth area, e.g. 400 µl per well of a 12-well plate. Without scraping, lysis was achieved by pipetting up and down a few times before transferring the sample to a 1.5 ml nuclease-free safelock tube and freezing at -20°C. At the day of isolation, samples were thawed at RT for ~30 min and supplemented with 0.2 ml chloroform per 1 ml of TRIzol and shaken vigorously for 2 min. After 2-3 min of incubation at RT for phase separation, samples were centrifuged at 12.000 g for 17 min at 4°C. The aqueous phase of the resulting separated mixture was transferred to a fresh tube, taking care to avoid

contamination from the DNA- and protein-containing interphase. RNA was precipitated from the aqueous phase by adding 0.5 ml isopropanol per 1 ml TRIzol, mixing by vortexing, incubating for 10 min at RT and centrifuging at 12.000 g for 20 min at 4°C to pellet the precipitate. The RNA pellet was washed by aspirating the supernatant and adding 1 ml ice cold 75% Ethanol per 1 ml TRIzol used. After centrifugation at 7.500 g for 6 min at 4°C, Ethanol was decanted and samples were air-dried or vacuum-dried at RT for 5-30 min. Subsequently, RNA was typically dissolved in 20 µl DEPC-treated RNAse-free water by pipetting up and down several times and incubating for 10 min at 55°C. RNA concentration as well as 260/280 and 260/230 ratios were determined using the NanoDrop spectrophotometer. RNA was frozen for long-term storage at -80°C.

RNA Isolation from mouse tissue

Snap-frozen tissue pieces were kept on dry ice and transferred one at a time to 5 ml tubes containing 1.5 ml TRIzol. The tissue pieces were homogenized using the Ultra-Turrax dispersion instrument for 2-5 sec, then put on ice. The Ultra-Turrax tip was cleaned with Ethanol before homogenizing the next sample.

Centrifugation for 10 min at maximum speed (15.000-20.000 g) at 4°C to separate out the fat cake. The rosé-transparant interphase was transferred to a clean 2 ml tube, to which 300 µl chloroform were added, followed by 10 sec vortexing and 15 min centrifugation as before. The aqueous phase (~800 µl) was transferred to a fresh tube and extracted again with approx. the same volume of chloroform (~800 µl), followed by another round of centrifugation as before. The aqueous phase is transferred to a clean 1.5 ml tube. Subsequently, isolation of RNA is continued as described for cultured cells, except that the washing with ethanol is repeated 3x with 800 µl.

cDNA synthesis from mRNA

RNA was thawed on ice and reverse transcribed to cDNA for RT-qPCR analysis using the Qiagen QuantiTect Reverse Transcription kit. Briefly, 1 µg of RNA is brought to a total volume of 12 µl with DEPC-treated nuclease free water. gDNA is removed by adding 2 µl gDNA Wipeout buffer and incubating for 2' at 42°C, then returning to ice. 6 µl of the prepared master mix containing 4 µl Quantitect RT Buffer, 1 µl RT primer mix and 1 µl RT enzyme were added per sample. The mixture was incubated for 30' at 42°C before stopping the reaction by a 3' incubation at 95°C.

Quantitative RT-PCR

For analysis by RT-qPCR, cDNA solutions were diluted with ddH_2O to the equivalent of 1 ng/µl RNA. RT-qPCR was performed in MicroAmp Optical 96-well or 384 well reaction plates.
Samples were assayed in triplicates using either the ABI PRISM 7000 Sequence Detection System or Thermo Fisher QuantStudio 6 Flex Real-Time PCR system.

Reaction mixes for the two respective systems are detailed in Tables Table 6 and Table 7, the temperature profile of the PCR reactions involved are shown in Figures Figure 16

and. Data were analyzed using the "QPCR real-time PCR data management and analysis" online tool by Stefan Pabinger.

Table 6: RT-qPCR reaction set-up for ABI Prism 7000 sequence detection instrument, 96-well block

COMPONENT	VOLUME [µL]
Invitrogen SYBR QPCR Supermix	9 µl
Forward + Reverse primer mix, 800 nM stock	4.5 µl
1 ng/µl cDNA	4.5 µl

Table 7: RT-qPCR reaction set-up for Quantstudio 6 Flex instrument, 384-well block

COMPONENT	VOLUME [µL]
Invitrogen PowerUp! SYBR Green Mix	5 µl
Forward + Reverse primer mix, 2 µM stock	2 µl
1 ng/µl cDNA	3 µl

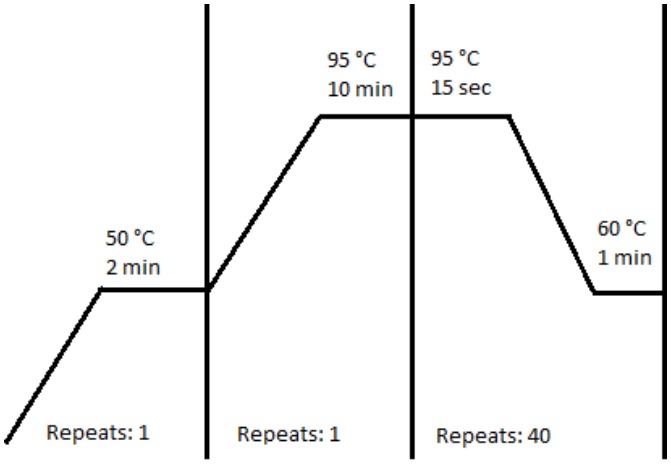

Figure 16: PCR temperature profile for ABI PRISM 7000 Sequence detection machine RT-qPCR runs

Detection of miRNAs by quantitative RT-PCR

miRNAs were quantified using the miRCURY LNA™ Universal RT microRNA PCR system by Exiqon as described by the manufacturer. 20 ng of total RNA were brought to 14 µl total volume with nuclease-free water in 0.2 ml Eppendorf PCR tubes, mixed with 4 µl 5x reaction buffer and 2µl Enzyme mix, followed by incubation at 42°C for 60 min. The reaction is stopped by heat inactivation at 95°C for 5 min. The cDNA is then diluted 1:72 to 1:74 in nuclease-free H_2O.

Commercially available miRNA-specific primer pairs (Exiqon) were dissolved in nuclease-free H_2O as stated by the manufacturer. Primer-specific master mixes are prepared accounting for 5 µl SYBR Green Master Mix, 1 µl primer mix and 0,3 µl ROX stock solution per well (technical replicate). For the ABI PRISM 7000 Sequence Detection System, a 5 µM ROX stock solution was used, yielding a final concentration of 150 nM, while for the Thermo Fisher QuantStudio 6 Flex Real-Time PCR system, a 1 µM ROX stock solution was used to yield a final concentration of 30 nM. Samples were assayed in technical triplicates.

6.4 µl of the primer-specific master-mix were combined with 3.6 µl of diluted cDNA per well.
The remaining steps of the RT-qPCR procedure were carried out as for the conventional SYBR green RT-qPCR described above.

ChIP-qPCR

Buffers used for ChIP are specified in Table 8. Per ml of IP buffer, ChIP lysis buffers and Wash buffers, 20 µl cOmplete Mini Protease Inhibitor Cocktail were added as protease inhibitors.

Stimulation of cells

hMADS cells were grown to confluence in 15 cm dishes, with at least 3 dishes needed per experiment. At confluence, cells were kept in MI and stimulated with 5 µM dexamethasone for ~24h.

Fixing and harvesting cell pellets

At the time of harvest, medium was aspirated and replaced by 18 ml pre-chilled PBS containing 0.75% Methanol-free Formaldehyde (fresh vial opened each time). Cells are fixed for 10 min at RT while shaking at 60-70 rpm. Formaldehyde is quenched with 2 ml 1.25 M Glycine for 5 min at RT. Afterwards, cells are rinsed twice with 10 ml cold PBS and scraped into 5 ml cold PBS to be transferred into a 15 ml tube. Remaining cells are washed off the plate using 3 ml cold PBS and added to the tube. Cells are pelleted for 5 min at 1000 g at 4°C.

Lysing cell pellets

Cells are lysed by adding 1 ml cold IP buffer (+ protease inhibitors) to 1 pellet/tube, pipetted up and down to resuspend and incubated on ice for 10 min. This lysate is then transferred to 2 ml DNA LoBind tubes. The lysate is centrifuged for 1 min at 12000 g at 4°C to yield another pellet. This process is repeated.

Chromatin shearing – using the Qsonica Q800R2

190µl ChIP lysis buffer + protease inhibitors were added to nuclei pellet per 1x 15cm dishes and pipetted up and down. For sonication, 190µl additional ChIP lysis buffer + protease inhibitors were added, to approximate the final volume of our real sonication. Sonication is done in 1.5 ml tubes. Nuclei are sheared for 5 cycles of ~90% power, 30 sec on, 30 sec pause (total: 5min sonication). 25µl were taken out for fragment size check (labeled S1) while adding back 25µl ChIP lysis buffer + protease inhibitors. Nuclei were sheared for another 5 cycles (15c) of ~90% power, 30 sec on, 30 sec pause (total: 7,5min sonication). Again, 25 µl were taken out (labelled S2) and replaced by ChIP lysis lysis. The lysate is then cooled on ice for 5 min. The whole cycle was repeated for 5x to get S1-S7 (5 cycles to 35 cycles). Lysates were transferred to 1.5 ml Eppendorf vials. Lysates were cleared by centrifugation at 12.000 g for 10 min at 4°C. 25 µl aliquots were taken out of the cleared lysate to reverse cross-linking overnight and check fragment size: These were diluted 1+4 in ChIP lysis buffer + protease inhibitors and 5 µl NaCl 5 M, then heated 4-5h or overnight at 65°C. The remaining lysates were kept at 4°C overnight.

Phenol-chloroform DNA extraction of size-check fragments

An equal volume of phenol:chloroform:isoamylalcohol (Invitrogen UltraPure Phenol:Chloroform:Isoamylalcohol) was added to each fragment check sample to yield 125 µl total volume. This mixture was vortexed and centrifuged for 10min at max speed,

4°C. Aqueous upper phase was transferred to fresh tube. Twice the volume (~100µl) cold EtOH (200ul), 1/10th NaAcetate 3M (adjust to pH5,2) (10µl) and 1/20 of µl in µg glycogen were added and briefly vortexed. This mixture was incubated for at least 2h at -20°C or for at leaset 1h at -80°C. Samples were then centrifuge for 15 min at max speed at 4°C. Pellets were washed in 70% EtOH (1/2 vol, 50µl) and centrifuged for 5 min at max speed 4°C. Pellet was dried and resuspended in 30 µl H_2O. 10 µl were loaded on a 1% agarose gel to visualize fragment size. Shearing cycles were added as needed.

Blocking of beads in 2ml DNA LoBind tube

30 µl of Protein A Dynabeads 1ml 30mg/ml, stored at 4°C, were taken per immunoprecipitation (IP) and washed 2x in 0.5% BSA in PBS (1ml). Meanwhile, ssDNA was boiled for 5min at 95°C, then put on ice again. The BSA solution was aspirated and single-stranded herring sperm DNA was added to a final conc. of 75 ng/µl beads. 30 µl beads/IP vial were prepared, plus 15 µl per vial for pre-clearing. BSA was added to beads to a final concentration of 0.1 µg/µl beads. ChIP Lysis buffer was added to twice the bead volume and the resulting mixture was rotated for 2h at RT.

After blocking, the supernatant was removed using the magnetic rack and beads were resuspended in original bead volume of ChIP Lysis buffer + protease inhibitors, then kept on ice until use.

Pre-clearing of chromatin

Chromatin concentration was measured at the NanoDrop after blanking with ChIP lysis buffer. Chromatin was diluted to 150 ng/µl in ChIP lysis buffer + protease inhibitors. It was then pre-cleared by adding 15 µl pre-blocked beads per chromatin corresponding to one 15 cm dish, if necessary, distributed over several DNA LoBind tubes, and incubating for 1h at 4°C on a rotating wheel. Supernatant was then pooled and distributed to three DNA LoBind tubes, corresponding to the three pulldown reactions. 10% or 1% of total volume was taken as "input" before proceeding with the pulldown.

Immunoprecipitation

For each pulldown reaction, 1 µg/100 µl undiluted chromatin of antibody were added: 1.5 µl of 2 µg/µl GR antibody sc1003-x Rb (E-20), 3 µl 1 µg/µl H3K9ac antibody, and 0.6 µl 5 µg/µl IgG isotype control rabbit. These reactions were incubated overnight at 4°C on a rotating wheel.

Washes and elution

The next day, 30 µl pre-blocked beads were added to each IP vial and incubated for 4-6h at 4°C on a rotating wheel. Using the magnetic rack, beads were washed 3x by aspirating supernatant, adding 1 ml ChIP Lysis buffer, rotating for 5min in cold room at 4°C and putting the vial back into the magnetic rack. This wash was repeated twice. One last wash was completed using a 1:1 mixture of ChIP lysis buffer and ChIP Lysis buffer 500 mM (final NaCl concentration: 325 mM). During the washes, 200 µl Bead Elution Buffer were freshly prepared per IP vial. Beads were washed with 1 ml nuclease-free H_2O, which was aspirated carefully. 100 µl Elution buffer were added to the beads, which were vortexed and incubated in the Thermomixer for 15 min at 1000 rpm at RT. Afterwards, tubes were placed in the magnetic rack and the eluate was transferred to a fresh 1.5 ml tube. 100 µl Elution buffer were added to the beads again, and vortexing and incubation was repeated. Tubes were put back in the magnetic rack and the supernatant was combined with the previous eluate, yielding 200 µl eluted, ChIP'ed chromatin.

Reversing cross-linking

8 µl 5 M NaCl and 1 µl 10 mg/ml RNAse A were added to 200 µl of eluate. Samples were incubated at 37°C for 30min. 0.7 µl Proteinase K were added and the mixture was heated overnight at 65°C. The 1% or 10% input samples taken before IP are brought to 200 µl with Elution buffer and treated like the other eluates.

DNA purification

Next day, DNA was purified using the QIAquick PCR purification kit. Briefly, samples were diluted in 5 volumes Binding buffer and processed on the column as indicated by manufacturer's instructions. Purified DNA was eluted in 50 µl ddH_2O and stored at -20°C. Samples were analyzed by RT-qPCR using standard curves for each primer used, and relating the ng pulled down per antibody to the "total" input samples, yielding % pulldown. Samples were assayed in duplicates using 1 µl DNA per well.

Table 8: Buffers used for ChIP.

Lysis in:	**Sonication & IP, as well as first 3 washes:**	**Last wash:**	**Elute with:**
IP buffer	ChIP lysis buffer	ChIP lysis buffer 325 mM	Elution buffer:
150 mM NaCl	0.1% SDS	0.1% SDS	100 mM NaHCO3
5 mM EDTA pH 7.5	1% Triton X-100	1% Triton X-100	1% SDS
50 mM Tris HCl pH 7.5	150 mM NaCl	325 mM NaCl	
1% Triton X-100	1 mM EDTA	1 mM EDTA	
0.5% NP-40	50 mM Tris, pH8	50 mM Tris, pH8	
protease inhibitors			

Oil Red O staining

After aspirating media, monolayer cells were washed with PBS and fixated using 3.6% formaldehyde in PBS for 15 min. Oil Red O stock solution (10 g Oil Red O powder dissolved in 500 ml isopropanol) is diluted 3:2 in ddH_2O to yield the working solution. After 1-2 more washes with PBS, Oil Red O working solution was applied to the cells, which were then incubated for 30 min at RT. Cells are washed again twice with PBS, then overlaid with 50% glycerol in PBS to prevent drying out.

Quantification of triglyceride accumulation

Intracellular triglyceride accumulation was quantified with the Infinity Triglyceride kit. Cells were cultured in 12-well plates in technical duplicates, and harvested at the desired time point by aspirating media, washing with PBS, adding 300 µl PBS per well and scraping the cells. This suspension was transferred to 1.5 ml tubes. Cells were disrupted by ultrasonication for 20 sec at ~40% power of the Sonopuls UW2070.

For the assay, a 4 mM Glycerol stock solution was diluted 1:2 to create a 7-step dilution series. 15 µl of each sample and standard solution were pipetted into a 96-well plate in duplicates. 200 µl Triglycerides Reagent were added per well, followed by incubation of

the plate at 37°C for 10 min. The resulting color shift is recorded using an absorbance plate reader at 500 nm.
The µmolar amount of triglycerides/µl was normalized to mg protein/µl of the same sample. Protein concentration was determined using the Pierce BCA Assay Kit according to manufacturer's instructions. Briefly, the 2 mg/ml BSA standard was diluted in PBS to create a 5-step 1:2 dilution series. 20 µl of each sample, standard solution and the blank were pipetted into a 96-well plate. Reagent B and A were mixed at the ratio of 1:49. 200 µl of this mixture were added to each well, followed by 30 min incubation at 37°C. Afterwards, absorbance is recorded using a plate reader at 562 to 564 nm.

Generation of luciferase reporter vectors

cDNA templates for amplification of the 3'UTR of interest were created by retrotranscribing 1 µg of total hMADS RNA using the Superscript II RT kit. First, DNAse digestion was accomplished in 8 µl total volume containing RNA and 1.8 µl of a DNase + 10x reaction buffer master mix by incubation at 37°C for 1h. This reaction was stopped at 65°C for 5 min. 1 µl dNTP mix (10 mM), 1 µl oligo(dT) primers (500 ng/µl) and 1 µl random hexamer primers (250 ng/µl) were used per reaction.
For PCR amplification of the 3'UTR of interest, different reaction set-ups were used (see Tables Table 9, Table 10 and Table 11). In general terms, a master mix consisting of nuclease-free water, 10x High Fidelity PCR buffer with 15 mM $MgCl_2$, and dNTP mix was added to a solution containing forward and reverse primer as well as the template cDNA. The PCR enzyme mix was either added to the master mix or directly to each single reaction.

Table 9: PCR conditions for 3'UTR amplification of different potential target genes.

3'UTR	Template	Primer 10µM stock F+R[µL]	dNTP mix 10 mM each [µL]	10x High Fidelity PCR buffer 15 mM $MgCl_2$ [µL]	PCR enzyme mix [µL]	Annealing T [°C]	Elongation time [min:sec]	Reaction volume [µL]
EPAS1	25 ng in 0.5 µl	1.5	0.6	3	0.4	52	2:00	30
DKK1	25 ng in 0.5 µl	1.5	0.6	3	0.4	52	2:00	30
MAPK1	50 ng in 0.5 µl	1.5	0.6	3	0.4	56	2:00	30
S100A16	50 ng in 0.5 µl	1.5	0.6	3	0.4	56	1:00	30
SIAH2	50 ng in 0.5 µl	1.5	0.6	3	0.4	56	1:00	30
XBP1	50 ng in 0.5 µl	1.5	0.6	3	0.4	56	1:00	30
NR3C1	100 ng	2.5	0.6	3	0.5	57	2:50	30

	in 2 µl

Table 10: Cycling protocols for PCR amplification of 3'UTRs of potential target genes (EPAS1, DKK1, MAPK1, S100A16, SIAH2, XBP1).

CYCLING PROTOCOL FOR PCR

Step		T[°C]	time [min:sec]
Init. Denaturation		94	03:00
30x	Denaturation	94	00:30
	Annealing	see Table 9	00:30
	Elongation	72	see Table 9
Final Extension		72	10:00
End		4	∞

Table 11: Cycling protocol for PCR amplification of the NR3C1 3'UTR.

CYCLING PROTOCOL FOR PCR

Step		T[°C]	time [min:sec]
Init. Denaturation		94	03:00
35x	Denaturation	94	00:30
	Annealing	see Table 9	00:30
	Elongation	68	see Table 9
Final Extension		72	10:00
End		4	∞

PCR amplification products were mixed with 10 µl 6x loading dye visualized for size checking on an Ethidium bromide-containing agarose gel and subsequently eluted using the Promega Wizard SV Gel and PCR Clean-up System as suggested by the manufacturer. Double digestion using XhoI and NotI at 37°C for 1h in 45 µl reaction volume was followed by inactivation at 80°C for 20min. Alternatively, a reaction volume of 36 µl was used, including 10x buffer, 3µl 100u/µl XhoI and 1.5 µl NotI, following the same thermal protocol. The inserts were ligated into the psiCHECK-2 (pC2) vector backbone at a ratio of 3:1 molarity using T4 ligase. NEB5α C2987 competent *E. coli* were transformed acc. to the instruction manual with the resulting vectors. After incubation in 1 ml SOC medium, 100 µl were plated directly on Ampicillin LB culture plates, while the remaining 900 µl were centrifuged at 4000 g for 1.5 min. The resulting pellet was resuspended in 100 µl SOC and plated in the same way. All plates were incubated overnight at 37°C. Next morning, colonies were picked with one pipette tip to inoculate an ONC (LB medium + 100 µg/ml ampicillin) as well as provide material for performing a colony PCR. PCR conditions were 94°C for 2 min, followed by 30 cycles of 94°C for 30 sec, 50°C for 30 sec and72°C for 1 min, ended by an elongation step of 10 min at 72°C. ONCs were shaken at 37°C. Colony PCR amplification products were visualized on an agarose gel, comparing the size using the GeneRuler 1kB ladder. Glycerol stocks were created from positive colonies by removing 500 µl of the respective ONC, centrifuging for 10 min at 4°C at 4000 g, resuspending the pellet in 50% LB medium, 50% Glycerol and freezing at -80°C. The remaining ONC was mini prepped using the PureLink Quick Plasmid Miniprep Kit as per manufacturer's instructions.

Integrity of the inserts was confirmed by sequencing using primers surrounding the pC2 MCS (for sequences, see “Cloning of Luciferase vectors"). Vectors were used for transfection of HEK 293T cells and subsequent Luciferase reporter assays as described below.

For NR3C1, mutated versions of the pC2-3’UTR construct were generated using the Quik-Change Lightning Site-Directed Mutagenesis Kit. Primers were designed using the online software provided by Agilent (http://www.genomics.agilent.com/primerDesignProgram.jsp) to mutate each one of the 3 seed regions individually, then ordered from IDT (www.idtdna.com) at PAGE purification grade. For primer sequences, see “Cloning of Luciferase vectors”. Primer stocks were established at 1 µg/ml and diluted to 100 ng/ml working solutions in ddH_2O. Each reaction contained 50 ng of the unmutated pC2 construct in 39 µl ddH_2O, 5 µl 10x reaction buffer, 1.25 µl of the respective forward/reverse primer working solutions, 1 µl dNTP mix, 1.5 µl QuikSolution reagent and 1 µl QuikChange Lightning enzyme. PCR conditions were denaturation at 95°C for 2 min, 18 cycles of denaturation at 95°C for 20 sec, annealing for 10 sec at 60°C, and elongation at 68°C for 4 min 25 sec, followed by a final extension at 68°C for 5 min. Amplification products were digested with 2 µl DpnI enzyme solution by incubating at 37°C for 5 min and then placing on ice. This reaction was directly transformed into XL10-Gold ultracompetent cells thawed on ice by mixing the bacterial suspension with 2 µl β-mercaptoethanol and incubating on ice for 2 min. 2 µl of the digestion reaction were added to each bacterial aliquot for transformation, incubated for 30 min on ice, heat-shocked at 42°C for 30 sec and snap-cooled on ice for 2 min again. Transformation reactions were taken up in 500 µl pre-warmed SOC medium and incubated at 37°C for 1h while shaking at 250 rpm. 100 µl of the total bacterial solution were finally plated on LB + Ampicillin 100 µg/ml Agar plates and incubated overnight at 37°C. Next day, colonies were picked to inoculate ONCs (5 ml LB medium + 100 µg/ml Ampicillin). Mini preps were performed as described above and plasmids were sequenced to confirm mutational success. Mutated vectors were used for transfection of HEK 293T cells and subsequent Luciferase reporter assays as described below.

Luciferase reporter assays

HEK 293T cells were seeded at 20.000 cells/well into 96-well culture plates in 100 µl HEK medium per well without antibiotics. Vectors for Luciferase assays were diluted to ~50 ng/µl. miRNA mimic and ASO stocks were thawed on ice and diluted 1:4 in DMEM 4.5 g/L glucose to yield 5 µM working solutions.
Since each reaction was assayed in technical duplicates, 41.2 µl transfection mix was prepared per reaction. 100 ng of the vector, plus 1 µl of each 5 µM working solution of miRNA mimics and ASOs were used per reaction (the latter were omitted for the vector only reaction), yielding a final concentration of 50 nM oligonucleotide per well. Twice this amount (for 2 wells) was diluted in 20.6 µl DMEM and combined with 20.6 µl of a 1:50 Dharmafecten Duo:DMEM mixture. This transfection mixture was mixed by vortexing briefly, and incubated at RT for 20 min.

Old medium was aspirated and replaced by 80 µl antibiotic-free HEK Medium. 20 µl of the transfection mix were added to each well and cells were incubated at 37°C 5% CO_2 overnight.

Luciferase assays were performed using the Promega Dual-Luciferase Reporter Assay System. 30 µl 1x Passive Lysis Buffer (PLB) per well * 1.5 as a volume buffer were prepared prior to harvesting. Medium was aspirated and 96-well plates were washed with 30 µl PBS per well. 30 µl 1x PLB was added per well followed by incubation at RT for 25 min on a shaker at 100 rpm. The resulting lysate was frozen at -20°C or -80°C and thawed to facilitate cell lysis.
Stop & Glo Buffer 50x was pre-warmed at 37°C to resolubilize any precipitates, then diluted 1:50 to yield the volume required (25 µl * 1.5 per well). Aliquots of the Luciferase Assay Buffer II (LARII), stored at -80°C, were thawed (volumes as for Stop & Glo Buffer).
The ORION II microplate luminometer was primed with 70% Ethanol and ddH_2O for cleaning before priming with LARII and Stop & Glo reagents. 6 µl of each lysis sample were transferred to a well of an opaque white 96-well plate. The assay program was started, and the luminometer was washed again after the assay.
The assay program consisted of addition of 25 µl LARII reagent per well, followed by 2s pre-measurement delay, and the measurement of Firefly Luciferase (FL) activity at a photon flux integration time of 10 sec. Then, 25 µl Stop & Glo reagent were added and Renilla luciferase (RL) activity was recorded in the same manner. For analysis, FL values were normalized to respective RL activity. Technical replicates were averaged before comparing samples, which were normalized to the vector only reaction.

Western Blot analysis

Cultured cells were harvested by scraping in a protein extraction buffer (PEB) containing 25 mM Tris-HCl pH 7.4, 100 mM NaCl, 1 mM EDTA, 0.5% Triton X-100, 0.5% Nonidet P40, 0.5 mM sodium orthovanadate, 10 mM NaF, 10 mM β-glycerophosphate, and 1x cOmplete Mini Protease Inhibitor Cocktail. Medium was aspirated, cells were washed on ice with cold PBS and then scraped into ½ of 150 µl per 6-well plate well. After transferring the cell suspension to a 1.5 ml vial, the remaining cells were washed out of the scraped well using the second half of the allocated volume of PEB and pooled with the first suspension. Samples were then sonicated 3x 10 sec at about 40% power of the Sonopuls UW2070 while keeping them on ice. To pellet debris, lysates were centrifuged at 16000 g for 10 min at 4°C and supernatants were aliquoted to 40 µl per vial and stored at -20°C until use.
For tissue samples, tissues were homogenized in Qiagen TissueLyser with 20x (v/w) Buffer A until no visible particles remain. Then, 1:10 volume of buffer B were added and tissues were lysed for another 30-60 sec. For buffer composition see Table 12. Lysates were mixed on a rotating wheel at 4°C for 30 min, then centrifuged at 15000 g for 15 min at 4°C. For a typical piece of WAT (50-100 mg), 500 µl Buffer A and 50 µl Buffer B were used. Protein lysates were aliquoted as described above.
Protein concentration was determined with the Pierce BCA Assay kit. A 5-step 1:2 dilution series of the 2 mg/ml BSA standard was prepared in 0.9% NaCl. 10 µl of each

standard plus 2 µl of PEB were pipetted into a 96-well plate, while 2 µl of each sample plus 10 µl of 0.9% NaCl were used. The remaining BCA assay was conducted as described under "Quantification of triglyceride accumulation".
For PAGE, 40-50 µg of protein per sample and 10 µl SeeBlue Plus2 pre-stained standard were completed with NuPAGE LDS Sample Buffer and 0.5 M DTE to a final volume of 40 µl. Samples were denatured at 70°C for 10 min, then snap-cooled on ice and loaded into the wells of a 10% or 4-12% precast NuPAGE Bis-Tris gel, which had been placed in a gel chamber filled with 1x MOPS SDS Running Buffer supplemented with 500 µl Invitrogen antioxidant solution. Electrophoresis was performed for 1h – 1h 15min at 175V. Subsequently, proteins were transferred to an activated nitrocellulose membrane by wet transfer in a Tris-Gylcine-SDS buffer containing 25 mM Tris, 192 mM glycine, 0.1% SDS and 20% methanol, pH8.3, for 1.5h at 4°C and 0.5 A. Effective transfer was confirmed by Ponceau S staining.
Membranes were blocked in 1-5% Skim Milk Powder in TBST for 1h at RT while shaking, then incubated with the primary antibody overnight at 4°C again in a 1-5% SMP in TBST solution. Specifics for the antibodies used are given in Table 13. The next day, membranes were washed 3x in TBST for 5-10 min by shaking at RT, followed by incubation with the secondary antibody solution for 1-2h as stated in Table 13. Secondary antibody was removed and membranes were washed again 3x for 5-10 min. ECL Plus or SuperSignal West Pico were applied to the membrane as substrate for the HRP-conjugated secondary antibody and incubated for 2-5 min at RT while swaying gently. Chemiluminescence was visualized by exposing and developing Lucent Blue X-ray films, or digitally using the Syngene G:BOX chemi imaging system or the Biorad ChemiDoc.
Membranes were washed with TBST and kept in TBS at 4°C for short term storage. Stripping was performed by incubating with Restore Plus Western Blot stripping buffer for 5-15 min and RT, followed by blocking and re-incubation as indicated by the manufacturer.

Table 12: Buffers used for lysis of tissue samples for Western blot analysis

BUFFER A	BUFFER B
50 mM Tris pH 8	10% NP40
150 mM NaCl	5% sodium deoxycholate
1 tablet cOmplete Mini protease inhibitor per 45 ml	1% SDS

Table 13: Antibody-specific Western blot information

PRIMARY ANTIBODY	PRIMARY ANTIBODY SOLUTION	SECONDARY ANTIBODY SOLUTION	MEMBRANE BLOCKING
Anti-NR3C1 BuGR2 MA1-510 Thermo fisher	1:800 in 5% skim milk powder in TBST	Dako goat anti-mouse 1:5000 in 5% skim milk powder in TBST	5% skim milk powder in TBST
Anti-β-Tubulin	1:2000 in 1% skim	Dako goat anti-	5% skim milk

Sigma	milk powder in TBST	mouse 1:5000 in 1% skim milk powder in TBST	powder in TBST
Anti-NR3C1 sc-1004 (M-20)	1:500 in 2.5 skim milk powder in PBST	Dako swine anti-rabbit 1:5000 in 2.5% skim milk powder in PBST	5% skim milk powder in TBST
Anti-VCP mouse Abcam ab11433	1:10000 in 5% skim milk powder in TBST	Dako goat anti-mouse 1:5000 in 2% skim milk powder in TBST	5% skim milk powder in TBST

Table 14: Primer pairs designed for site-specific point-mutation of the pC2-NR3C1 reporter vector

WT REPORTER VECTOR	PRIMER	PRIMER SEQUENCE 5'-3'	GENERATED REPORTER
pC2-NR3C1	F	ctgatagctaagtgccatcaggttagaatagtcaacccattttcacacagatgattgatt	pC2-N-M1, pC2-N-M-all
	R	aatcaatcatctgtgtgaaaatgggttgactattctaacctgatggcacttagctatcag	
	F	ctattagatggtgcctttaaggatgtaatagtcaccttcctgtctcctgtttacatactt	pC2-N-M2, pC2-N-M-all
	R	aagtatgtaaacaggagacaggaaggtgactattacatccttaaaggcaccatctaatag	
	F	aacacatacataggaaataaatctgctttcaaacatagtcaccatatagcacttaaatccacaattaaacataa	pC2-N-M3, pC2-N-M-all
	R	ttatgtttaattgtggatttaagtgctatatggtgactatgtttgaaagcagatttatttcctatgtatgtgtt	

Abbreviations

11βHSD1	11β-hydroxysteroid dehydrogenase type 1
18F-FDG	18F-fluorodeoxyglucose
ACTH	adrenocorticotropic hormone
AGO	Argonaute
Akt	also known as Protein kinase B
ANGPTL4	Angiopoietin-like 4
AP1	Activator protein 1
AP2/FABP4	adipocyte protein 2/fatty acid binding protein 4
BAT	brown adipose tissue
BCA	bicinchoninic acid
BIO	6-bromoindirubin-3'-oxime
BMI	body mass index
BMP	bone morphogenetic proteins
C/EBPα	CCAAT/Enhancer Binding Protein Alpha
C/EBPɣ	CCAAT/Enhancer Binding Protein Gamma
C/EBPβ	CCAAT/Enhancer Binding Protein Beta
C/EBPδ	CCAAT/Enhancer Binding Protein Delta
CAMK	Ca2+/calmodulin-dependent protein kinase
cAMP	cyclic adenosine monophosphate
CDS	coding sequence
ChIP	chromatin immunoprecipitation
Cidea	Cell death activator
COX8B	cytochrome c oxidase subunit VIIIb
CREB	cAMP-responsive element-binding
CRH	corticotropin releasing hormone
CT	computerized tomography
Dex	dexamethasone
DIO2	Type II iodothyronine deiodinase
DKK1	dickkopf homologue 1
DMEM	Dulbecco's Modified Eagle Medium
ECM	extracellular matrix
EPAS1	endothelial PAS domain protein 1
ERK1/2	Mitogen-activated protein kinase 3 and 1
eWAT	epididymal WAT
FKBP5	FK506 Binding Protein 5
FTO	Fat mass and obesity-associated protein
GAP	GTPase-activating protein
GCR	glucocorticoid receptor resistance
GCs	Glucocorticoids
gDNA	genomic DNA
GEF	guanine nucleotide exchange factors
GFP	green fluorescent protein
GLUT4	Glucose transporter type 4
GLUT4	glucose transporter type 4
GPDH	glycerol-3-phosphate dehydrogenase

GR	glucocorticoid receptor
GWAS	genome-wide association study
H3K9ac	Histone 3 Lysine 9 acetylation
HCV	hepatitis C virus
HDAC1	Histone deacetylase 1
hMADS cells	human Multipotent Adipose-Derived Stem cells
hnRNPA1	Heterogeneous nuclear ribonucleoprotein A1
HPA	hypothalamo-pituitary-adrenal
HSP	heat shock protein
IBMX	3-isobutyl-1-methylxanthine
IL-1β	interleukin 1 beta
IL-5	interleukin 5
IRS2	insulin receptor 1
IRS2	insulin receptor 2
iWAT	inguinal WAT
KLF	kruppel-like factor
KRAS	V-Ki-ras2 Kirsten rat sarcoma viral oncogene homolog
LiCl	lithium chloride
LNA	locked nucleic acid
LPL	lipoprotein lipase
LPL	lipoprotein lipase
LPS	lipopolysaccharide
MAPK1	mitogen-activated protein kinase 1
MED1	Mediator of RNA Polymerase II transcription subunit 1
MEST	mesoderm-specific transcript homologue
miRISC	miRNA-Induced Silencing Complex
miRNA	microRNA
MMP	matrix metalloproteinase peptidase
MOI	multiplicity of infection
MRE	microRNA regulatory element
MSCs	multipotent stem cells
NGT	normal glucose tolerant/tolerance
pASO	power antisense oligonucleotide
PBS	phosphate-buffered saline
PCR	polymerase chain reaction
PEB	protein extraction buffer
PET	positron emission tomography
PGC-1α	Peroxisome proliferator-activated receptor gamma coactivator 1-alpha
PI3K	Phosphoinositide 3-kinase
PKA	protein kinase A
PKC	protein kinase C
POMC	Pro-opiomelanocortin
PPARα	peroxisome proliferator-activated receptor alpha
PPARɣ	Peroxisome proliferator-activated receptor gamma
PPARɣ	peroxisome proliferator-activated receptor gamma
PRDM16	PR domain containing 16
pre-miRNA	precursor microRNA

pri-miRNA	primary microRNA
RB2/p130	Retinoblastoma-like protein 2
RHO	Ras homolog gene family
RT	reverse transcription, or room temperature
RT-qPCR	Real-time quantitative PCR
S100A16	S100 calcium binding protein A16
scWAT	subcutaneous WAT
SIAH2	seven in absentia homologue 2
SNP	single nucleotide polymorphism
T1DM	type I diabetes mellitus
T2DM	type II diabetes mellitus
TCF/LEF	T-cell factor/lymphoid enhancer factor
TCF7L2	transcription factor 7 like 2
TG	triglyceride
TGFBR2	TGF beta receptor 2
TGFβ	Transforming Growth factor β
TNFα	Tumor necrosis factor alpha
TNFα	tumor necrosis factor alpha
TRBP	HIV-1 TAR RNA binding protein
TSS	transcription start site
UCP1	uncoupling protein 1
UTR	untranslated region
visWAT	visceral WAT
WAT	white adipose tissue
Wnt	Wingless-related integration site
XBP1	x-box binding protein
ZBTB16	Zinc Finger And BTB Domain Containing 16

List of Figures

List of Tables

Bibliography

Allison, D.B., Kaprio, J., Korkeila, M., Koskenvuo, M., Neale, M.C., and Hayakawa, K. (1996). The heritability of body mass index among an international sample of monozygotic twins reared apart. Int. J. Obes. Relat. Metab. Disord. *20*, 501–506.

Arner, P., Bernard, S., Salehpour, M., Possnert, G., Liebl, J., Steier, P., Buchholz, B. a., Eriksson, M., Arner, E., Hauner, H., et al. (2011). Dynamics of human adipose lipid turnover in health and metabolic disease. Nature *478*, 110–113.

Bader, A.G. (2012). miR-34 - a microRNA replacement therapy is headed to the clinic. Front. Genet. *3*, 120.

Bannister, A.J., and Kouzarides, T. (2011). Regulation of chromatin by histone modifications. Cell Res. *21*, 381–395.

Bartel, D.P. (2009). MicroRNAs: Target Recognition and Regulatory Functions. Cell *136*, 215–233.

Beg, M.S., Brenner, A.J., Sachdev, J., Borad, M., Kang, Y.-K., Stoudemire, J., Smith, S., Bader, A.G., Kim, S., and Hong, D.S. (2016). Phase I study of MRX34, a liposomal miR-34a mimic, administered twice weekly in patients with advanced solid tumors. Invest. New Drugs.

Bernstein, E., Kim, S.Y., Carmell, M.A., Murchison, E.P., Alcorn, H., Li, M.Z., Mills, A.A., Elledge, S.J., Anderson, K. V, and Hannon, G.J. (2003). Dicer is essential for mouse development. *35*, 215–217.

Berry, R., Jeffery, E., and Rodeheffer, M.S. (2014). Weighing in on adipocyte precursors. Cell Metab. *19*, 8–20.

Betel, D., Wilson, M., Gabow, A., Marks, D.S., and Sander, C. (2008). The microRNA.org resource: Targets and expression. Nucleic Acids Res. *36*, D149–D153.

Birkenmeier, E.H., Gwynn, B., Howard, S., Jerry, J., Gordon, J.I., Landschulz, W.H., and McKnight, S.L. (1989). Tissue-specific expression, developmental regulation, and genetic mapping of the gene encoding {CCAAT}/enhancer binding protein. Genes Dev. *3*, 1146–1156.

Böttcher, Y., Unbehauen, H., Klöting, N., Ruschke, K., Körner, A., Schleinitz, D., Tönjes, A., Enigk, B., Wolf, S., Dietrich, K., et al. (2009). Adipose tissue expression and genetic variants of the bone morphogenetic protein receptor 1A gene (BMPR1A) are associated with human obesity. Diabetes *58*, 2119–2128.

Brestoff, J.R., and Artis, D. (2015). Immune Regulation of Metabolic Homeostasis in Health and Disease. Cell *161*, 146–160.

Campbell, J.E., Peckett, A.J., D'souza, A.M., Hawke, T.J., and Riddell, M.C. (2011). Adipogenic and lipolytic effects of chronic glucocorticoid exposure. Am. J. Physiol. Cell Physiol. *300*, C198-209.

Carè, A., Catalucci, D., Felicetti, F., Bonci, D., Addario, A., Gallo, P., Bang, M.-L., Segnalini, P., Gu, Y., Dalton, N.D., et al. (2007). MicroRNA-133 controls cardiac hypertrophy. Nat. Med. *13*, 613–618.

Cecil, J.E., Tavendale, R., Watt, P., Hetherington, M.M., and Palmer, C.N.A. (2008). An obesity-associated FTO gene variant and increased energy intake in children. N. Engl. J. Med. *359*, 2558–2566.

Chen, Z., Zhang, L., Xia, L., Jin, Y., Wu, Q., Guo, H., Shang, X., Dou, J., Wu, K., Nie, Y., et al. (2014). Genomic analysis of drug resistant gastric cancer cell lines by combining mRNA and microRNA expression profiling. Cancer Lett.

Chikanza, I.C., and Kozaci, D.L. (2004). Corticosteroid resistance in rheumatoid arthritis: Molecular and cellular perspectives. Rheumatology *43*, 1337–1345.

Cidlowski, J.A., and Cidlowski, N.B. (1981). Regulation of glucocorticoid receptors by glucocorticoids in cultured HeLa S3 cells. Endocrinology *109*, 1975–1982.

Cinti, S. (2001). The adipose organ: morphological perspectives of adipose tissues. Proc. Nutr. Soc. *60*, 319–328.

Cinti, S. (2005). The adipose organ. Prostaglandins. Leukot. Essent. Fatty Acids *73*, 9–15.

Clevers, H., and Nusse, R. (2012). Wnt/β-catenin signaling and disease. Cell *149*, 1192–1205.

Clop, A., Marcq, F., Takeda, H., Pirottin, D., Tordoir, X., Bibé, B., Bouix, J., Caiment, F., Elsen, J.-M., Eychenne, F., et al. (2006). A mutation creating a potential illegitimate microRNA target site in the myostatin gene affects muscularity in sheep. Nat. Genet. *38*, 813–818.

Cohade, C., Osman, M., Pannu, H.K., and Wahl, R.L. (2003). Uptake in supraclavicular area fat ("USA-Fat"): description on 18F-FDG PET/CT. J. Nucl. Med. *44*, 170–176.

Cohen, S., Janicki-Deverts, D., Doyle, W.J., Miller, G.E., Frank, E., Rabin, B.S., and Turner, R.B. (2012). Chronic stress, glucocorticoid receptor resistance, inflammation, and disease risk. Proc. Natl. Acad. Sci. U. S. A. *109*, 5995–5999.

Cole, T.J., Blendy, J.A., Monaghan, A.P., Krieglstein, K., Schmid, W., Aguzzi, A., Fantuzzi, G., Hummler, E., Unsicker, K., and Schütz, G. (1995). Targeted disruption of the glucocorticoid receptor gene blocks adrenergic chromaffin cell development and severely retards lung maturation. Genes Dev. *9*, 1608–1621.

Cortez, M.A., Bueso-Ramos, C., Ferdin, J., Lopez-Berestein, G., Sood, A.K., and Calin, G.A. (2011). MicroRNAs in body fluids--the mix of hormones and biomarkers. Nat. Rev. Clin. Oncol. *8*, 467–477.

Cristancho, A.G., and Lazar, M.A. (2011). Forming functional fat: a growing understanding of adipocyte differentiation. Nat. Rev. Mol. Cell Biol. *12*, 722–734.

Cypess, A.M., Lehman, S., Williams, G., Tal, I., Rodman, D., Goldfine, A.B., Kuo, F.C., Palmer, E.L., Tseng, Y.-H., Doria, A., et al. (2009). Identification and importance of brown adipose tissue in adult humans. N. Engl. J. Med. *360*, 1509–1517.

Dai, X., Pang, W., Zhou, Y., Yao, W., Xia, L., Wang, C., Chen, X., Zen, K., Zhang, C.Y., and Yuan, Y. (2016). Altered profile of serum microRNAs in pancreatic cancer-associated new-onset diabetes mellitus. J. Diabetes *8*, 422–433.

Dangwal, S., and Thum, T. (2013). microRNA Therapeutics in Cardiovascular Disease Models. Annu. Rev. Pharmacol. Toxicol.

Davis, E.K., Zou, Y., and Ghosh, A. (2008). Wnts acting through canonical and noncanonical signaling pathways exert opposite effects on hippocampal synapse formation. Neural Dev. *3*, 32.

Deng, M., Tufan, T., Raza, M.U., Jones, T.C., and Zhu, M.-Y. (2016). MicroRNAs 29b and 181a down-regulate the expression of the norepinephrine transporter and glucocorticoid receptors in PC12 cells. J. Neurochem. *139*, 197–207.

Deree, J., Martins, J.O., Melbostad, H., Loomis, W.H., and Coimbra, R. (2008). Insights into the regulation of TNF-alpha production in human mononuclear cells: the effects of non-specific phosphodiesterase inhibition. Clinics (Sao Paulo). *63*, 321–328.

Dong, Y., Poellinger, L., Gustafsson, J.A., and Okret, S. (1988). Regulation of glucocorticoid receptor expression: evidence for transcriptional and posttranslational mechanisms. Mol. Endocrinol. *2*, 1256–1264.

Dooley, J., Garcia-Perez, J.E., Sreenivasan, J., Schlenner, S.M., Vangoitsenhoven, R., Papadopoulou, A.S., Tian, L., Schonefeldt, S., Serneels, L., Deroose, C., et al. (2016). The microRNA-29 family dictates the balance between homeostatic and pathological glucose handling in diabetes and obesity. Diabetes *65*, 53–61.

Ebert, M.S., and Sharp, P.A. (2012). Roles for MicroRNAs in conferring robustness to biological processes. Cell *149*, 505–524.

Elabd, C., Chiellini, C., Massoudi, A., Cochet, O., Zaragosi, L.-E., Trojani, C., Michiels, J.-F., Weiss, P., Carle, G., Rochet, N., et al. (2007). Human adipose tissue-derived multipotent stem cells differentiate in vitro and in vivo into osteocyte-like cells. Biochem. Biophys. Res. Commun. *361*, 342–348.

Elabd, C., Chiellini, C., Carmona, M., Galitzky, J., Cochet, O., Petersen, R., Pénicaud, L., Kristiansen, K., Bouloumié, A.,

Casteilla, L., et al. (2009). Human multipotent adipose-derived stem cells differentiate into functional brown adipocytes. Stem Cells *27*, 2753–2760.
Esau, C., Kang, X., Peralta, E., Hanson, E., Marcusson, E.G., Ravichandran, L. V, Sun, Y., Koo, S., Perera, R.J., Jain, R., et al. (2004). {MicroRNA}-143 {Regulates} {Adipocyte} {Differentiation}. J. Biol. Chem. *279*, 52361–52365.
Essayan, D.M. (2001). Cyclic nucleotide phosphodiesterases. J. Allergy Clin. Immunol. *108*, 671–680.
Euskirchen, G.M., Rozowsky, J.S., Wei, C.-L., Lee, W.H., Zhang, Z.D., Hartman, S., Emanuelsson, O., Stolc, V., Weissman, S., Gerstein, M.B., et al. (2007). Mapping of transcription factor binding regions in mammalian cells by ChIP: Comparison of array- and sequencing-based technologies. Genome Res. *17*, 898–909.
Evangelia Charmandari, Tomoshige Kino, G.P.C. (2007). Primary Generalized Familial and Sporadic Glucocorticoid Resistance (Chrousos Syndrome) and Hypersensitivity. October *454*, 42–54.
Farmer, S.R. (2006). Transcriptional control of adipocyte formation. Cell Metab. *4*, 263–273.
Fasshauer, M., Klein, J., Neumann, S., Eszlinger, M., and Paschke, R. (2002). Hormonal Regulation of Adiponectin Gene Expression in 3T3-L1 Adipocytes. Biochem. Biophys. Res. Commun. *290*, 1084–1089.
Frontini, A., and Cinti, S. (2010). Distribution and development of brown adipocytes in the murine and human adipose organ. Cell Metab. *11*, 253–256.
Galic, S., Oakhill, J.S., and Steinberg, G.R. (2010). Adipose tissue as an endocrine organ. Mol. Cell. Endocrinol. *316*, 129–139.
Gesta, S., Tseng, Y.-H., and Kahn, C.R. (2007). Developmental origin of fat: tracking obesity to its source. Cell *131*, 242–256.
Ginty, D.D., Bonni, A., and Greenberg, M.E. (1994). Nerve growth factor activates a Ras-dependent protein kinase that stimulates c-fos transcription via phosphorylation of CREB. Cell *77*, 713–725.
Giordano, A., Murano, I., Mondini, E., Perugini, J., Smorlesi, A., Severi, I., Barazzoni, R., Scherer, P.E., and Cinti, S. (2013). Obese adipocytes show ultrastructural features of stressed cells and die of pyroptosis. J. Lipid Res. *54*, 2423–2436.
Girard, J., and Lafontan, M. (2008). Impact of visceral adipose tissue on liver metabolism and insulin resistance. Part II: Visceral adipose tissue production and liver metabolism. Diabetes Metab. *34*, 439–445.
Goudenege, S., Pisani, D.F., Wdziekonski, B., Di Santo, J.P., Bagnis, C., Dani, C., and Dechesne, C.A. (2009). Enhancement of myogenic and muscle repair capacities of human adipose-derived stem cells with forced expression of MyoD. Mol. Ther. *17*, 1064–1072.
Green, H., and Kehinde, O. (1975). An established preadipose cell line and its differentiation in culture. II. Factors affecting the adipose conversion. Cell *5*, 19–27.
Green, H., and Meuth, M. (1974). An established pre-adipose cell line and its differentiation in culture. Cell *3*, 127–133.
Grøntved, L., John, S., Baek, S., Liu, Y., Buckley, J.R., Vinson, C., Aguilera, G., and Hager, G.L. (2013). C/EBP maintains chromatin accessibility in liver and facilitates glucocorticoid receptor recruitment to steroid response elements. EMBO J. *32*, 1–16.
Gross, B., Pawlak, M., Lefebvre, P., and Staels, B. (2016). PPARs in obesity-induced T2DM, dyslipidaemia and NAFLD. Nat. Rev. Endocrinol. *13*, 36–49.
Gross, B., Pawlak, M., Lefebvre, P., and Staels, B. (2017). PPARs in obesity-induced T2DM, dyslipidaemia and NAFLD. Nat. Rev. Endocrinol. *13*, 36–49.
Guo, C.M., Kasaraneni, N., Sun, K., and Myatt, L. (2012). Cross talk between PKC and CREB in the induction of COX-2 by PGF2α in human amnion fibroblasts. Endocrinology *153*, 4938–4945.
Han, B.W., Hung, J.-H., Weng, Z., Zamore, P.D., and Ameres, S.L. (2011). The 3'-to-5' exoribonuclease Nibbler shapes the 3' ends of microRNAs bound to Drosophila Argonaute1. Curr. Biol. *21*, 1878–1887.
Han, J., Lee, Y., Yeom, K.H., Nam, J.W., Heo, I., Rhee, J.K., Sohn, S.Y., Cho, Y., Zhang, B.T., and Kim, V.N. (2006). Molecular Basis for the Recognition of Primary microRNAs by the Drosha-DGCR8 Complex. Cell *125*, 887–901.
Hany, T.F., Gharehpapagh, E., Kamel, E.M., Buck, A., Himms-Hagen, J., and von Schulthess, G.K. (2002). Brown adipose tissue: a factor to consider in symmetrical tracer uptake in the neck and upper chest region. Eur. J. Nucl. Med. Mol. Imaging *29*, 1393–1398.
Hauner, H., and Entenmann, G. (1991). Regional variation of adipose differentiation in cultured stromal-vascular cells from the abdominal and femoral adipose tissue of obese women. Int. J. Obes. *15*, 121–126.
He, A., Zhu, L., Gupta, N., Chang, Y., and Fang, F. (2007a). Overexpression of Micro Ribonucleic Acid 29, Highly Up-Regulated in Diabetic Rats, Leads to Insulin Resistance in 3T3-L1 Adipocytes. Mol. Endocrinol. *21*, 2785–2794.
He, A., Zhu, L., Gupta, N., Chang, Y., and Fang, F. (2007b). Overexpression of micro ribonucleic acid 29, highly up-regulated in diabetic rats, leads to insulin resistance in 3T3-{L}1 adipocytes. Mol. Endocrinol. *21*, 2785–2794.
Hilton, C., Neville, M.J., and Karpe, F. (2013). {MicroRNAs} in adipose tissue: their role in adipogenesis and obesity. Int. J. Obes. (Lond). *37*, 325–332.
Hinds, T.D., Stechschulte, L.A., Cash, H.A., Whisler, D., Banerjee, A., Yong, W., Khuder, S.S., Kaw, M.K., Shou, W., Najjar, S.M., et al. (2011). Protein phosphatase 5 mediates lipid metabolism through reciprocal control of glucocorticoid receptor and peroxisome proliferator-activated receptor-?? (PPAR??)*. J. Biol. Chem. *286*, 42911–42922.
Hoppmann, J., Perwitz, N., Meier, B., Fasshauer, M., Hadaschik, D., Lehnert, H., and Klein, J. (2010). The balance between gluco- and mineralo-corticoid action critically determines inflammatory adipocyte responses. J. Endocrinol. *204*, 153–164.
Huang, H., Song, T.-J., Li, X., Hu, L., He, Q., Liu, M., Lane, M.D., and Tang, Q.-Q. (2009). BMP signaling pathway is required for commitment of C3H10T1/2 pluripotent stem cells to the adipocyte lineage. Proc. Natl. Acad. Sci. *106*, 12670–12675.
Hudson, M.E., and Snyder, M. (2006). High-throughput methods of regulatory element discovery. Biotechniques *41*, 673, 675, 677 passim.
Iliopoulos, D., Drosatos, K., Hiyama, Y., Goldberg, I.J., and Zannis, V.I. (2010). {MicroRNA}-370 controls the expression of {microRNA}-122 and {Cpt}1{alpha} and affects lipid metabolism. J. Lipid Res.
Inui, M., Martello, G., and Piccolo, S. (2010). MicroRNA control of signal transduction. Nat. Rev. Mol. Cell Biol. *11*, 252–263.
Janssen, H.L.A., Reesink, H.W., Lawitz, E.J., Zeuzem, S., Rodriguez-Torres, M., Patel, K., van der Meer, A.J., Patick, A.K., Chen, A., Zhou, Y., et al. (2013). Treatment of HCV infection by targeting microRNA. N. Engl. J. Med. *368*, 1685–1694.
Jeong Kim, Y., Jin Hwang, S., Chan Bae, Y., and Sup Jung, J. (2009). MiR-21 regulates adipogenic differentiation through the modulation of TGF-beta signaling in mesenchymal stem cells derived from human adipose tissue. Stem Cells *27*, 3093–3102.
Ji, J., Shi, J., Budhu, A., Yu, Z., Forgues, M., Roessler, S., Ambs, S., Chen, Y., Meltzer, P.S., Croce, C.M., et al. (2009). {MicroRNA} expression, survival, and response to interferon in liver cancer. N. Engl. J. Med. *361*, 1437–1447.
Jinek, M., and Doudna, J.A. (2009). A three-dimensional view of the molecular machinery of RNA interference. Nature *457*, 405–412.
John, K., Marino, J.S., Sanchez, E.R., and Hinds, T.D. (2015). The Glucocorticoid Receptor: Cause or Cure for Obesity? Am. J. Physiol. - Endocrinol. Metab. ajpendo.00478.2015.
John, S., Sabo, P.J., Thurman, R.E., Sung, M.-H., Biddie, S.C., Johnson, T.A., Hager, G.L., and Stamatoyannopoulos, J.A. (2011). Chromatin accessibility pre-determines glucocorticoid receptor binding patterns. Nat. Genet. *43*, 264–268.
Jung, H., Lee, S.K., and Jho, E. (2011). Mest/Peg1 inhibits Wnt signalling through regulation of LRP6 glycosylation. Biochem. J. *436*, 263–269.
Juvvuna, P.K., Khandelia, P., Lee, L.M., and Makeyev, E. V (2012). Argonaute identity defines the length of mature mammalian microRNAs. Nucleic Acids Res. *40*, 6808–6820.
Kadota, Y., Yanagawa, M., Nakaya, T., Kawakami, T., Sato, M.,

and Suzuki, S. (2012). Gene expression of mesoderm-specific transcript is upregulated as preadipocytes differentiate to adipocytes in vitro. J. Physiol. Sci. JPS *62*, 403–411.
Kajimoto, K., Naraba, H., and Iwai, N. (2006). MicroRNA and 3T3-L1 pre-adipocyte differentiation. RNA *12*, 1626–1632.
Kapinas, K., Kessler, C.B., and Delany, A.M. (2009). {miR}-29 suppression of osteonectin in osteoblasts: regulation during differentiation and by canonical {Wnt} signaling. J. Cell. Biochem. *108*, 216–224.
Kapinas, K., Kessler, C., Ricks, T., Gronowicz, G., and Delany, A.M. (2010). miR-29 modulates Wnt signaling in human osteoblasts through a positive feedback loop. J. Biol. Chem. *285*, 25221–25231.
Karbiener, M., Fischer, C., Nowitsch, S., Opriessnig, P., Papak, C., Ailhaud, G., Dani, C., Amri, E.-Z., and Scheideler, M. (2009). {microRNA} {miR}-27b impairs human adipocyte differentiation and targets {PPARgamma}. Biochem. Biophys. Res. Commun. *390*, 247–251.
Karbiener, M., Pisani, D.F., Frontini, A., Oberreiter, L.M., Lang, E., Vegiopoulos, A., Mössenböck, K., Bernhardt, G.A., Mayr, T., Hildner, F., et al. (2014). {MicroRNA}-26 {Family} {Is} {Required} for {Human} {Adipogenesis} and {Drives} {Characteristics} of {Brown} {Adipocytes}. Stem Cells *32*, 1578–1590.
Karbiener, M., Glantschnig, C., Pisani, D.F., Laurencikiene, J., Dahlman, I., Herzig, S., Amri, E.-Z., and Scheideler, M. (2015). Mesoderm-specific transcript (MEST) is a negative regulator of human adipocyte differentiation. Int. J. Obes. *39*, 1–9.
Kertesz, M., Iovino, N., Unnerstall, U., Gaul, U., and Segal, E. (2007). The role of site accessibility in microRNA target recognition. TL - 39. Nat. Genet. *39 VN-r*, 1278–1284.
Kilroy, G., Kirk-Ballard, H., Carter, L.E., and Floyd, Z.E. (2012). The Ubiquitin Ligase Siah2 Regulates PPARγ Activity in Adipocytes. Endocrinology *153*, 1206–1218.
Kinoshita, M., Ono, K., Horie, T., Nagao, K., Nishi, H., Kuwabara, Y., Takanabe-Mori, R., Hasegawa, K., Kita, T., and Kimura, T. (2010). Regulation of adipocyte differentiation by activation of serotonin (5-HT) receptors 5-HT2AR and 5-HT2CR and involvement of microRNA-448-mediated repression of KLF5. Mol. Endocrinol. *24*, 1978–1987.
Van Der Klaauw, A.A., and Farooqi, I.S. (2015). The hunger genes: Pathways to obesity. Cell *161*, 119–132.
Klöting, N., Berthold, S., Kovacs, P., Schön, M.R., Fasshauer, M., Ruschke, K., Stumvoll, M., and Blüher, M. (2009). MicroRNA expression in human omental and subcutaneous adipose tissue. PLoS One *4*, e4699.
Knittle, J.L., Timmers, K., Ginsberg-Fellner, F., Brown, R.E., and Katz, D.P. (1979). The growth of adipose tissue in children and adolescents. Cross-sectional and longitudinal studies of adipose cell number and size. J. Clin. Invest. *63*, 239–246.
Kong, L., Zhu, J., Han, W., Jiang, X., Xu, M., Zhao, Y., Dong, Q., Pang, Z., Guan, Q., Gao, L., et al. (2011). Significance of serum microRNAs in pre-diabetes and newly diagnosed type 2 diabetes: A clinical study. Acta Diabetol. *48*, 61–69.
Kornfeld, J.-W., Baitzel, C., Könner, A.C., Nicholls, H.T., Vogt, M.C., Herrmanns, K., Scheja, L., Haumaitre, C., Wolf, A.M., Knippschild, U., et al. (2013). Obesity-induced overexpression of miR-802 impairs glucose metabolism through silencing of Hnf1b. Nature *494*, 111–115.
Kota, J., Chivukula, R.R., O'Donnell, K.A., Wentzel, E.A., Montgomery, C.L., Hwang, H.-W., Chang, T.-C., Vivekanandan, P., Torbenson, M., Clark, K.R., et al. (2009). Therapeutic {microRNA} delivery suppresses tumorigenesis in a murine liver cancer model. Cell *137*, 1005–1017.
Kozomara, A., and Griffiths-Jones, S. (2014). miRBase: annotating high confidence microRNAs using deep sequencing data. Nucleic Acids Res. *42*, D68–D73.
Krek, A., Grün, D., Poy, M.N., Wolf, R., Rosenberg, L., Epstein, E.J., MacMenamin, P., da Piedade, I., Gunsalus, K.C., Stoffel, M., et al. (2005). Combinatorial microRNA target predictions. Nat. Genet. *37*, 495–500.
Kriegel, A.J., Liu, Y., Fang, Y., Ding, X., and Liang, M. (2012). The miR-29 family: genomics, cell biology, and relevance to renal and cardiovascular injury. Physiol. Genomics *44*, 237–244.
Krol, J., Loedige, I., and Filipowicz, W. (2010). The widespread regulation of microRNA biogenesis, function and decay. Nat. Rev. Genet. *11*, 597–610.
Kuo, T., Lew, M.J., Mayba, O., Harris, C.A., Speed, T.P., and Wang, J.-C. (2012). Genome-wide analysis of glucocorticoid receptor-binding sites in myotubes identifies gene networks modulating insulin signaling. Proc. Natl. Acad. Sci. U. S. A. *109*, 11160–11165.
Lagos-quintana, M., Rauhut, R., Lendeckel, W., and Tuschl, T. (2001). Identification of novel genes Coding for RNAs of Small expressed RNAs. Science (80-.). *294*, 853–858.
Lanford, R.E., Hildebrandt-Eriksen, E.S., Petri, A., Persson, R., Lindow, M., Munk, M.E., Kauppinen, S., and Ørum, H. (2010). Therapeutic silencing of {microRNA}-122 in primates with chronic hepatitis {C} virus infection. Science *327*, 198–201.
Langley, S.C., and York, D.A. (1990). Effects of antiglucocorticoid RU 486 on development of obesity in obese fa/fa Zucker rats. Am. J. Physiol. *259*, R539-44.
Lau, Nelson C.; Lim, Lee P.; Weinstein, Earl G.; Bartel, D.P. (2001). An abundant class of tiny RNAs with probable regulatory roles in Caenorhabditis elegans. Science (80-.). *294*, 858–862.
Lee, Y.-K., and Cowan, C.A. (2013). White to brite adipocyte transition and back again. Nat. Cell Biol. *15*, 568–569.
Lee, E.K., Lee, M.J., Abdelmohsen, K., Kim, M.M., Srikantan, S., Jennifer, L., Hutchison, E.R., Kim, H.H., Marasa, S., Selimyan, R., et al. (2011). miR-130 Suppresses Adipogenesis by Inhibiting Peroxisome Proliferator-Activated Receptor γ Expression miR-130 Suppresses Adipogenesis by Inhibiting Peroxisome Proliferator-Activated Receptor ✐ Expression □. Mol. Cell. Biol. *31*, 626–638.
Lee, M.-J., Pramyothin, P., Karastergiou, K., and Fried, S.K. (2014a). Deconstructing the roles of glucocorticoids in adipose tissue biology and the development of central obesity. Biochim. Biophys. Acta *1842*, 473–481.
Lee, M.J., Pramyothin, P., Karastergiou, K., and Fried, S.K. (2014b). Deconstructing the roles of glucocorticoids in adipose tissue biology and the development of central obesity. Biochim. Biophys. Acta - Mol. Basis Dis. *1842*, 473–481.
Lee, R.C., Feinbaum, R.L., and Ambros, V. (1993). The C. elegans heterochronic gene lin-4 encodes small RNAs with antisense complementarity to lin-14. Cell *75*, 843–854.
Lee, R.C., Ambros, V., Erdmann, V.A., Lee, R.C., Feinbaum, R.L., Ambros, V., Reinhart, B., Wightman, B., Ha, I., Ruvkun, G., et al. (2001). An extensive class of small RNAs in Caenorhabditis elegans. Science *294*, 862–864.
Lefterova, M.I., Zhang, Y., Steger, D.J., Schupp, M., Schug, J., Cristancho, A., Feng, D., Zhuo, D., Stoeckert Jr, C.J., Liu, X.S., et al. (2008). {PPARgamma} and {C}/{EBP} factors orchestrate adipocyte biology via adjacent binding on a genome-wide scale. Genes Dev. *22*, 2941–2952.
Lewis, B.P., Burge, C.B., and Bartel, D.P. (2005). Conserved seed pairing, often flanked by adenosines, indicates that thousands of human genes are microRNA targets. Cell *120*, 15–20.
Li, Z., Huang, H., Chen, P., He, M., Li, Y., Arnovitz, S., Jiang, X., He, C., Hyjek, E., Zhang, J., et al. (2012). miR-196b directly targets both HOXA9/MEIS1 oncogenes and FAS tumour suppressor in MLL-rearranged leukaemia. Nat. Commun. *3*, 688.
Lin, Q., Gao, Z., Alarcon, R.M., Ye, J., and Yun, Z. (2009). A role of miR-27 in the regulation of adipogenesis. FEBS J. *276*, 2348–2358.
Lindroos, J., Husa, J., Mitterer, G., Haschemi, A., Rauscher, S., Haas, R., Gröger, M., Loewe, R., Kohrgruber, N., Schrögendorfer, K.F., et al. (2013). Human but Not Mouse Adipogenesis Is Critically Dependent on LMO3. Cell Metab. *18*, 62–74.
Ling, H.Y., Wen, G.B., Feng, S.D., Tuo, Q.H., Ou, H.S., Yao, C.H., Zhu, B.Y., Gao, Z.P., Zhang, L., and Liao, D.F. (2011). MicroRNA-375 promotes 3T3-L1 adipocyte differentiation through modulation of extracellular signal-regulated kinase signalling. Clin. Exp. Pharmacol. Physiol. *38*, 239–246.
Lingel, A., and Izaurralde, E. (2004). RNAi: finding the elusive endonuclease. RNA *10*, 1675–1679.
Linhart, H.G., Ishimura-Oka, K., DeMayo, F., Kibe, T., Repka, D., Poindexter, B., Bick, R.J., and Darlington, G.J. (2001).

C/{EBPalpha} is required for differentiation of white, but not brown, adipose tissue. Proc. Natl. Acad. Sci. U. S. A. *98*, 12532–12537.

Linsley, P.S., Schelter, J., Burchard, J., Kibukawa, M., Martin, M.M., Bartz, S.R., Johnson, J.M., Cummins, J.M., Raymond, C.K., Dai, H., et al. (2007). Transcripts targeted by the microRNA-16 family cooperatively regulate cell cycle progression. Mol. Cell. Biol. *27*, 2240–2252.

Liu, N., Abe, M., Sabin, L.R., Hendriks, G.-J., Naqvi, A.S., Yu, Z., Cherry, S., and Bonini, N.M. (2011a). The exoribonuclease Nibbler controls 3' end processing of microRNAs in Drosophila. Curr. Biol. *21*, 1888–1893.

Liu, Y., Nakagawa, Y., Wang, Y., Sakurai, R., Tripathi, P. V, Lutfy, K., and Friedman, T.C. (2005). Increased Glucocorticoid Receptor and 11b-Hydroxysteroid Dehydrogenase Type 1 Expression in Hepatocytes May Contribute to the Phenotype of Type 2 Diabetes in db / db Mice. Blood *54*, 32–40.

Liu, Y., Zhang, R., Xin, J., Sun, Y., Li, J., Wei, D., and Zhao, A.Z. (2011b). Identification of S100A16 as a novel adipogenesis promoting factor in 3T3-L1 cells. Endocrinology *152*, 903–911.

Livingstone, D.E.W., Grassick, S.L., Currie, G.L., Walker, B.R., and Andrew, R. (2009). Dysregulation of glucocorticoid metabolism in murine obesity: comparable effects of leptin resistance and deficiency. J. Endocrinol. *201*, 211–218.

Longo, K.A., Wright, W.S., Kang, S., Gerin, I., Chiang, S.-H., Lucas, P.C., Opp, M.R., and MacDougald, O.A. (2004). Wnt10b inhibits development of white and brown adipose tissues. J. Biol. Chem. *279*, 35503–35509.

Lu, N.Z., Collins, J.B., Grissom, S.F., and Cidlowski, J.A. (2007). Selective regulation of bone cell apoptosis by translational isoforms of the glucocorticoid receptor. Mol. Cell. Biol. *27*, 7143–7160.

MacDougald, O.A., and Lane, M.D. (1995). Transcriptional regulation of gene expression during adipocyte differentiation. Annu. Rev. Biochem. *64*, 345–373.

Maltese, P., Palma, L., Sfara, C., de Rocco, P., Latiano, a, Palmieri, O., Corritore, G., Annese, V., and Magnani, M. (2012). Glucocorticoid resistance in Crohn's disease and ulcerative colitis: an association study investigating GR and FKBP5 gene polymorphisms. Pharmacogenomics J. *12*, 432–438.

van Marken Lichtenbelt, W.D., Vanhommerig, J.W., Smulders, N.M., Drossaerts, J.M.A.F.L., Kemerink, G.J., Bouvy, N.D., Schrauwen, P., and Teule, G.J.J. (2009). Cold-activated brown adipose tissue in healthy men. N. Engl. J. Med. *360*, 1500–1508.

Marques, L.J., Zheng, L., Poulakis, N., Guzman, J., and Costabel, U. (1999). Pentoxifylline inhibits TNF-alpha production from human alveolar macrophages. Am. J. Respir. Crit. Care Med. *159*, 508–511.

Masuzaki, H., and Flier, J.S. (2003). Tissue-specific glucocorticoid reactivating enzyme, 11 beta-hydroxysteroid dehydrogenase type 1 (11 beta-HSD1)--a promising drug target for the treatment of metabolic syndrome. Curr. Drug Targets. Immune. Endocr. Metabol. Disord. *3*, 255–262.

Masuzaki, H., Paterson, J., Shinyama, H., Morton, N.M., Mullins, J.J., Seckl, J.R., and Flier, J.S. (2001). A Transgenic Model of Visceral Obesity and the Metabolic Syndrome. Science (80-.). *294*, 2166–2170.

Melo, A.K.G., Melo, M.R., Saramago, A.B.A., Demartino, G., Souza, B.D.B., and Longui, C.A. (2013). Persistent glucocorticoid resistance in systemic lupus erythematosus patients during clinical remission. Genet. Mol. Res. *12*, 2010–2019.

Mendell, J.T., and Olson, E.N. (2012). MicroRNAs in stress signaling and human disease. Cell *148*, 1172–1187.

Miller, R.E., Hackenberg, R., and Gershman, H. (1978). Regulation of glutamine synthetase in cultured 3T3-L1 cells by insulin, hydrocortisone, and dibutyryl cyclic AMP. Proc. Natl. Acad. Sci. U. S. A. *75*, 1418–1422.

Mudhasani, R., Imbalzano, A.N., and Jones, S.N. (2010). An essential role for Dicer in adipocyte differentiation. J. Cell. Biochem. *110*, 812–816.

Mudhasani, R., Puri, V., Hoover, K., Czech, M.P., Imbalzano, A.N., and Jones, S.N. (2011). Dicer is required for the formation of white but not brown adipose tissue. J. Cell. Physiol. *226*, 1399–1406.

Mueller, K.M., Hartmann, K., Kaltenecker, D., Vettorazzi, S., Bauer, M., Mauser, L., Amann, S., Jall, S., Fischer, K., Esterbauer, H., et al. (2017). Adipocyte Glucocorticoid Receptor Deficiency Attenuates Aging- and HFD-Induced Obesity and Impairs the Feeding-Fasting Transition. Diabetes *66*, 272–286.

Nedergaard, J., Bengtsson, T., and Cannon, B. (2007). Unexpected evidence for active brown adipose tissue in adult humans. Am. J. Physiol. Endocrinol. Metab. *293*, E444--452.

Nguyen, N.T., and Varela, J.E. (2016). Bariatric surgery for obesity and metabolic disorders: state of the art. Nat. Rev. Gastroenterol. Hepatol.

O'Donnell, K.A., Wentzel, E.A., Zeller, K.I., Dang, C. V., and Mendell, J.T. (2005). c-Myc-regulated microRNAs modulate E2F1 expression. Nature *435*, 839–843.

Oishi, Y., Manabe, I., Tobe, K., Tsushima, K., Shindo, T., Fujiu, K., Nishimura, G., Maemura, K., Yamauchi, T., Kubota, N., et al. (2005). Krüppel-like transcription factor KLF5 is a key regulator of adipocyte differentiation. Cell Metab. *1*, 27–39.

Okret, S., Poellinger, L., Dong, Y., and Gustafsson, J. a (1986). Down-regulation of glucocorticoid receptor mRNA by glucocorticoid hormones and recognition by the receptor of a specific binding sequence within a receptor cDNA clone. Proc. Natl. Acad. Sci. U. S. A. *83*, 5899–5903.

Oskowitz, A.Z., Lu, J., Penfornis, P., Ylostalo, J., McBride, J., Flemington, E.K., Prockop, D.J., and Pochampally, R. (2008). Human multipotent stromal cells from bone marrow and {microRNA}: regulation of differentiation and leukemia inhibitory factor expression. Proc. Natl. Acad. Sci. U. S. A. *105*, 18372–18377.

Park, Y.-K., and Ge, K. (2017). Glucocorticoid Receptor Accelerates, but Is Dispensable for, Adipogenesis. Mol. Cell. Biol. *37*, e00260-16.

Pasquinelli, A.E. (2012). MicroRNAs and their targets : recognition , regulation and an emerging reciprocal relationship. Nat. Publ. Gr. *13*, 271–282.

Patel, R., Williams-Dautovich, J., and Cummins, C.L. (2014). Minireview: new molecular mediators of glucocorticoid receptor activity in metabolic tissues. Mol. Endocrinol. *28*, 999–1011.

Peng, H., Zhong, M., Zhao, W., Wang, C., Zhang, J., Liu, X., Li, Y., Paudel, S.D., Wang, Q., Lou, T., et al. (2013). Urinary miR-29 Correlates with Albuminuria and Carotid Intima-Media Thickness in Type 2 Diabetes Patients. PLoS One *8*, e82607.

Pereira, M.J., Palming, J., Svensson, M.K., Rizell, M., Dalenbäck, J., Hammar, M., Fall, T., Sidibeh, C.O., Svensson, P.A., and Eriksson, J.W. (2014). FKBP5 expression in human adipose tissue increases following dexamethasone exposure and is associated with insulin resistance. Metabolism. *63*, 1198–1208.

Phillips, D.I.W., Barker, D.J.P., Fall, C.H.D., Seckl, J.R., Whorwood, C.B., Wood, P.J., and Walker, B.R. (1998). Elevated Plasma Cortisol Concentrations: A Link between Low Birth Weight and the Insulin Resistance Syndrome? [1]. J. Clin. Endocrinol. Metab. *83*, 757–760.

Pickering, R.T., Lee, M., Karastergiou, K., Gower, A., and Fried, S.K. (2016). Depot Dependent Effects of Dexamethasone on Gene Expression in Human Omental and Abdominal Subcutaneous Adipose Tissues from Obese Women. 1–19.

Pisani, D.F., Djedaini, M., Beranger, G.E., Elabd, C., Scheideler, M., Ailhaud, G., and Amri, E.Z. (2011). Differentiation of human adipose-derived stem cells into "brite" (brown-in-white) adipocytes. Front. Endocrinol. (Lausanne). *2*, 1–9.

Poy, M.N., Hausser, J., Trajkovski, M., Braun, M., Collins, S., Rorsman, P., Zavolan, M., and Stoffel, M. (2009). {miR}-375 maintains normal pancreatic alpha- and beta-cell mass. Proc. Natl. Acad. Sci. U. S. A. *106*, 5813–5818.

Ravussin, Y., Leibel, R.L., and Ferrante, A.W. (2014). A missing link in body weight homeostasis: The catabolic signal of the overfed state. Cell Metab. *20*, 565–572.

Rayner, K.J., Esau, C.C., Hussain, F.N., McDaniel, A.L., Marshall, S.M., van Gils, J.M., Ray, T.D., Sheedy, F.J., Goedeke, L., Liu, X., et al. (2011). Inhibition of miR-33a/b in non-human primates raises plasma HDL and lowers VLDL triglycerides. Nature *478*,

404–407.
Rebuffé-Scrive, M., Krotkiewski, M., Elfverson, J., and Bj??rntorp, P. (1988). Muscle and adipose tissue morphology and metabolism in cushing???s syndrome. J. Clin. Endocrinol. Metab. *67*, 1122–1128.
van der Ree, M.H., van der Meer, A.J., van Nuenen, A.C., de Bruijne, J., Ottosen, S., Janssen, H.L., Kootstra, N.A., and Reesink, H.W. (2016). Miravirsen dosing in chronic hepatitis C patients results in decreased microRNA-122 levels without affecting other microRNAs in plasma. Aliment. Pharmacol. Ther. *43*, 102–113.
Van Der Ree, M., de Vree, M.L., Stelma, F., Willemse, S., van der Valk, M., Rietdijk, S., Molenkamp, R., Schinkel, J., Hadi, S., Harbers, M., et al. (2015). LO7 : A single subcutaneous dose of 2mg/kg or 4mg/kg of RG-101, a GalNAc-conjugated oligonucleotide with antagonist activity against MIR-122, results in significant viral load reductions in chronic hepatitis C patients. J. Hepatol. *62*, S261.
Rega-Kaun, G., Kaun, C., and Wojta, J. (2013). More than a simple storage organ: adipose tissue as a source of adipokines involved in cardiovascular disease. Thromb. Haemost. *110*, 641–650.
Reichardt, H.M., Kaestner, K.H., Tuckermann, J., Kretz, O., Wessely, O., Bock, R., Gass, P., Schmid, W., Herrlich, P., Angel, P., et al. (1998). DNA binding of the glucocorticoid receptor is not essential for survival. Cell *93*, 531–541.
Reusch, J.E., Colton, L.A., and Klemm, D.J. (2000). CREB activation induces adipogenesis in 3T3-L1 cells. Mol. Cell. Biol. *20*, 1008–1020.
Reynolds, R.M., Walker, B.R., Syddall, H.E., Whorwood, C.B., Wood, P.J., and Phillips, D.I. (2001). Elevated plasma cortisol in glucose-intolerant men: differences in responses to glucose and habituation to venepuncture. J. Clin. Endocrinol. Metab. *86*, 1149–1153.
Rodriguez, A.-M., Pisani, D., Dechesne, C.A., Turc-Carel, C., Kurzenne, J.-Y., Wdziekonski, B., Villageois, A., Bagnis, C., Breittmayer, J.-P., Groux, H., et al. (2005). Transplantation of a multipotent cell population from human adipose tissue induces dystrophin expression in the immunocompetent mdx mouse. J. Exp. Med. *201*, 1397–1405.
Rooij, E. Van, and Kauppinen, S. (2014). Development of microRNA therapeutics is coming of age. *6*, 851–864.
van Rooij, E., Sutherland, L.B., Qi, X., Richardson, J.A., Hill, J., and Olson, E.N. (2007). Control of Stress-Dependent Cardiac Growth and Gene Expression by a MicroRNA. Science (80-.). *316*, 575–579.
van Rooij, E., Purcell, A.L., and Levin, A.A. (2012). Developing microRNA therapeutics. Circ. Res. *110*, 496–507.
Rosen, E.D., and MacDougald, O. a (2006). Adipocyte differentiation from the inside out. Nat. Rev. Mol. Cell Biol. *7*, 885–896.
Rosen, E.D., and Spiegelman, B.M. (2006). Adipocytes as regulators of energy balance and glucose homeostasis. Nature *444*, 847–853.
Ross, S.E., Hemati, N., Longo, K.A., Bennett, C.N., Lucas, P.C., Erickson, R.L., and MacDougald, O.A. (2000). Inhibition of adipogenesis by {Wnt} signaling. Science *289*, 950–953.
Rössger, K., Charpin-El-Hamri, G., and Fussenegger, M. (2013). A closed-loop synthetic gene circuit for the treatment of diet-induced obesity in mice. Nat. Commun. *4*, 2825.
Roux, C., Pisani, D.F., Yahia, H. Ben, Djedaini, M., Beranger, G.E., Chambard, J.C., Ambrosetti, D., Michiels, J.F., Breuil, V., Ailhaud, G., et al. (2013). Chondrogenic potential of stem cells derived from adipose tissue: A powerful pharmacological tool. Biochem. Biophys. Res. Commun. *440*, 786–791.
Ru, P., Hu, P., Geng, F., Mo, X., Cheng, C., Yoo, J.Y., Cheng, X., Wu, X., Guo, J.Y., Nakano, I., et al. (2015). Feedback Loop Regulation of SCAP/SREBP-1 by miR-29 Modulates EGFR Signaling-Driven Glioblastoma Growth. Cell Rep. *16*, 1527–1535.
Rubin, C.S., Hirsch, A., Fung, C., and Rosen, O.M. (1978). Development of hormone receptors and hormonal responsiveness in vitro. Insulin receptors and insulin sensitivity in the preadipocyte and adipocyte forms of 3T3-L1 cells. J. Biol. Chem. *253*, 7570–7578.
Russell, T.R., and Ho, R. (1976a). Conversion of 3T3 fibroblasts into adipose cells: triggering of differentiation by prostaglandin {F}2alpha and 1-methyl-3-isobutyl xanthine. Proc. Natl. Acad. Sci. U. S. A. *73*, 4516–4520.
Russell, T.R., and Ho, R. (1976b). Conversion of 3T3 fibroblasts into adipose cells: triggering of differentiation by prostaglandin F2alpha and 1-methyl-3-isobutyl xanthine. Proc. Natl. Acad. Sci. U. S. A. *73*, 4516–4520.
Saito, M., Okamatsu-Ogura, Y., Matsushita, M., Watanabe, K., Yoneshiro, T., Nio-Kobayashi, J., Iwanaga, T., Miyagawa, M., Kameya, T., Nakada, K., et al. (2009). High incidence of metabolically active brown adipose tissue in healthy adult humans: effects of cold exposure and adiposity. Diabetes *58*, 1526–1531.
Saltiel, A.R., and Kahn, C.R. (2001). Insulin signalling and the regulation of glucose and lipid metabolism. Nature *414*, 799–806.
Sanchez-Gurmaches, J., and Guertin, D.A. (2014). Adipocytes arise from multiple lineages that are heterogeneously and dynamically distributed. Nat. Commun. *5*, 4099.
Sanchez-Gurmaches, J., Hung, C.-M., Sparks, C.A., Tang, Y., Li, H., and Guertin, D.A. (2012). PTEN Loss in the Myf5 Lineage Redistributes Body Fat and Reveals Subsets of White Adipocytes that Arise from Myf5 Precursors. Cell Metab. *16*, 348–362.
Scheideler, M., Elabd, C., Zaragosi, L.-E., Chiellini, C., Hackl, H., Sanchez-Cabo, F., Yadav, S., Duszka, K., Friedl, G., Papak, C., et al. (2008). Comparative transcriptomics of human multipotent stem cells during adipogenesis and osteoblastogenesis. BMC Genomics *9*, 340.
Scheideler, M., Karbiener, M., Dani, C., Ailhaud, G., and Amri, E.-Z. (2013). UCP1 (Thermogenin) - inducing agents for use in the treatment of a disorder of the energy homeostasis.
Schlossmacher, G., Stevens, A., and White, A. (2011). Glucocorticoid receptor-mediated apoptosis: Mechanisms of resistance in cancer cells. J. Endocrinol. *211*, 17–25.
Seale, P., Bjork, B., Yang, W., Kajimura, S., Chin, S., Kuang, S., Scimè, A., Devarakonda, S., Conroe, H.M., Erdjument-Bromage, H., et al. (2008). {PRDM}16 controls a brown fat/skeletal muscle switch. Nature *454*, 961–967.
Seckl, J.R., and Walker, B.R. (2001). Minireview: 11β-Hydroxysteroid Dehydrogenase Type 1— A Tissue-Specific Amplifier of Glucocorticoid Action [1]. Endocrinology *142*, 1371–1376.
Sethupathy, P., and Collins, F.S. (2008). MicroRNA target site polymorphisms and human disease. Trends Genet. *24*, 489–497.
Sha, H., He, Y., Chen, H., Wang, C., Zenno, A., Shi, H., Yang, X., Zhang, X., and Qi, L. (2009). The IRE1α-XBP1 Pathway of the Unfolded Protein Response Is Required for Adipogenesis. Cell Metab. *9*, 556–564.
Sharma, G., and Goalstone, M.L. (2005). Dominant negative FTase (DNFTalpha) inhibits ERK5, MEF2C and CREB activation in adipogenesis. Mol. Cell. Endocrinol. *245*, 93–104.
Sharma, S., and Fulton, S. (2013). Diet-induced obesity promotes depressive-like behaviour that is associated with neural adaptations in brain reward circuitry. Int. J. Obes. (Lond). *37*, 382–389.
Sharp, L.Z., Shinoda, K., Ohno, H., Scheel, D.W., Tomoda, E., Ruiz, L., Hu, H., Wang, L., Pavlova, Z., Gilsanz, V., et al. (2012). Human BAT Possesses Molecular Signatures That Resemble Beige/Brite Cells. PLoS One *7*, e49452.
Sheng, M., Thompson, M.A., and Greenberg, M.E. (1991). CREB: a Ca(2+)-regulated transcription factor phosphorylated by calmodulin-dependent kinases. Science *252*, 1427–1430.
Shibli-Rahhal, A., Van Beek, M., and Schlechte, J.A. (2006). Cushing's syndrome. Clin. Dermatol. *24*, 260–265.
Siersbæk, R., Rabiee, A., Nielsen, R., Sidoli, S., Traynor, S., Loft, A., Poulsen, L., Rogowska-Wrzesinska, A., Jensen, O.N., and Mandrup, S. (2014a). Transcription factor cooperativity in early adipogenic hotspots and super-enhancers. Cell Rep. *7*, 1443–1455.
Siersbæk, R., Baek, S., Rabiee, A., Nielsen, R., Traynor, S., Clark, N., Sandelin, A., Jensen, O.N., Sung, M.H., Hager, G.L., et al.

(2014b). Molecular architecture of transcription factor hotspots in early adipogenesis. Cell Rep. *7*, 1434–1442.
Ślusarz, A., and Pulakat, L. (2015). The two faces of miR-29. J. Cardiovasc. Med. (Hagerstown). *16*, 480–490.
Sørensen, T.I., Price, R.A., Stunkard, A.J., and Schulsinger, F. (1989). Genetics of obesity in adult adoptees and their biological siblings. BMJ *298*, 87–90.
Spalding, K.L., Arner, E., Westermark, P.O., Bernard, S., Buchholz, B.A., Bergmann, O., Blomqvist, L., Hoffstedt, J., Näslund, E., Britton, T., et al. (2008a). Dynamics of fat cell turnover in humans. Nature *453*, 783–787.
Spalding, K.L., Arner, E., Westermark, P.O., Bernard, S., Buchholz, B.A., Bergmann, O., Blomqvist, L., Hoffstedt, J., Näslund, E., Britton, T., et al. (2008b). Dynamics of fat cell turnover in humans. Nature *453*, 783–787.
Di Stefano, V., Zaccagnini, G., Capogrossi, M.C., and Martelli, F. (2011). microRNAs as peripheral blood biomarkers of cardiovascular disease. Vascul. Pharmacol. *55*, 111–118.
Steger, D.J., Grant, G.R., Schupp, M., Tomaru, T., Lefterova, M.I., Schug, J., Manduchi, E., Stoeckert, C.J., and Lazar, M.A. (2010). Propagation of adipogenic signals through an epigenomic transition state. Genes Dev. *24*, 1035–1044.
Styner, M., Sen, B., Xie, Z., Case, N., and Rubin, J. (2010). Indomethacin promotes adipogenesis of mesenchymal stem cells through a cyclooxygenase independent mechanism. J. Cell. Biochem. *111*, 1042–1050.
Sun, F., Wang, J., Pan, Q., Yu, Y., Zhang, Y., Wan, Y., Wang, J., Li, X., and Hong, A. (2009a). Characterization of function and regulation of miR-24-1 and miR-31. Biochem. Biophys. Res. Commun. *380*, 660–665.
Sun, T., Fu, M., Bookout, A.L., Kliewer, S.A., and Mangelsdorf, D.J. (2009b). MicroRNA *let - 7* Regulates 3T3-L1 Adipogenesis. Mol. Endocrinol. *23*, 925–931.
Szefler, S.J., and Leung, D.Y.M. (1997). Glucocorticoid-resistant asthma: pathogenesis and clinical implications for management. Eur. Respir. J. *10*, 1640–1647.
Taganov, K.D., Boldin, M.P., Chang, K.-J., and Baltimore, D. (2006). NF-kappaB-dependent induction of microRNA miR-146, an inhibitor targeted to signaling proteins of innate immune responses. Proc. Natl. Acad. Sci. U. S. A. *103*, 12481–12486.
Tang, Q.Q., and Lane, M.D. (2012). Adipogenesis : From Stem Cell to Adipocyte. Annu. Rev. Biochem. *81*, 715–736.
Tata, J.R. (2002). Signalling through nuclear receptors. Nat. Rev. Mol. Cell Biol. *3*, 702–710.
The UniProt Consortium (2015). UniProt: a hub for protein information. Nucleic Acids Res. *43*, D204-12.
Thum, T., Gross, C., Fiedler, J., Fischer, T., Kissler, S., Bussen, M., Galuppo, P., Just, S., Rottbauer, W., Frantz, S., et al. (2008). MicroRNA-21 contributes to myocardial disease by stimulating MAP kinase signalling in fibroblasts. Nature *456*, 980–984.
Tijsen, A.J., Creemers, E.E., Moerland, P.D., de Windt, L.J., van der Wal, A.C., Kok, W.E., and Pinto, Y.M. (2010). MiR423-5p as a circulating biomarker for heart failure. Circ. Res. *106*, 1035–1039.
Tome, M., Lopez-Romero, P., Albo, C., Sepulveda, J.C., Fernandez-Gutierrez, B., Dopazo, A., Bernad, A., and Gonzalez, M.A. (2011). miR-335 orchestrates cell proliferation, migration and differentiation in human mesenchymal stem cells. Cell Death Differ. *18*, 985–995.
Tontonoz, P., and Spiegelman, B.M. (2008). Fat and beyond: the diverse biology of {PPARgamma}. Annu. Rev. Biochem. *77*, 289–312.
Torres, A.G., Fabani, M.M., Vigorito, E., and Gait, M.J. (2011). {MicroRNA} fate upon targeting with anti-{miRNA} oligonucleotides as revealed by an improved {Northern}-blot-based method for {miRNA} detection. RNA *17*, 933–943.
Trayhurn, P. (2014). Hypoxia and {Adipocyte} {Physiology}: {Implications} for {Adipose} {Tissue} {Dysfunction} in {Obesity}. Annu. Rev. Nutr.
Tseng, Y.-H., Kokkotou, E., Schulz, T.J., Huang, T.L., Winnay, J.N., Taniguchi, C.M., Tran, T.T., Suzuki, R., Espinoza, D.O., Yamamoto, Y., et al. (2008). New role of bone morphogenetic protein 7 in brown adipogenesis and energy expenditure. Nature *454*, 1000–1004.
Uhlenhaut, N.H., Barish, G.D., Yu, R.T., Downes, M., Karunasiri, M., Liddle, C., Schwalie, P., Hübner, N., and Evans, R.M. (2013). Insights into Negative Regulation by the Glucocorticoid Receptor from Genome-wide Profiling of Inflammatory Cistromes. Mol. Cell *49*, 158–171.
Underwood, E.L., and Thompson, L.T. (2016). A High-Fat Diet Causes Impairment in Hippocampal Memory and Sex-Dependent Alterations in Peripheral Metabolism. Neural Plast. *2016*, 7385314.
Vegiopoulos, A., and Herzig, S. (2007a). Glucocorticoids, metabolism and metabolic diseases. Mol. Cell. Endocrinol. *275*, 43–61.
Vegiopoulos, A., and Herzig, S. (2007b). Glucocorticoids, metabolism and metabolic diseases. Mol. Cell. Endocrinol. *275*, 43–61.
Ventura, A., and Jacks, T. (2009). MicroRNAs and Cancer: Short RNAs Go a Long Way. Cell *136*, 586–591.
Viengchareun, S., Zennaro, M.-C., Pascual-Le Tallec, L., and Lombes, M. (2002). Brown adipocytes are novel sites of expression and regulation of adiponectin and resistin. FEBS Lett. *532*, 345–350.
Virtanen, K.A., Lidell, M.E., Orava, J., Heglind, M., Westergren, R., Niemi, T., Taittonen, M., Laine, J., Savisto, N.-J., Enerbäck, S., et al. (2009). Functional brown adipose tissue in healthy adults. N. Engl. J. Med. *360*, 1518–1525.
Visweswaran, M., Schiefer, L., Arfuso, F., Dilley, R.J., Newsholme, P., and Dharmarajan, A. (2015). Wnt antagonist secreted frizzled-related protein 4 upregulates adipogenic differentiation in human adipose tissue-derived mesenchymal stem cells. PLoS One *10*, 1–13.
Wang, Q., Li, Y.C., Wang, J., Kong, J., Qi, Y., Quigg, R.J., and Li, X. (2008a). {miR}-17-92 cluster accelerates adipocyte differentiation by negatively regulating tumor-suppressor {Rb}2/p130. Proc. Natl. Acad. Sci. U. S. A. *105*, 2889–2894.
Wang, Q., Li, Y.C., Wang, J., Kong, J., Qi, Y., Quigg, R.J., and Li, X. (2008b). miR-17-92 cluster accelerates adipocyte differentiation by negatively regulating tumor-suppressor Rb2/p130. Proc. Natl. Acad. Sci. *105*, 2889–2894.
Wang, W.-X., Rajeev, B.W., Stromberg, A.J., Ren, N., Tang, G., Huang, Q., Rigoutsos, I., and Nelson, P.T. (2008c). The expression of microRNA miR-107 decreases early in Alzheimer's disease and may accelerate disease progression through regulation of beta-site amyloid precursor protein-cleaving enzyme 1. J. Neurosci. Off. J. Soc. Neurosci. *28*, 1213–1223.
Wardle, J., Carnell, S., Haworth, C.M., and Plomin, R. (2008a). Evidence for a strong genetic influence on childhood adiposity despite the force of the obesogenic environment. Am. J. Clin. Nutr. *87*, 398–404.
Wardle, J., Carnell, S., Haworth, C.M.A., Farooqi, I.S., O'Rahilly, S., and Plomin, R. (2008b). Obesity Associated Genetic Variation in *FTO* Is Associated with Diminished Satiety. J. Clin. Endocrinol. Metab. *93*, 3640–3643.
Wiper-Bergeron, N., Wu, D., Pope, L., Schild-poulter, C., and Hache, R.J.G. (2003). Stimulation of preadipocyte differentiation by steroid through targeting of an HDAC1 complex. EMBO *22*, 2135–2145.
Wiper-Bergeron, N., Salem, H.A., Tomlinson, J.J., Wu, D., and Hache, R.J.G. (2007). Glucocorticoid-stimulated preadipocyte differentiation is mediated through acetylation of C/EBPbeta by GCN5. Proc. Natl. Acad. Sci. *104*, 2703–2708.
World Health Organisation (2016). Obesity and overweight. Fact Sheet.
World Health Organization, R.O. for E. (2017). Obesity: Data and statistics (World Health Organization).
Wu, J.-H., Gao, Y., Ren, A.-J., Zhao, S.-H., Zhong, M., Peng, Y.-J., Shen, W., Jing, M., and Liu, L. (2011). Altered {MicroRNA} {Expression} {Profiles} in {Retinas} with {Diabetic} {Retinopathy}. Ophthalmic Res. *47*, 195–201.
Xi, Y., Shen, W., Ma, L., Zhao, M., Zheng, J., Bu, S., Hino, S., and Nakao, M. (2016). HMGA2 promotes adipogenesis by activating C/EBPβ-mediated expression of PPARγ. Biochem. Biophys. Res. Commun. *472*, 617–623.

Xie, H., Lim, B., and Lodish, H.F. (2009). MicroRNAs induced during adipogenesis that accelerate fat cell development are downregulated in obesity. Diabetes *58*, 1050–1057.
Xin, M., Small, E.M., Sutherland, L.B., Qi, X., McAnally, J., Plato, C.F., Richardson, J.A., Bassel-Duby, R., and Olson, E.N. (2009). MicroRNAs miR-143 and miR-145 modulate cytoskeletal dynamics and responsiveness of smooth muscle cells to injury. Genes Dev. *23*, 2166–2178.
Yates, L.A., Norbury, C.J., and Gilbert, R.J.C. (2013). The long and short of microRNA. Cell *153*, 516–519.
Yu, J., Yu, B., He, J., Zheng, P., Mao, X., Han, G., and Chen, D. (2014). Chronic Glucocorticoid Exposure-Induced Epididymal Adiposity Is Associated with Mitochondrial Dysfunction in White Adipose Tissue of Male C57BL/6J Mice. PLoS One *9*, e112628.
Zampetaki, A., Kiechl, S., Drozdov, I., Willeit, P., Mayr, U., Prokopi, M., Mayr, A., Weger, S., Oberhollenzer, F., Bonora, E., et al. (2010). Plasma {microRNA} profiling reveals loss of endothelial {miR}-126 and other {microRNAs} in type 2 diabetes. Circ. Res. *107*, 810–817.
Zeng, W., van den Berg, A., Huitema, S., Gouw, A.S.H., Molema, G., and de Jong, K.P. (2014). Correlation of MicroRNA-16, MicroRNA-21 and MicroRNA-101 Expression with Cyclooxygenase-2 Expression and Angiogenic Factors in Cirrhotic and Noncirrhotic Human Hepatocellular Carcinoma. PLoS One *9*, e95826.
Zingaretti, M.C., Crosta, F., Vitali, A., Guerrieri, M., Frontini, A., Cannon, B., Nedergaard, J., and Cinti, S. (2009). The presence of {UCP}1 demonstrates that metabolically active adipose tissue in the neck of adult humans truly represents brown adipose tissue. FASEB J. Off. Publ. Fed. Am. Soc. Exp. Biol. *23*, 3113–3120.
miR-29a entry in miRbase.